Stony Brook University

Structural and Biochemical Characterization of the Interaction between Gephyrin and Dynein Light Chains

A Dissertation Presented

By

Eun-Young Lee

To

The Graduate School

In Partial Fulfillment of the

Requirements for the Degree of

Doctor of Philosophy

In

Biochemistry and Structural Biology

Stony Brook University

August 2009

Stony Brook University

The Graduate School

Eun-Young Lee

We, the dissertation committee for the above candidate for the

Doctor of Philosophy Degree,

hereby recommend acceptance of this dissertation.

Hermann Schindelin, Ph.D. – Dissertation Advisor
Professor, Rudolf Virchow Center, University of Würzburg, Germany
Formerly Associate Professor, Department of Biochemistry and Cell Biology,
Stony Brook University

Erwin London, Ph.D. – Dissertation Co-advisor
Professor, Department of Biochemistry and Cell Biology, Stony Brook University

Steven O. Smith, Ph.D. – Chairperson of Defense
Professor, Department of Biochemistry and Cell Biology, Stony Brook University

Dax Fu, Ph.D.
Biochemist, Department of Biology, Brookhaven National Laboratory

Lonnie P. Wollmuth, Ph.D.
Associate Professor, Department of Neurobiology and Behavior, Stony Brook University

This dissertation is accepted by the Graduate School

Lawrence Martin
Dean of the Graduate School

Abstract of the Dissertation

Structural and Biochemical Characterization

of the Interaction between Gephyrin and Dynein Light Chains

By

Eun-Young Lee

Doctor of Philosophy

In

Biochemistry and Structural Biology

Stony Brook University

2009

Gephyrin is a dynamic receptor-associated protein that plays a crucial role in the clustering and anchoring as well as trafficking of inhibitory neuronal receptors. Gephyrin is composed of three regions, an N-terminal G-domain, a C-terminal E-domain, and a presumably unstructured linker region connecting the two domains. The isolated G- and E-domains form trimers and dimers, respectively, and the two independent oligomerization interfaces led to the proposal that gephyrin oligomers can assemble into a hexagonal lattice below the postsynaptic membrane providing binding sites for the inhibitory neurotransmitter receptors on one side and components of the cytoskeleton on the opposite side, thereby anchoring the receptors either directly or indirectly.

The interactions with the light chains of the dynein motor (DYNLL1 and DYNLL2) mediate the retrograde transport of glycine receptor-gephyrin complexes via the dynein motor. A short peptide (residues 203-214) within the central linker of gephyrin has been

identified as the DYNLL-binding site. I determined the crystal structures of DYNLL1 and DYNLL2 in their apo-state and in complex with a peptide derived from gephyrin's linker. The peptide is present in an extended conformation and binds as an additional β-strand to either DYNLL. The analysis of the binary complexes revealed the contribution of individual amino acids to this interaction and revealed that Tyr65, His68 and Phe73 of DYNLL and Gln211 of gephyrin are critical for this interaction. Comparisons with other DYNLL-peptide complexes demonstrate a remarkable plasticity in the ligand-binding pocket.

The gephyrin linker region revealed that it contains the binding sites of additional gephyrin interacting proteins besides DYNLL, but its structural properties are not well characterized. The functional significance of gephyrin linker region which is presumably unstructured has been analyzed here. A thermostablility analysis revealed that the C-terminal end of the linker region stabilizes the E-domain. The oligomerization potential of the linker fused to either the G- or E-domain has been biochemically analyzed since the isolated linker cannot be analyzed due to its proteolytic sensitivity. These studies revealed that the linker of gephyrin contains an independent oligomerization site. The N-terminal half of linker region including the C-terminal end of the G-domain was deduced as an important region for oligomerization of the linker. The binding on G- or E-domain fused linkers to DYNLL revealed that interactions involving on the linker region can modulate the oligomerization of gephyrin.

Table of Contents

List of Figures

List of Tables

List of Abbreviations

µM: Micromolar

Å: Angstrom (10^{-10} m)

Apg3: Autophagy-related protein 3

Apg7: Autophagy-related protein 7

Apg8: Autophagy-related protein 8

Cα: alpha Carbon

DHHC: Asp-His-His-Cys motif

DYNLL1/2: Dynein light chain 1 and 2

kDa: Kilo-dalton

DTT: Dithiothreitol

E.coli: *Escherichia coli*

EDTA: Ethylenediamine-tetraacetic acid

GABA: γ-amino-butyric acid

$GABA_AR$: GABA type A receptor

GABARAP: GABA receptor associated protein

GlyR: Glycine receptor

GDP: Guanosine 5'-diphosphate

GEF: Guanine nucleotide exchange factor

GTP: Guanosine 5'-triphosphate

ΔH: Enthalpy change

H-: Hydrogen

His_6-tag: 6xHistidine affinity tag

IAP: Integrin associate protein

IPTG: Isopropyl β-D-thiogalactopyranoside

ITC: Isothermal titration calorimetry

K_d: Dissociation constant

LB: Luria Bertani broth

Moco: Molybdenum cofactor

MPT: Molybdopterin

N: Stoichiometry

NCS: Non-crystallographic symmetry

NMDA: N-methyl-D-aspartate

OD_{600}: Optical density at 600 nm

PCR: Polymerase chain reaction

PDB: Protein data bank

PEG: Polyethylene glycol

RMS: Root mean square

ΔS: Entropy change

SDS-PAGE: Sodium dodecyl sulfate-polyacrylamide gel electrophoresis

Tris: Tris(hydroxymethyl) aminomethane

WT: wild-type

Acknowledgements

I would like to thank our collaborators Oliver Schwiese and his advisor, Prof. Günter Schwarz at the University of Cologne (Germany) for the fruitful collaboration on the gephyrin project. I deeply thank all my committee members, Profs. Erwin London who is also my co-advisor, Dax Fu, Lonnie P. Wollmuth and Steven O. Smith for their suggestion and guidance during my dissertation research. I would like to acknowledge Prof. William Lennarz for his academic advising and support. I would like to express my sincere gratitude towards my extraordinary advisor Prof. Hermann Schindelin together with Prof. Caroline Kisker for their continuous support, immense knowledge and encouragement. I sincerely thank the members of Schindelin, Kisker and Lennarz lab. I miss them so much and I will always remember every one of them. I would like to especially thank my husband, Keunyoung Kim who has been an inspiration during my graduate studies.

I dedicate this thesis to my loving parents and brothers. Without their love and encouragement, this work would not have been possible.

CHAPTER1:

MAIN INTRODUCTION

A. Trafficking of inhibitory neurotransmitter receptors and their postsynaptic anchoring

In the central nervous system neurotransmitters are released from the presynapse into the synaptic cleft and bind to neurotransmitter receptors located in the postsynaptic membrane. This leads to conformational changes and induces the opening of the intrinsic ion conducting pores in the cognate receptors. Subsequently, the ionic flux across the postsynaptic membrane induces a change in the postsynaptic membrane potential. The neurotransmitter receptors are distributed on the one hand between the plasma membrane and intracellular sites and on the other hand between synaptic and extrasynaptic sites.

For fast and precise signal transmission neurotransmitter receptors are required to be highly enriched in the postsynaptic membrane and positioned opposite the presynaptic specializations where neurotransmitters are released. This process is mediated by receptor associated proteins which deliver the receptors from sites of synthesis to the neuronal plasma membrane or vice versa and anchor them to the cytoskeletal matrix to control the lateral diffusion within the plasma membrane (1,2) (Figure 1.1). The receptor associated scaffold proteins are directly or indirectly interconnected and together form the postsynaptic density (PSD) at postsynaptic sites. Interestingly, the postsynaptic scaffold proteins are often used as cargo adaptors to link the neurotransmitter receptors to different motor proteins (3-5).

The motor proteins involved in transport of the complex of the vesicular neurotransmitter receptors and the adaptor proteins include kinesins (6) and cytoplasmic dynein (7) which are both microtubule-based motor systems, as well as unconventional myosins (8) that are actin filament-based motor systems. Microtubule-based motor

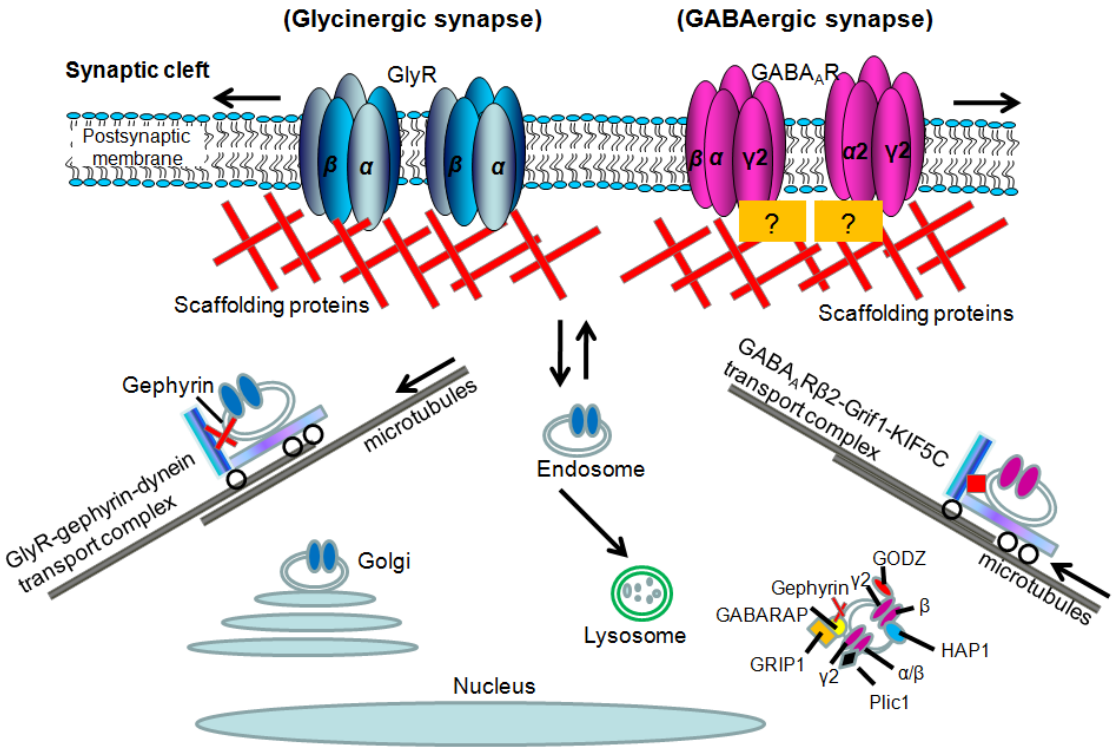

Figure 1.1 Trafficking and synaptic anchoring of inhibitory neurotransmitter receptors. The trafficking of neurotransmitter receptors between intracellular organelles and the plasma membrane is accomplished mainly by microtubule-dependent motor systems through motor protein-cargo transport complexes. The postsynaptic scaffold proteins that anchor and cluster the receptors at postsynaptic sites are often used as cargo adaptors to link the neurotransmitter receptor to the motor proteins. Endosomally internalized receptors either recycle back to the cell surface, or are degraded within the lysosome. Several proteins that are involved in trafficking and anchoring of $GABA_AR$ have been identified. In contrast, it has been described that gephyrin is the only known protein for anchoring and trafficking of GlyRs. This figure has been modified from Kneussel and Loebrich (1).

systems are thought to mediate the long-distance transport since microtubules are distributed throughout neurons, however, they are absent from the cerebral cortex. In contrast, actin filaments are known to serve as tracks for short distance transport because they are mainly localized in the cerebral cortex.

The major inhibitory neurotransmitter receptors in the central nervous system are γ-aminobutyric type A receptors ($GABA_A$Rs) and glycine receptors (GlyRs). $GABA_A$Rs are distributed throughout the brain whereas GlyRs are restricted to the spinal cord and brain stem. $GABA_A$Rs feature a heteropentameric quarternary architecture, which is assembled from the following subunit types: α1-6, β1-3, γ1-3, δ, ε, and π (9). The α/β/γ2 subunits are major components of $GABA_A$Rs in the central nervous system (9). $GABA_A$Rs interact through their intracellular domains with several proteins including the $GABA_A$R-interaction factor1 (GRIF1), the Huntingtin-associated protein1 (HAP1), the Golgi-specific DHHC domain-containing zinc-finger protein (GODZ), the protein linking IAP to the cytoskeleton 1 (PLIC-1), the GABA-receptor associated protein (GABARAP) and gephyrin. These proteins regulate the clustering and trafficking of $GABA_A$Rs. GRIF1 binds to the β2 subunits of $GABA_A$Rs and is an adaptor candidate for the transport of $GABA_A$Rs by the kinesin motor KIF5C although the functional evidence for cargo movement is not clear at present (10). HAP1 which interacts with the β subunit of $GABA_A$Rs associates with kinesin motor proteins (11) and cytoplamic dynein motors (12). The γ2 subunits of $GABA_A$Rs bind to GABARAP (13) and GODZ (14). GABARAP shows ~30% amino acid identity to microtubule-associate proteins and prompts $GABA_A$ receptor clustering (15). However, further studies revealed that GABARAP did not colocalize with $GABA_A$Rs at synaptic sites (16) and was not important for the synaptic delivery of $GABA_A$Rs to synapse (17). Rather the structural similarity of GABARAP to the ubiquitin-like protein Apg8 which is activated by the E1-like enzyme Apg7 and the E2-

like enzyme Apg3 during autophagy suggested its involvement in the degradation of $GABA_A$Rs (18). GODZ, a palmitoyltransferase, is thought to be important for receptor coupling to vesicular membranes and trafficking of receptors. PLIC1, which is a ubiquitin like protein, binds to the α and β subunits of the receptor (19) and facilitates the exit of $GABA_A$Rs from the Golgi and promotes their accumulation in the plasma membrane (19,20). Once inserted at synapses, $GABA_A$Rs are stabilized by their interaction with gephyrin and other clustering molecules (21,22). The interaction between gephyrin and $GABA_A$ receptors is not fully defined. It has been demonstrated that a knockout of $GABA_A$R γ2 subunits in mice leads to loss of $GABA_A$R clustering which is paralleled by the depletion of gephyrin expression (23). Recently, a direct interaction between gephyrin and the α2 subunit of the $GABA_A$ receptor has been described (24). The accumulation of $GABA_A$Rs as well as GlyRs at inhibitory synapse is regulated in a gephyrin dependent manner.

Like $GABA_A$Rs, GlyRs assemble into pentamers, however, they are less diverse since they are constructed only from α1-4 and β subunits. During development, a predominant expression of homopentameric α subunit containing receptors in immature neurons switches to a predominant expression of heteromeric α/β receptor types in mature neurons (25). The stoichiometry of the heteropentameric receptors was initially assumed to be $3\alpha:2\beta$, however, recent data from the same group indicate a $2\alpha:3\beta$ architecture instead (26).

Gephyrin ($\gamma\varepsilon\phi\upsilon\rho\alpha$; Greek: bridge) was originally isolated by copurification with the GlyR from rat spinal cord (27). Gephyrin binds directly to the large cytoplasmic loop located between the third and fourth transmembrane segments of the β-subunit of the GlyRs (28). Gephyrin is critical for GlyR clustering and anchoring at neuronal

membranes as well as for trafficking. The inhibition of gephyrin synthesis by antisense oligonucleotides (29) and in gephyrin knockout mice (30) leads to significant interference of GlyR clustering at synapses although overall GlyR expression levels are not reduced. NMDA receptors containing the gephyrin binding motif located in the GlyR β subunit co-cluster with gephyrin (31). Gephyrin coexpression with GlyR α and β subunits in human HEK293 cells redirects the β subunits into intracellular aggregates (32). Gephyrin links vesicular GlyR to the dynein motor complex and gephyrin-GlyR complexes are subject to retrograde transport from synaptic sites to intracellular destinations (3).

B. The diverse functions of gephyrin

Gephyrin is encoded by a highly mosaic gene (referred to as GPHN) that harbors multiple splice sites, and so far more than 12 splice variants of gephyrin have been reported. Gephyrin is widely expressed in the brain and spinal cord but also in many other peripheral tissues that do not express GlyRs, and shows species-specific differences. The wide expression in non-neuronal tissue and various gephyrin isoforms suggest multiple functions for this protein (33-35).

Gephyrin is composed of three regions (Figure 1.2), an N-terminal G-domain (Geph-G) and a C-terminal E-domain (Geph-E) that are homologous to the bacterial MogA and MoeA proteins, respectively, which participate in molybdenum cofactor (Moco) biosynthesis (30), connected by a linker. The Moco biosynthesis pathway (Figure 1.3) is highly conserved from prokaryotes and archaea to humans and can be divided into three common steps: (i) Conversion of guanosine triphosphate (5'-GTP) to a sulfur-free tricyclic pyranopterin derivative termed precursor Z by MoaA and MoaC (MOCS1A and MOCS1B in humans); (ii) Transformation of precursor Z into the dithiolene containing

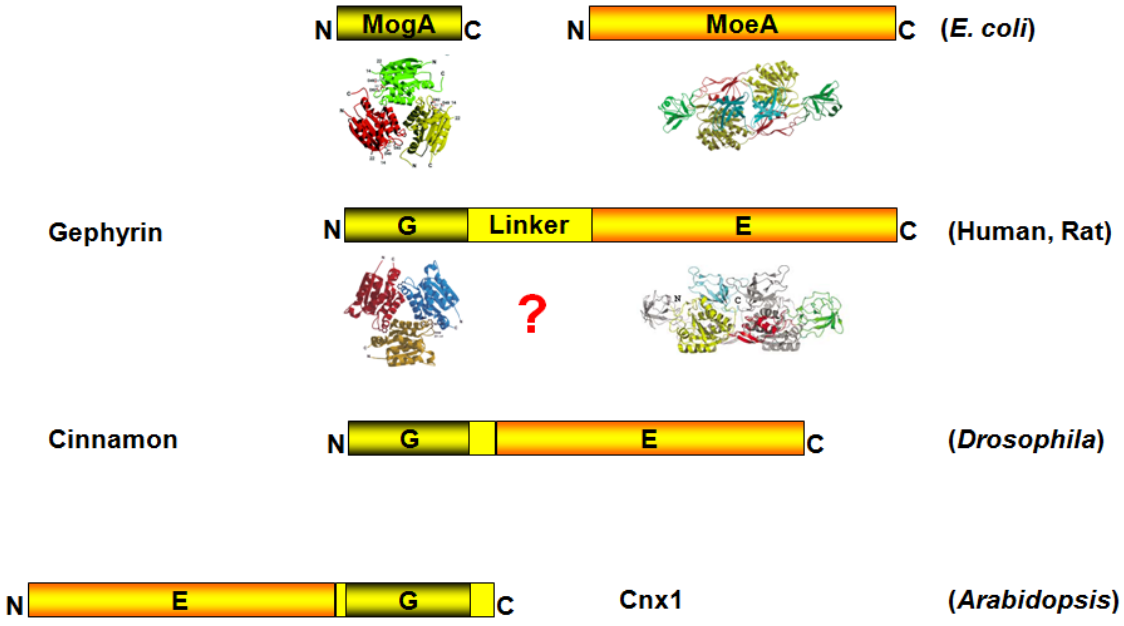

Figure 1.2 Schematic representation of gephyrin related proteins. Gephyrin, cinnamon and Cnx1 proteins from eukaryotes are fusion proteins of domains homologous to the bacterial MogA and MoeA proteins which are connected by a linker region of variable length. In the plant Cnx1 protein, the G-domain and E-domain are fused together in reversed order. This figure has been modified from Stallmeyer *et al*. (36). Crystal structures of the individual proteins/domains (37-40) have been added as ribbon diagrams. MogA and the G-domain form homotrimers (each domain is colored differently), whereas MoeA (viewed along its twofold axis with subdomains in different shapes of the same color) and the E-domain (viewed perpendicular to the twofold axis with one subunit in gray) dimerize.

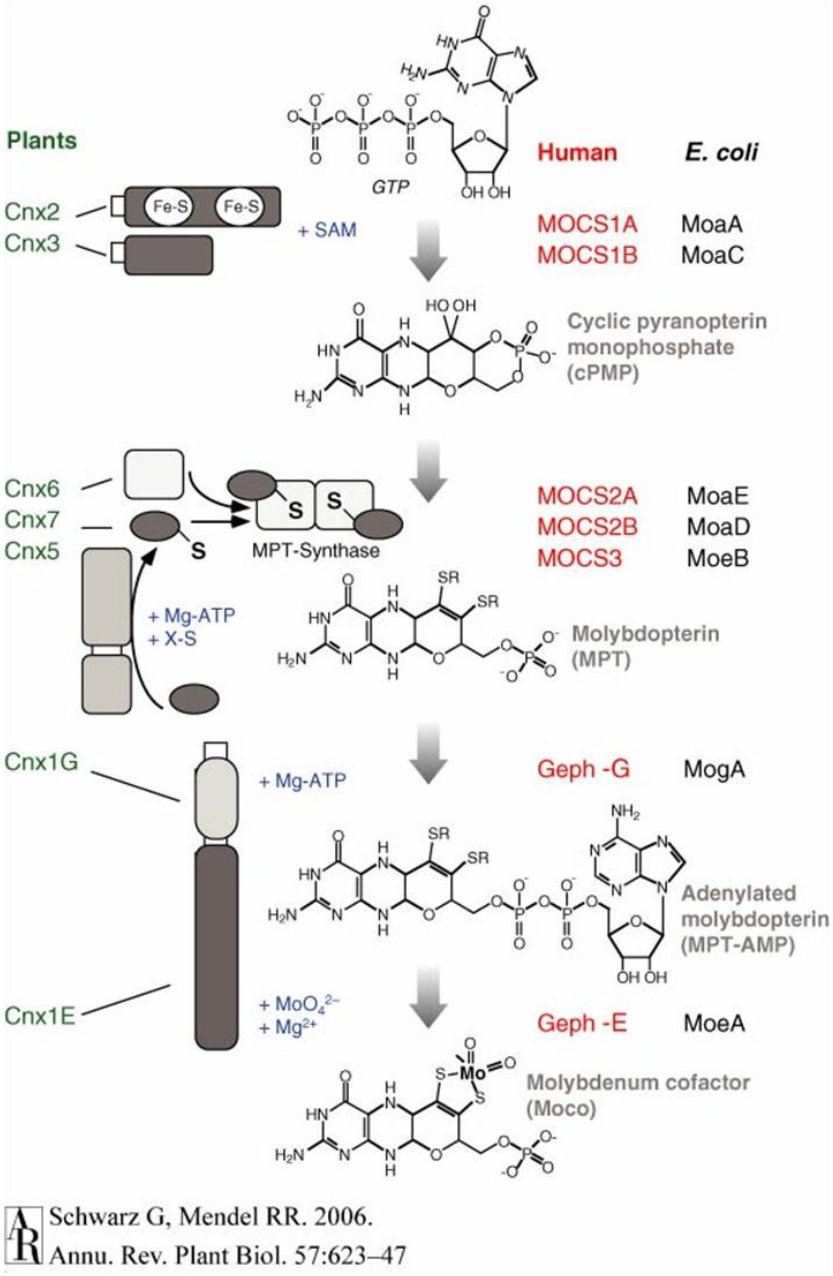

Figure 1.3 Biosynthesis pathway of molybdenum cofactor (Moco). This figure has been adopted from Schwarz and Mendel (41). The functional homologues among bacteria, human, and plant proteins are represented. The human proteins (Molydenum cofactor synthesis MOCS1A/1B/2A/2B/3) are indicating in red and the plant proteins (Cofactor for nitrate reductase and xanthine dehydrogenase Cnx1/2/3/5/6/7) are shown in green, respectively.

product molybdopterin (MPT) by MPT synthase which is composed of the MoaD and MoaE subunits (MOCS2A and MOCS2B in humans); (iii) MPT adenylation by MogA and insertion of molybdenum into MPT by MoeA to generate mature Moco (collectively catalyzed by gephyrin in humans via its G- and E- domains) (41).

Gephyrin's G- and E-domains are connected via a presumably unstructured central region. However, neither the relative orientation of the two domains nor the structure of the linker region is defined at present. The crystal structures of the Geph-G and the Geph-E (Figure 1.2) revealed that Geph-G timerizes like the bacterial MogA protein, while isolated Geph-E dimerizes like its bacterial MoeA counterpart, in agreement with biochemical data (37,38,42,43). The two independent oligomerization interfaces led to the proposal that gephyrin oligomers can assemble into a hexagonal scaffold (40) (Figure 1.4) below the postsynaptic membrane. However, bacterially expressed holo-gephyrin is known to form a trimer (42,44). The postulated hexagonal lattice would be located below the postsynaptic membrane providing on one side binding sites for the inhibitory neurotransmitter receptors and on the opposite side for components of the cytoskeleton, thereby anchoring the receptors.

Gephyrin also interacts with a number of other proteins (Figure 1.5) which are somehow involved in synaptic scaffold formation, either by coupling with the cytoskeleton or by modulating signaling cascades. In addition, the function of gephyrin can be regulated by its binding partners. For example, a recent study has shown that in a phosphorylation dependent manner, Pin1 (peptidyl-prolyl cis/trans isomerase NIMA-interacting 1) interacts with gephyrin and triggers conformational changes in gephyrin that enhance the binding of GlyRs (45). Collybistin, a Cdc42 specific guanine nucleotide exchange factor (GEF) was initially identified as a gephyrin-binding protein (46). Collybistin occurs in four splice forms referred to as collybistin I to IV.

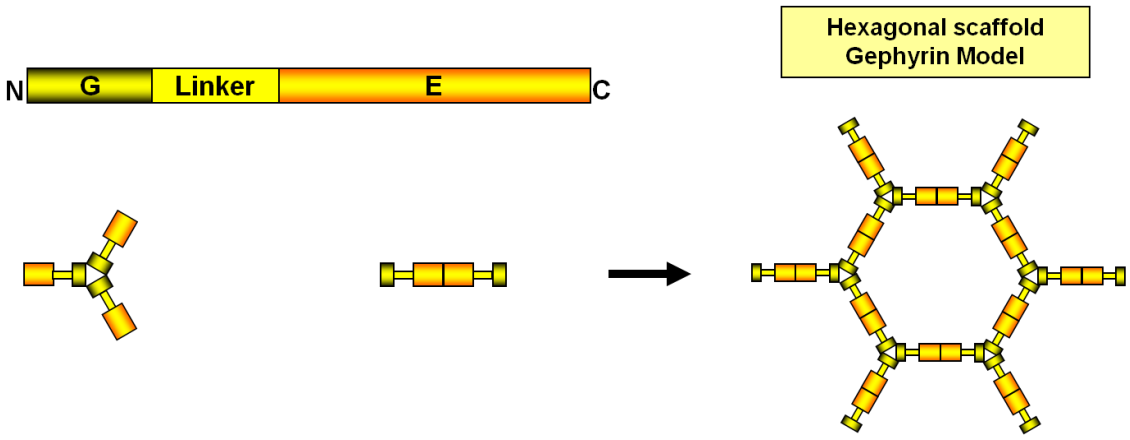

Figure 1.4 Model for a hexagonal gephyrin scaffold. Gephyrins oligomerize by trimerization and dimerization of its G-domains and E-domains, respectively, as observed in the crystal structures of the isolated domains in agreement with biochemical studies. This figure has been modified from Xiang *at al*. (40).

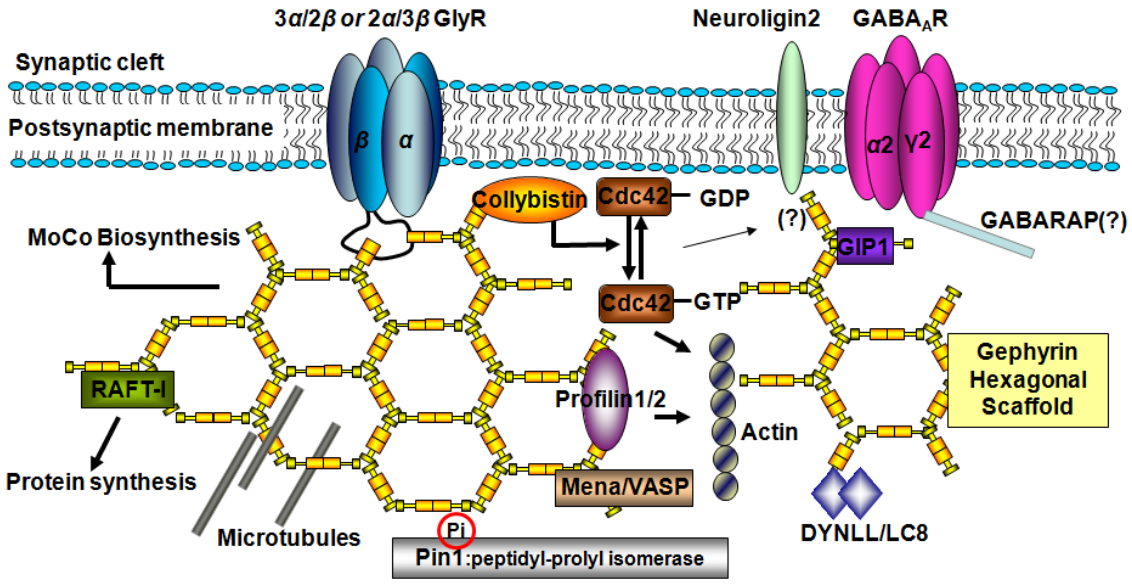

Figure 1.5 Anchoring of inhibitory neurotransmitter receptors by gephyrin. The hexagonal gephyrin scaffold below the postsynaptic membrane is based on the oligomeric states of its isolated E- and G-domains. Identified gephyrin binding partners are indicated. This figure has been modified from Kneussel *et al*. (47).

Collybistin I and II are expressed mainly in the brain, and collybistin I associates with intracellular gephyrin aggregates, while collybistin II, containing an additional N-terminal SH3 domain and a C-terminal coiled coil region, is frequently translocated together with gephyrin-GlyRs to the cell surface (46). The similar pattern of GlyR and collybistin clustering (28,46) at inhibitory synapses implies that collybistin might be an important molecule for the postsynaptic clustering by gephyrin. However, how collybistin is recruited for synaptic clustering of GlyRs is not clear. As a Rho-like GTPase, Cdc42 is involved in actin remodeling, indicating that collybistin is a possible candidate which plays an essential role in gephyrin clustering by regulating the actin cytoskeleton. The interaction between gephyrin and RAFT1 (mammalian FKBP12-rapamycin binding protein, also referred to as mTOR and FRAP) has also been reported (48). RAFT1 is involved in the immunosuppressive effects of rapamycin and the regulation of protein kinase translation. A RAFT1 mutant deficient in gephyrin-binding is not able to signal to its downstream target, thus implying that the interaction between gephyrin and RAFT1 is significant for translational control at synapse. Gephyrin is also directly or indirectly connected to microfilaments and microtubules. Gephyrin colocalizes with profilin (an actin binding protein) (49) and Mena/VASP (mammalian enabled/vasodilator stimulated phosphoprotein) at synapses of rat spinal cord and neurons. This might regulate the microfilament-dependent receptor packing density and dynamics at inhibitory synapses (50). Gephyrin binds also with high affinity to polymerized tubulin (35,51) although the significance of this interaction is not clear. Finally, gephyrin also interacts with dynein light chains, which have been identified as components of the microtubule-based dynein motor complex (52).

C. Function of dynein light chains

Dynein is a large multisubunit motor that binds to microtubules through its C-terminal heavy chains and hydrolyzes ATP to generate force toward the minus end of microtubules. Based on their structure and function dyneins are divided into two major classes, axonemal dynein required for the generation of cilia and flagellar movements, and cytoplasmic dyneins involved in intracellular events such as transports of vesicles, mRNA localization and static anchoring, mitosis, as well as neuronal development and maintenance (53-56). Cytoplasmic dynein is comprised of two dynein heavy chains (~530 kDa), intermediate chains (~74 kDa), light intermediate chains (~50-60 kDa) and three classes of light chains: 14 kDa Tctex1, 12 kDa Roadblock and 10 kDa LC8 (DYNLL in mammals) (57) (Figure 1.6). Dynein intermediate chains are associated with the N-terminal region of the heavy chains and contain binding sites for dynein light chains and the dynactin complex. Through interactions with the dynactin complex, the intermediate chains bind to kinetochores and the Golgi apparatus (58). The intermediate chains have also been suggested to interact directly with cargo molecules (59). The light intermediate chain is a component of cytoplamic dyneins, but is not present in axonemal dynein. The light intermediate chains interact with the centrosomal protein pericentrin (60) and have also been implicated in direct cargo binding. Finally the three light chains interact with a large number of proteins and are thought to play a role as adaptors for cargo recognition which allows cargo to be transported in a retrograde manner.

The 10 kDa dynein light chain is ubiquitously expressed in and highly conserved among different species. It was originally identified as an internal component of the *Chlamydomonas reinhardtii* outer dynein arm where it is associated with the dynein intermediate chains (52) and was subsequently discovered in mammalian brain

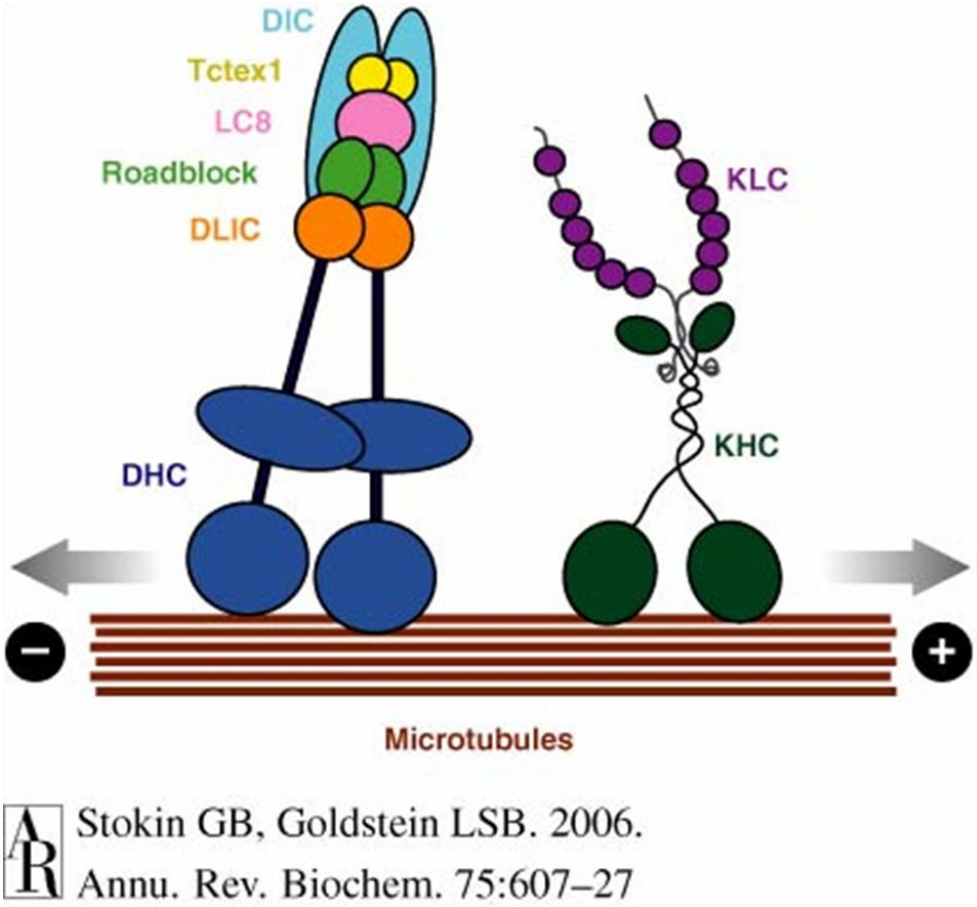

Figure 1.6 Schematic structures of microtubule-based motor proteins. Cytoplasmic dynein which migrates to the minus end of microtubules assembles as a homodimer composed of dynein heavy chain (DHC), dynein intermediate chain (DIC), dynein light intermediate chain (DLIC) and three different members of dynein light chains: Tctex1, LC8, Roadblock. Kinesins regulate the microtubule-based anterograde transport. Among the 14 classes, kinesin-1 represents the best studied example. It is a heteroteramer composed of two kinesin heavy chains (KHC) that contain microtubule binding sites and two kinesin light chains (KLC) that are involved in cargo binding and in the regulation of transport. This figure has been adopted from Stokin *et al*.(54).

cytoplamic dyneins (61). The evidence for an active transport of cargo molecules along microtubules by dynein motor complex comes from the Drosophila swallow protein which requires the interaction with dynein light chain for its proper localization to the anterior pole of the oocyte of bicoid mRNA in mid-oogenesis (62).

However, significant amounts of DYNLL exist in a soluble form in the cytoplasm (61) and recent thermodynamic and structural characterizations (63,64) support that DYNLL has additional functions which are independent of dynein.

Mammalian dynein light chain (DYNLL) occurs in two isoforms (Figure 1.7), DYNLL1 also known as either LC8, DLC1 or PIN (protein inhibitor of neuronal nitric oxide synthase), a light chain of cytoplasmic dynein, and DYNLL2, a light chain component of the myosin V motor complex (65,66). The functional significance of having two light chains in mammalian cells is currently not clear. There are six amino acids that are different between the two isoforms, and it has been suggested that *in vivo* DYNLL1/2 display selectivity for their binding partners as well as either dynein or myosin (67). Nevertheless, *in vitro* both DYNLLs can interact with the same proteins and currently it is almost impossible to distinguish their binding partners and function *in vivo* due to their high sequence and structural identities.

Both DYNLLs interact with a number of proteins, as well as the dynein intermediate chain, that display diverse functions, including nNOS (neuronal nitric oxide synthase) (68), IκBα (the inhibitor of the NF-κB/Rel family of transcription factors) (69), p53-binding protein 1 (70), Pak1 (p21-activated kinase-1) (71), the product of the Drosophila swallow gene (62), phosphoprotein of viruses (72), the proapoptotic member of the Bcl-2 family, Bim (Bcl-2 interacting mediator) and Bmf (Bcl-2 modifying factor) (67), KIBRA (dendrin interacting protein in kidney and brain) (73), GKAP (PSD-95/Guanylate

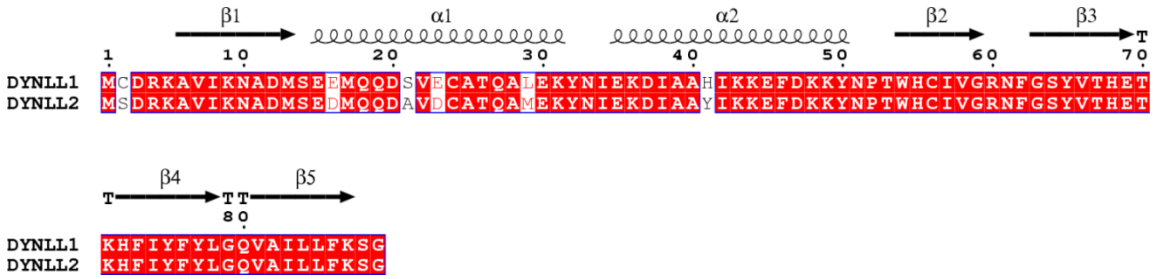

Figure 1.7 Sequence alignment of human DYNLL1 and DYNLL2. Secondary structure elements are indicated above the DYNLL1 sequence with arrows representing β-strands and ribbons representing α-helices. Identical residues are indicated in white letters on red background, conserved substitutions in red letters and non-conserved residues in black. Alignments were performed using ClustalW (http://www.ebi.ac.uk/clustalw) and were visualized with ESPript (http://espript.ibcp.fr).

kinase domain-associated protein) (66), gephyrin (74), and possibly other proteins (75). It has been proposed that when DYNLL is bound to its various binding partners, including the dynein intermediate chain, it promotes their structural stabilization as a dimerization hub, or directly regulates functional characteristics of its binding partners (76-78). For example, upon DYNLL binding, the content of helical structure in the intermediate chain required for its efficient dimerization is increased (78) and in the presence of DYNLL, the monomer-dimer equilibrium of myosin V is shifted to a dimer-tetramer equilibrium (79). DYNLL also controls nitric oxide levels by inhibiting the activity of nNOS (77), and is involved in activating NF-κB by binding to IκBα in a redox dependent manner (80). DYNLL1/2 also regulate the apoptotic process by interacting with the proapoptotic proteins, Bim and Bmf, and facilitate estrogen induced estrogen receptor transactivation through binding with KIBRA and growth stimulation in cancer cells (73,81).

Through biochemical and mutagenesis studies the canonical sequence motifs in DYNLL target proteins were identified as either (K/R)XTQT or G(I/V)QV(D/E) (where *"X"* denotes any amino acid) (75,82). However, some of the putative DYNLL-binding proteins do not feature either one of the canonical binding motifs (Table 1.1) indicating that additional binding partners exist (71).

Table 1.1 DYNLL recognition motifs in target proteins (75,82)

Target protein	Binding motif
(K/R/T)XTQT motif	
Dynein intermediate chain	TYT **KETQT** PL
Dynein heavy chain	QD **KLVQT** PL
BCL-2 interacting mediator: Bim	CD **KSTQT** PS
BCL-2 modifying factor: Bmf	ED **KATQT** LS
Drosophila swallow gene (Drosophila bicoid mRNA localization)	TSA **KATQT** DF
BS69 (Adenovirus E1A-binding protein)	LH **RSTQT** TN
Rabies virus P protein	ED **KSTQT** TS
Mokola virus	ED **KSTQT** PE
P54 (African swine virus protein)	QN **TASQT** MW
C82 (Novel protein)	HS **KGTQT** AK
Kid-1 (Renal transcription factor)	TT **KSTQT** PS
Protein 4 (Microtubule-associated protein)	GS **KSTQT** VA
P53 binding protein	TVS**AATQT**IK
G(I/V)QV(D/E) motif	
Rat neuronal nitric oxide synthase: nNOS	MKDT **GIQVD**
DNA cytosine methyl transferase	KDL **GIQVD**
Guanylate kinase domain associated protein	LSI **GIQVD /** QSV **GVQVE**
P53 binding protein	NNI**GIQTM**E
Gephyrin	TEDK**GVQC**E
Non canonical motif	
Myosin Va	DDKNTMTD
Pak1	TPTRDVATSPI

CHAPTER2:
STRUCTURAL AND BIOCHEMICAL CHARACTERIZATION OF THE INTERACTION BETWEEN GEPHYRIN AND DYNEIN LIGHT CHAIN1/2

The work presented in this chapter has been submitted to the *Journal of Molecular Biology* with me as the first author.

I. Introduction

To ensure a fast and precise signal transmission in the central nervous system, the receptor associated scaffolding protein gephyrin mediates the cytoskeletal anchoring and localized clustering as well as subcellular transport of inhibitory neurotransmitter receptors on the cytoplasmic side of the postsynaptic membrane at inhibitory synapses. Gephyrin consists of a presumably unstructured central linker region which connects two oligomerization domains, a trimeric N-terminal G-domain and a dimeric C-terminal E-domain. Gephyrin interacts directly with the β-subunit of the glycine receptor and the α2 subunit of $GABA_A$ receptors (24,28), and with a variety of additional proteins most of which are linked directly or indirectly to the cytoskeleton.

Among these binding partners, the 10 kDa light chains of the dynein motor (DYNLL1 and DYNLL2) mediate the retrograde transport of vesicular glycine receptor-gephyrin complexes within neuronal dendrites via the microtubule-based dynein motor system (3) (Figure 2.1). The interaction between gephyrin and DYNLL1/2 was originally identified in a yeast two-hybrid screen using full-length gephyrin as bait and subsequently verified by *in vitro* co-sedimentation analysis and GST pull down assays, and *in vivo* colocalization studies in transfected HEK293 cells and cultured neurons (74). The interacting region in gephyrin has been mapped to residues 203-214 with the sequence KQTEDKGVQCEE located in its linker region by mutagenesis studies and a pepscan analysis (75). Through monitoring the trypsin-mediated degradation of the proteolytically sensitive linker region in the presence or absence of DYNLL1/2, the group of our collaborator Günter Schwarz demonstrated that the tight interaction between gephyrin and DYNLL1/2 stabilizes gephyrin.

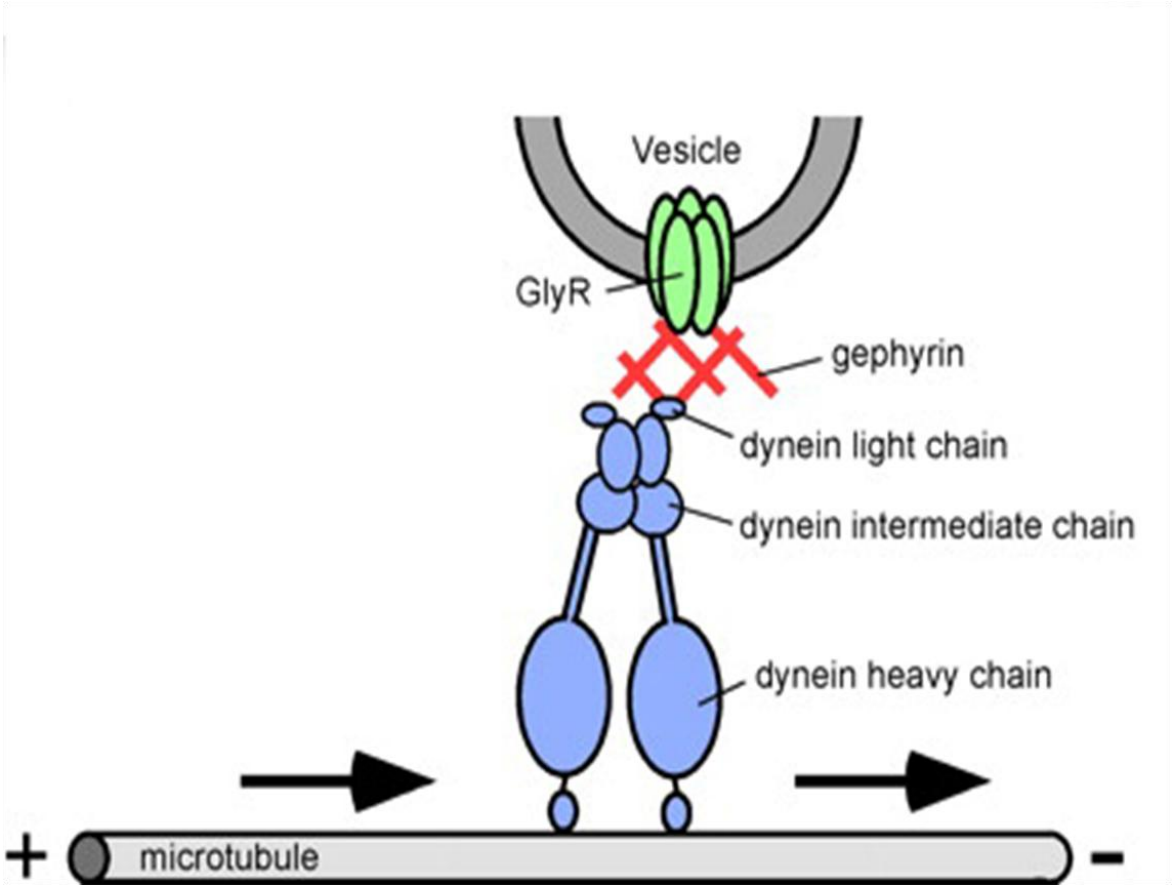

Figure 2.1 Neuronal cotransport of the glycine receptor and the scaffold protein gephyrin towards the minus end of microtubules by the dynein motor. It has been observed that gephyrin coimmunoprecipitated with vesicular GlyR, and colocalized with dynein intermediate chain and heavy chain which are exclusive components of the dynein motor as well as the dynein light chain. This figure has been reproduced from Mass *et al*. (3).

In this study, first, the binding affinities between gephyrin and DYNLL1/2 were determined and possible effects on gephyrin's oligomeric state upon binding DYNLL1/2 were analyzed. Second, to provide insights into the molecular basis of how DYNLLs recognize gephyrin, the crystal structures of DYNLL1 and DYNLL2 in their apo-state and in complex with a chemically synthesized peptide derived from gephyrin's linker have been solved at medium to high resolution. Third, residues located in the interface between gephyrin and DYNLL1/2 were analyzed in detail using isothermal titration calorimetry. Finally, the crystal structures of DYNLL complexes with gephyrin were compared with other DYNLL-peptide complexes.

II. Materials and methods

A. Molecular cloning and site directed mutagenesis

cDNA templates encoding DYNLL1/2 were purchased from Openbiosystems (www.openbiosysems.com). Genes of interest were amplified by PCR and inserted into the NdeI/SapI restriction sites of the pTXB1 vector (IMPACT TM-CN, New England Biolabs). For expression of DYNLL1/2 with an N-terminal His_6-tag, the amplified genes were cloned into the NdeI/XhoI restriction enzyme sites of the pET28a vector (Novagen).

To analyze the contribution of residues in the interface of the full-length gephyrin (Geph-P2; P2 splice variant)(44) and DYNLL the Q204A, T205A, E206A, E206K, D207A, K208A, K208T, G209A, G209E, V210A, V210N, V210T, Q211A, Q211E and C212A Geph-P2 point mutations, and the E35A, E35K, K36A, K36P, K44A, N61A, F62A, Y65A, Y65F, Y65D, H68A, T70A, F73A, Y75A and Y77A variants of DYNLL1 were generated. Site directed mutagenesis was performed with the QuickChange kit (STRATAGENE) and all mutations were verified by sequencing.

B. Protein overexpression and purification

For overexpression, DYNLL1/2 (pTXB1 or pET28a) were transformed into *E. coli* BL21 (DE3) cells and Geph-P2 (pQE30) was cotransformed with pREP4 into *E. coli* BL21 (DE3) cells. Fresh overnight cultured cells were inoculated in LB medium containing 100 µg/mL of ampicillin or 50 µg/mL of kanamycin. The cells were grown at 37°C until the optical density (OD_{600}) reached 1.0 and then isopropyl-β-D-1-thiogalactopyranoside (IPTG) was added to a final concentration of 0.5 mM. After IPTG induction, cells were grown for 16-20 h at 16°C and harvested by centrifugation at 4,000

Table 2.1 Primers for mutagenesis of Geph-P2

Primers	Sequence
Geph-P2 Q204A Forward	5’ GCCCACATAAGGCGACAGAAGACAAAGG 3’
Reverse	3’ CCTTTGTCTTCTGTCGCCTTATGTGGGC 5’
Geph-P2 T205A Forward	5’ GCCCACATAAGCAGGCAGAAGACAAAGGAG 3’
Reverse	3’ CTCCTTTGTCTTCTGCCTGCTTATGTGGGC 5’
Geph-P2 E206A Forward	5’ CCACATAAGCAGACAGCAGACAAAGGAGTTCAGTGTG 3’
Reverse	3’ CACACTGAACTCCTTTGTCTGCTGTCTGCTTATGTGG 5’
Geph-P2 E206K Forward	5’ CCACATAAGCAGACAAAGGACAAAGGAGTTCAGTG 3’
Reverse	3’ CACTGAACTCCTTTGTCCTTTGTCTGCTTATGTGG 5’
Geph-P2 D207A Forward	5’ CATAAGCAGACAGAAGCCAAAGGAGTTCAGTGTGAAG 3’
Reverse	3’ CTTCACACTGAACTCCTTTGGCTTCTGTCTGCTTATG 5’
Geph-P2 K208A Forward	5’ AAGCAGACAGAAGACGCAGGAGTTCAGTGTGAAG 3’
Reverse	3’ CTTCACACTGAACTCCTGCGTCTTCTGTCTGCTT 5’
Geph-P2 K208T Forward	5’ AAGCAGACAGAAGACACAGGAGTTCAGTGTGAAG 3’
Reverse	3’ CTTCACACTGAACTCCTGTGTCTTCTGTCTGCTT 5’
Geph-P2 G209A Forward	5’ ACAGAAGACAAAGCAGTTCAGTGTGAAGAG 3’
Reverse	3’ CTCTTCACACTGAACTGCTTTGTCTTCTGT 5’
Geph-P2 G209E Forward	5’ ACAGAAGACAAAGAAGTTCAGTGTGAAGAG 3’
Reverse	3’ CTCTTCACACTGAACTTCTTTGTCTTCTGT 5’
Geph-P2 V210A Forward	5’ ACAGAAGACAAAGGAGCTCAGTGTGAAGAGGAGG 3’
Reverse	3’ CCTCCTCTTCACACTGAGCTCCTTTGTCTTCTGT 5’
Geph-P2 V210N Forward	5’ AGACAGAAGACAAAGGAAATCAGTGTGAAGAGGAGG 3’
Reverse	3’ CCTCCTCTTCACACTGATTTCCTTTGTCTTCTGTCT 5’
Geph-P2 V210T Forward	5’ ACAGAAGACAAAGGAACTCAGTGTGAAGAGGAGG 3’
Reverse	3’ CCTCCTCTTCACACTGAGTTCCTTTGTCTTCTGT 5’
Geph-P2 Q211A Forward	5’ CAGACAGAAGACAAAGGAGTTGCGTGTGAAGAGGAGGAAG 3’
Reverse	3’ CTTCCTCCTCTTCACACGCAACTCCTTTGTCTTCTGTCTG 5’
Geph-P2 Q211E Forward	5’ CAGAAGACAAAGGAGTTGAATGTGAAGAGGAGGAAG 3’
Reverse	3’ CTTCCTCCTCTTCACATTCAACTCCTTTGTCTTCTG 5’
Geph-P2 C212A Forward	5’ GAAGACAAAGGAGTTCAGGCGGAAGAGGAGGAAG 3’
Reverse	3’ CTTCCTCCTCTTCCGCCTGAACTCCTTTGTCTTC 3’

Table 2.2 Primers for mutagenesis of DYNLL1

Primers		Sequence
DYNLL1 E35K	Forward	5’ GAAATACAACATAAAGAAGGACATTGCGGCC 3’
	Reverse	3’ GGCCGCAATGTCCTTCTTTATGTTGTATTTC 5’
DYNLL1 E35A	Forward	5’ GAAATACAACATAGCGAAGGACATTGCGGC 3’
	Reverse	3’ GCCGCAATGTCCTTCGCTATGTTGTATTTC 5’
DYNLL1 K36A	Forward	5’ TACAACATAGAGGCGGACATTGCGGCTCA 3’
	Reverse	3’ TGAGCCGCAATGTCCGCCTCTATGTTGTA 5’
DYNLL1 K36P	Forward	5’ GAAATACAACATAGAGCCGGACATTGCGGCT 3’
	Reverse	3’ AGCCGCAATGTCCGGCTCTATGTTGTATTTC 5’
DYNLL1 K44A	Forward	5’ GCTCATATCAAGGCGGAATTTGACAAGAAG 3’
	Reverse	3’ CTTCTTGTCAAATTCCGCCTTGATATGAGC 5’
DYNLL1 N61A	Forward	5’ CGTGGGGAGGGCCTTCGGTAGTTATGTG 3’
	Reverse	3’ CACATAACTACCGAAGGCCCTCCCCACG 5’
DYNLL1 F62A	Forward	5’ CGTGGGGAGGAACGCCGGTAGTTATGTG 3’
	Reverse	3’ CACATAACTACCGGCGTTCCTCCCCACG 5‘
DYNLL1 Y65A	Forward	5’ AACTTCGGTAGTGCTGTGACACATGAAAC 3’
	Reverse	3’ GTTTCATGTGTCACAGCACTACCGAAGTT 5’
DYNLL1 Y65F	Forward	5’ AACTTCGGTAGTTTTGTGACACATGAAACC 3’
	Reverse	3’ GGTTTCATGTGTCACAAAACTACCGAAGTT 5’
DYNLL1 Y65D	Forward	5’ AACTTCGGTAGTGATGTGACACATGAAAC 3’
	Reverse	3’ GTTTCATGTGTCACATCACTACCGAAGTT 5’
DYNLL1 T67A	Forward	5’ CGGTAGTTATGTGGCACATGAAACCAAACG 3’
	Reverse	3’ CGTTTGGTTTCATGTGCCACATAACTACCG 5’
DYNLL1 H68A	Forward	5’ GTTATGTGACAGCTGAAACCAAACACTTCA 3’
	Reverse	3’ TGAAGTGTTTGGTTTCAGCTGTCACATAAC 5’
DYNLL1 T70A	Forward	5’ GTGACACATGAAGCCAAACACTTCATCTACT 3’
	Reverse	3’ AGTAGATGAAGTGTTTGGCTTCATGTGTCAC 5’
DYNLL1 F73A	Forward	5’ CATGAAACCAAACACGCCATCTACTTCTACCTG 3’
	Reverse	3’ CAGGTAGAAGTAGATGGCGTGTTTGGTTTCATG 5’
DYNLL1 Y75A	Forward	5’ CAAACACTTCATCGCCTTCTACCTGGGC 3’
	Reverse	3’ GCCCAGGTAGAAGGCGATGAAGTGTTTG 5’
DYNLL1 Y77A	Forward	5’ CTTCATCTACTTCGCCCTGGGCCAAGT 3’
	Reverse	3’ ACTTGGCCCAGGGCGAAGTAGATGAAG 5’

x g for 30 min. Cell pellets were resuspended in lysis buffer containing 40 mM Tris-HCl (pH 8.0), 300 mM NaCl, 10% glycerol plus a protease inhibitor cocktail (Roche), and lysed by passing them twice through a French pressure cell operating at 1,000-1,500 psi. The cleared lysate containing the intein-fused proteins was incubated with chitin agarose beads (New England Biolabs) for 1 h at 4°C with constant rocking. Beads were washed with 20 column volumes of wash buffer containing 40 mM Tris-HCl (pH 8.0), 1 M NaCl and 1 mM EDTA. DYNLL proteins were eluted with 20 mM Tris-HCl (pH 8.0), 250 mM NaCl and 50 mM DTT following cleavage of the intein with 50 mM DTT for 1 day at 4°C and then for 2 days at room temperature. The proteins were further purified by size exclusion chromatography on a Superdex 200 (26/60) column (GE Healthcare) equilibrated with 20 mM Tris-HCl (pH 8.0),100 mM NaCl and 5 mM DTT. The resulting pure DYNLL proteins were concentrated to 5-7 mg/mL and immediately subjected to crystallization.

Each soluble fraction of Geph-P2 wild-type and variants (pQE30) as well as DYNLL1/2 containing an N-terminal His_6-tag was directly transferred onto a column with Ni-nitrilotriacetic acid (NTA) superflow beads (Qiagen) at 4°C and beads were washed with 20 mM Tris-HCl (pH 8.0), 250 mM NaCl and 10 mM imidazole. After elution with 10 column volumes of buffer containing 20 mM Tris-HCl (pH 8.0), 250 mM NaCl and 250 mM imidazole the resulting protein pool was loaded onto a Q sepharose column (GE Healthcare) and purified by using a linear NaCl gradient (Buffer A: 20 mM Tris-HCl (pH 8.0), 50 mM NaCl and 5 mM DTT; Buffer B: same as Buffer A with 1 M instead of 20 mM NaCl). The peak fractions from the Q sepharose were loaded on a Superdex 200 (26/60) column (GE Healthcare), which was pre-equilibrated with 20 mM Tris-HCl (pH 8.0), 250 mM NaCl and 5 mM DTT. The purity of the final protein batches was analyzed by sodium dodecyl sulfate polyacrylamide gel electrophoresis (SDS-PAGE) and the protein

concentration was calculated by UV spectroscopy at 280 nm on the basis of calculated extinction coefficients of 28590 $M^{-1}cm^{-1}$, 12089 $M^{-1}cm^{-1}$ and 13370 $M^{-1}cm^{-1}$ for Geph-P2, DYNLL1 and DYNLL2, respectively. All purified proteins were flash frozen in liquid nitrogen after concentrating them to ~5 mg/ml with Centricon-20 (Millipore).

For complex purification, Geph-P2 and DYNLL proteins at a molar ratio of 1 to ~2-4 were incubated at 4°C for 1 h and then loaded onto a Superdex 200 (26/60) preparative column or a Superdex 200 (10/30) analytical size exclusion chromatography column (GE Healthcare) to separate the complex from unbound proteins. The purified complex proteins were immediately used for all subsequent experiments.

C. Isothermal titration calorimetry (ITC)

All ITC experiments were performed with a VP-ITC microcalorimeter (MicroCal) at 37°C. Prior to each experiment, the samples were prepared by dialyzing them overnight at 4°C against a buffer containing 10 mM Tris-HCl (pH 8.0), 1 mM β-mercaptoethanol and either 100 mM NaCl or 250 mM NaCl. Proteins (Geph-P2 wild-type or variants) at concentrations of 10-20 µM were titrated with DYNLL1/2 at concentrations of 200-400 µM, while DYNLL1/2 wild-type (20-25 µM) were titrated with gephyrin-derived dodecamer peptide 1 (KQTEDKGVQCEE, 12-mer, Anaspec) and gephyrin-derived peptide 2 (DSIISRGVQVLP, 12-mer, Anaspec) at concentrations of 400 µM, or 350 µM for the intermediate chain 1 derived peptide (VVSYSKETQTPL, 12-mer Anaspec). The binding parameters were calculated with the MicroCal Origin (version 7.0) software by fitting the data to a single site binding model.

D. Circular dichroism (CD)

The CD spectra of gephyrin-derived peptide 1 (KQTEDKGVQCEE, 12-mer, Anaspec) and 2 (DSIISRGVQVLP, 12-mer, Anaspec) were measured at 20°C, using a Jasco J810 CD spectropolarimeter flushed with N_2, and a cuvette with 1.0 mm path length. 0.5 mg/mL of concentrated peptide was in a buffer containing 20 mM Na phosphate (pH 8.0). The spectra were collected from 185 to 265 nm at 20 nm/sec intervals. 5 spectra were accumulated at room temperature and averaged to achieve an appropriate signal-to-noise ratio. The spectrum of the buffer was subtracted. The secondary structure composition of the peptides was analyzed with the Spectrum Analysis software provided by the manufacturer (Jasco, Inc).

E. Analytical size exclusion chromatography

To determine the binding stoichiometry between full-length gephyrin and DYNLL1/2, gephyrin in complex with DYNLL1/2 and gephyrin without DYNLL1/2 were diluted to final concentrations between 0.15 and 2 mg/mL. 500 µL of each protein sample was injected onto a Superdex 200 (10/30) analytical size exclusion chromatography column (GE Healthcare) equilibrated with buffer containing 20 mM Tris-HCl (pH 8.0), 250 mM NaCl and 5 mM DTT.

The molecular weight standards (GE Healthcare) used for calibration of the column were blue dextran (2000 kDa to determine the void volume V_o of the column), ferritin (440 kDa), catalase (232 kDa), aldolase (158 kDa), ovalbumin (43 kDa), chymotrypsinogen (25 kDa), ribonuclease A (13.7 kDa) in order to estimate the molecular mass of the analyzed proteins (Figure 2.2).

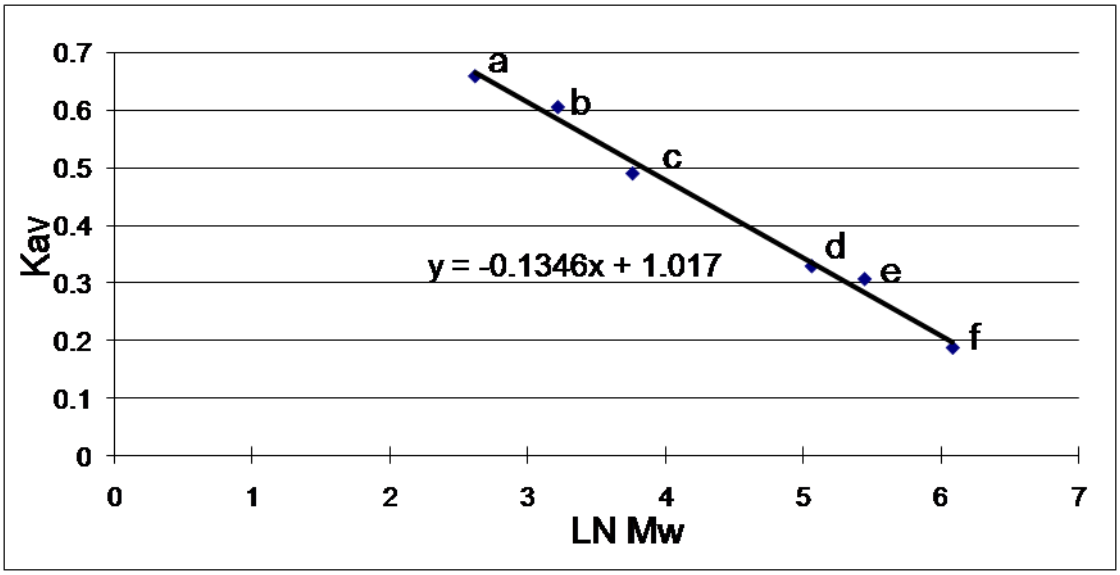

Figure 2.2 Size exclusion chromatography calibration curve of molecular weight standards. The following standard proteins were used to generate the calibration curve. a: Ribonuclease A (13.7 kDa), b: Chymotrypsinogen (25 kDa), c: Ovalbumin (43 kDa), d: Aldolase (158 kDa), e: Catalase (232 kDa), f: Ferritin (440 kDa). $K_{av}=(V_e-V_o)/(V_t-V_o)$, V_e is the elution volume and V_t the column volume (23.56 mL for the Superdex 200 (10/30) analytical size exclusion chromatography column (GE Healthcare) . The void volume (V_o) was determined by the elution volume of blue dextran (2000 kDa). The correlation coefficient was 0.99.

F. Analytical Ultracentrifugation (AUC) studies on DYNLL1/2

Sedimentation velocity (SV) experiments were carried out with a Beckman XL-I Optima analytical ultracentrifuge (Beckman Coulter, Fullerton, CA) with an eight-hole An-50 Ti rotor at 40,000 rpm and 20°C. Prior to each experiment, the samples were dialyzed overnight at 4°C against a buffer containing 10 mM Tris-HCl (pH 8.0), 1 mM β-mercaptoethanol and either 100 mM NaCl or 250 mM NaCl. Data were collected using absorbance optical detection at a wavelength of 280 nm and were analyzed with the DCDT+ program of John Philo (http://www.jphilo.mailway.com).

G. Dynamic light scattering (DLS)

DLS experiments were conducted at 4°C, 10°C and 20°C using 20 µL of 1 to 2.6 mg/mL protein with a DYNAPRO molecular sizing instrument (Protein Solutions) in buffer containing 20 mM Tris-HCl (pH 8.0), 250 mM NaCl and 5 mM DTT. All protein solutions were centrifuged for 20 min at 4°C prior to loading the cell at 16,000 x g. For each sample, at least 30 individual measurements of 10 sec acquisitions were taken, and the data were analyzed using the DYNAMICS software (Protein Solutions).

H. Fluorescence-based thermal shift assay

DYNLL1/2 proteins were diluted with buffer containing 20 mM Tris-HCl (pH 8.0), 250 mM NaCl and 5 mM DTT to 1 mg/mL. The fluorescence change was monitored in the temperature range from 30°C to 95°C using an Opticon real time PCR cycler (Bio-Rad). SYPRO Orange was diluted 2500-fold and the total protein used was 25 µg. Buffer

contained 20 mM Tris-HCl (pH 8.0), 250 mM NaCl and 5 mM DTT. The ratio of protein to peptide was 1:100.

I. Crystallization, data collection, structure determination and refinement

Using the hanging drop vapor diffusion method with 1 µL of fresh protein and 1 µL of crystallization buffer on pre-silanized coverslides, crystals were produced from Topaz Optimix screen 4. The peptide KQTEDKGVQCEE (gephyrin derived peptide 1) which represents the DYNLL-binding region (75) of gephyrin and the peptide VVSYSKETQTPL (dynein intermediate chain 1 (IC1) derived peptide) were chemically synthesized by Anaspec. After mixing the DYNLL1/2 proteins at concentration of 5-7 mg/mL and the gephyrin-derived peptide in a 1:2 molar ratio, the resulting complex was crystallized at 18°C against a reservoir solution containing 0.1 M sodium cacodylate (pH 6.5), 0.5 M L-proline and 27% w/v PEG 4000 for the DYNLL1-gephyrin peptide complex, and 0.1 M sodium citrate (pH 5.6), 0.8 M sodium formate and 23% w/v PEG 4000 for the DYNLL2-gephyrin peptide complex, respectively. Very thin, plate-shaped crystals of apo-DYNLL1 were grown under the same conditions as the DYNLL1-gephyrin peptide complex and crystals of apo-DYNLL2 were grown against a reservoir containing 0.1 M sodium citrate (pH 5.6), 0.4 M sodium acetate and 18% w/v PEG 4000. Except for the crystals of apo-DYNLL1 the remaining proteins form long rod-shaped crystals (Figure 2.3). In case of the DYNLL1-IC1 crystals, DYNLL1 at concentration of 4 mg/mL was incubated with IC1 peptide at a molar ratio of 1:4 at 4°C for 1 h and subjected to crystallization. The rod-shaped DYNLL1-IC1 crystals form against a reservoir containing 0.1 M ADA (pH 6.5) and 23% w/v PEG 4000.

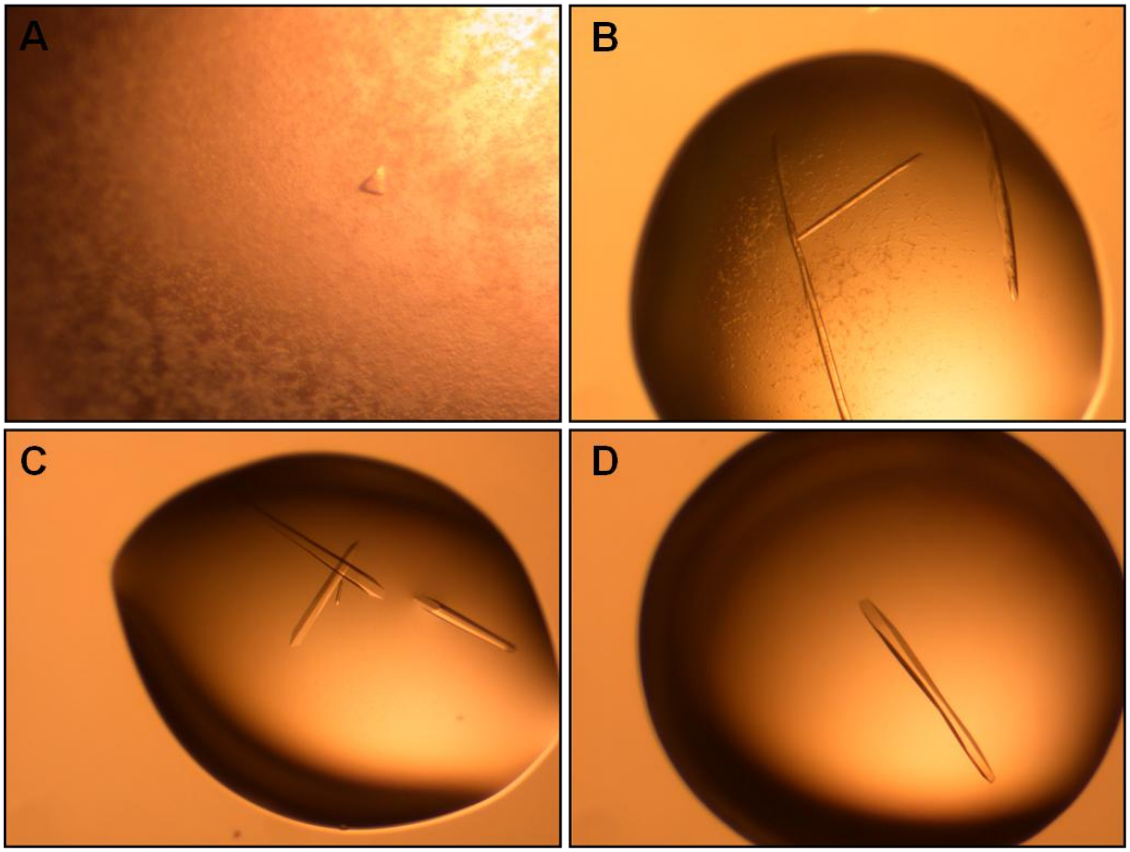

Figure 2.3 Crystals of DYNLL1/2 in the absence and presence of gephyrin derived peptides. (A) apo-DYNLL1, (B) DYNLL1-gephyrin peptide complex, (C) apo-DYNLL2, (D) DYNLL2-gephyrin peptide complex.

Prior to data collection crystals were soaked in mother liquor containing 15-30% (v/v) glycerol and flash cooled in liquid nitrogen. Diffraction data were collected at 100 K on beam lines X25, X26C or X29 of the National Synchrotron Light Source at Brookhaven National Laboratory. All diffraction data were indexed, integrated and scaled with HKL2000 (83). The structure of DYNLL1 was solved by molecular replacement with the program AMORE (84), and the remaining structures (DYNLL1-gephyrin complex, DYNLL2-gephyrin complex, DYNLL1-IC1 complex and apo-DYNLL2) with the program MOLREP (85) using a previously reported DYNLL1 structure without the bound nNOS peptide (PDB entry 1CMI) as a search model (68). Additional calculations were performed with the CCP4 suite of programs (86). The model was refined with REFMAC5 (87), initially using rigid body refinement followed by TLS and restrained refinement (88). For apo-DYNLL1 refinement, additionally NCS (non-crystallographic) restraints with tight main chain and medium side chain weight were applied. Water molecules were added with ARP (89) and model building was performed using the programs O (90) and COOT (91). Figures representing the structures were generated with PyMOL (DeLano, 2002 W.L. The Pymol Molecular Graphics System (2002), DeLano Scientific, San Carolos, CA).

III. Results and discussion

A. Characterization of the gephyrin-DYNLL interaction by ITC

To determine the binding affinity between gephyrin and DYNLL proteins, first, the gephyrin wild-type protein was titrated with untagged and His_6-tagged DYNLL wild-type proteins. Irrespective of whether DYNLL carries a His_6-tag or not, ITC analyses at 37°C reveal an exothermic reaction that nicely fits a one-site binding model (Table 2.3). The dissociation constant of the Geph-DYNLL1 complex is ~3 µM with an approximate ΔH of -8 kcal/mol and a slight decrease in entropy (ΔS of ~ -1 cal mol^{-1} K^{-1}). The dissociation constant of the Geph-DYNLL2 complex shows a very similar value of ~3 µM, however, the enthalpy is reduced by almost a factor of 2 (ΔH of -4.5 kcal/mol) which is compensated by an increase in entropy (ΔS of ~10 cal mol^{-1} K^{-1}). The stoichiometry of ~0.7 (0.77 for the Geph-DYNLL1 complex and 0.7 for the Geph-DYNLL2 complex) appears consistent with the binding of a DYNLL dimer to a gephyrin trimer, which would indicate that one DYNLL dimer binds to two of the three monomers within the gephyrin trimer leaving the third binding site vacant. For all subsequent ITC studies His_6-tagged DYNLL proteins were used.

Second, the binding of a gephyrin-derived peptide to full-length DYNLL1/2 was also analyzed by ITC. For DYNLL1 and DYNLL2 dissociation constants of ~8 µM and ~5 µM, respectively, were observed, with almost identical binding enthalpies of -6 kcal/mol and a slight increase in entropy of ~5 cal mol^{-1} K^{-1} (Table 2.3). The binding stoichiometry indicated the formation of a one to one complex as reflected by an average n-value of 1.03 (Figure 2.4). Although the dissociation constants for the peptides are on average approximately twofold higher compared to the titrations with full-length gephyrin, there is generally good agreement between the binding parameters with the exception of the

Table 2.3 Summary of ITC results of Geph-P2 wild-type with DYNLL1/2 wild-type, and DYNLL1/2 with gephyrin derived peptides

Cell	Injector	N	K_d (μM)	ΔH (kcal mol^{-1})	ΔS (cal mol^{-1} K^{-1})
Geph-P2	DYNLL1	0.70±0.05	6.7±0.4	-1.1±0.1	-10.4
Geph-P2	DYNLL2	0.70±0.04	2.4±0.3	-7.8±0.3	0.4
Geph-P2	His-DYNLL1	0.77±0.02	3.3±0.3	-8.1±0.2	-1.3
Geph-P2	His-DYNLL2	0.70±0.04	4.3±0.7	-4.5±0.3	10.1
DYNLL1	Geph-peptide1	1.09±0.04	7.5±0.9	-5.8±0.3	4.7
DYNLL2	Geph-peptide1	0.97±0.02	5.2±0.4	-6.2±0.2	4.2

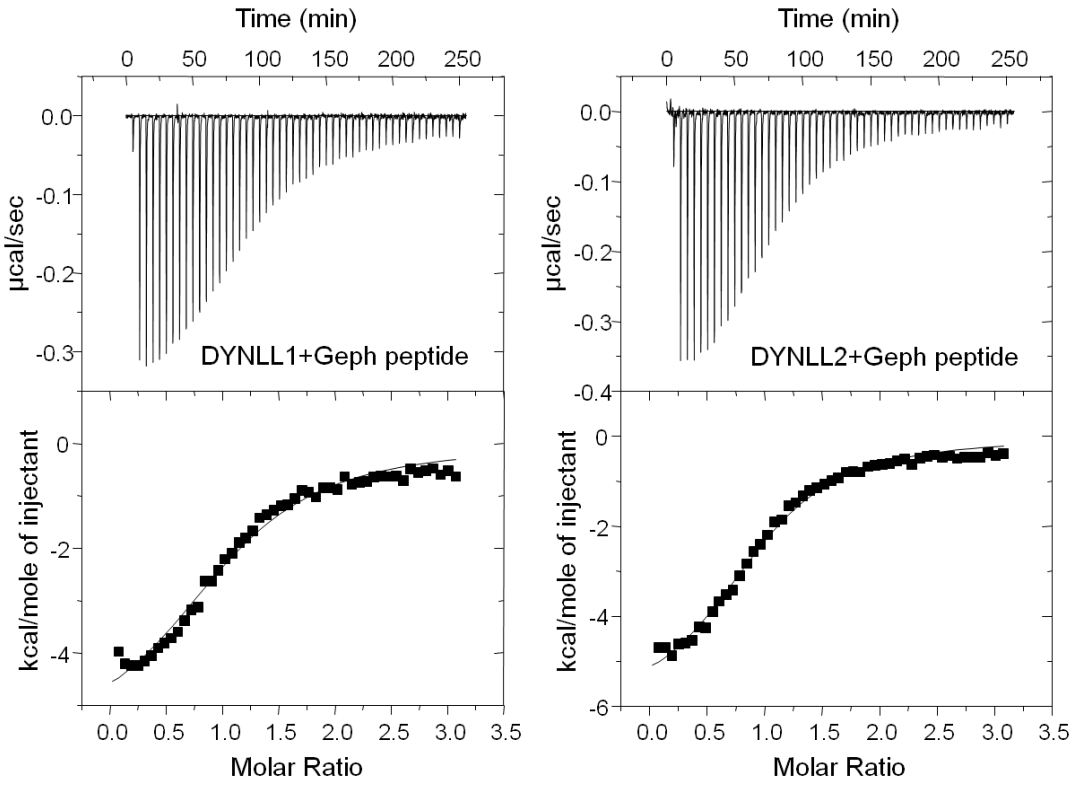

Figure 2.4 Raw ITC data with gephyrin peptide. Each DYNLL1 (left) and DYNLL2 (right) was titrated with gephyrin derived peptide 1.

binding stoichiometry (see next paragraph) indicating that all binding interactions with DYNLL1/2 are confined to residues 204-212 of gephyrin. Therefore, the gephyrin peptide serves as a useful model to study the DYNLL-gephyrin interaction by biophysical and structural techniques.

B. Oligomeric state of the Gephyrin-DYNLL complex

Recombinantly expressed full-length gephyrin predominantly forms a trimeric species (42,44). This is unusual among the DYNLL binding partners which generally form dimers. In fact, one of the functions proposed for DYNLL suggests that the protein acts as a dimerization hub. Based on this model the oligomeric state of gephyrin in the absence and presence of DYNLL was analyzed. Arguing against a DYNLL-induced dimerization the binding stoichiometry of 0.7 in the ITC experiments with full-length gephyrin is consistent with a complex in which one DYNLL dimer binds to two of the three monomers within the gephyrin trimer leaving the third binding site vacant. In contrast the dimerization hub model (76) should have resulted in a binding stoichiometry of one consistent with an assembly in which two gephyrin trimers bind to three DYNLL dimers such that either one or all three DYNLL dimers simultaneously bind to two different gephyrin trimers, thus resulting in the formation of a complex with approximately twice the molecular mass compared to the first model. Since the binding stoichiometry is sensitive to errors in the protein concentrations, size exclusion chromatography and dynamic light scattering studies were conducted to distinguish between the two models.

To address whether DYNLL binding to gephyrin leads to a shift in the oligomeric state of gephyrin, from the observed trimer to a hexamer, size exclusion chromatography studies were carried out (Table 2.4). Full-length gephyrin elutes from an analytical

Table 2.4 Size exclusion chromatography of Geph-P2 in the absence or presence of DYNLL1/2

Protein	Theoretical monomer mass (kDa)	Theoretical oligomeric state	Elution Vo (ml)	Experimental molecular mass (kDa)
Geph-P2	83	Trimer (249 kDa)	11.17	516
Geph-P2+DYNLL1	83 + 10	Trimer+Dimer (269 kDa)	11.26	484
Geph-P2+DYNLL2	83 + 10	Trimer+Dimer (269 kDa)	11.00	547
DYNLL1	10	Dimer (20 kDa)	17.67	20
DYNLL2	10	Dimer (20 kDa)	17.59	24

Superdex 200 (10/30) column at a volume of 11.17 mL. On the basis of a calibration for this column this corresponds to a mass of 516 kDa, which would be consistent with a hexamer, however, this result shows a discrepancy with previously reported predominant trimeric form of gephyin. It is presumably due to the large deviation of gephyrin's structure from a spherical shape, so this value should be treated with caution. Upon addition of either DYNLL1 or DYNLL2 only small changes in the elution volume are observed to 11.0 mL in case of the gephyrin-DYNLL1 complex and 11.26 mL for the gephyrin-DYNLL2 complex (Figure 2.5). Although it is somewhat surprising that both DYNLLs do not behave in an identical fashion, the shift is not consistent with a doubling of gephyrin's molecular mass and hence the more likely scenario is that a DYNLL dimer binds to a gephyrin trimer by bringing two linker regions together while leaving the third binding site unoccupied consistent with the binding stoichiometry of ~0.7 observed in the ITC experiments.

In DLS experiments, the mass of gephyrin was estimated to be 285 kDa, 274 kDa and 226 kDa (Table 2.5) at 4°C, 10°C and 20°C, respectively, corresponding in all cases to approximately a trimer (expected mass of 249 kDa). The theoretical mass for a complex between a gephyrin trimer and a DYNLL dimer is 269 kDa, and the observed mass of the complex is in the range of 236-336 kDa depending on the temperature, in general agreement with the theoretical mass and clearly incompatible with an assembly consisting of two gephyrin trimers which are bridged by three DYNLL dimers (calculated mass of 558 kDa). The molecular mass of gephyrin in complex with either DYNLL1 or DYNLL2 as deduced by size exclusion chromatography and dynamic light scattering demonstrated that no change in gephyrin's oligomeric state occurs upon binding to DYNLL.

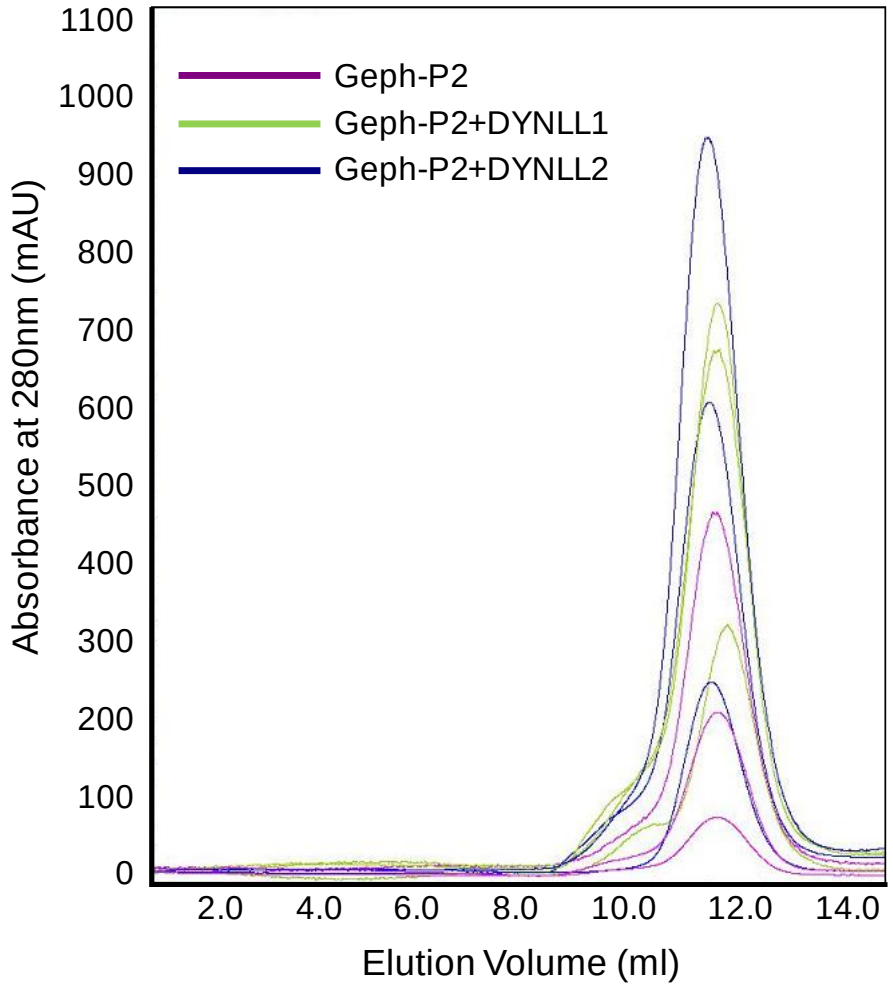

Figure 2.5 Size exclusion chromatography of Geph-P2 in the absence (purple) or presence of DYNLL1/2 (green/blue). In each case three different protein concentrations were analyzed which differ by a factor of 10 between the highest and lowest protein concentration to determine whether there are concentration-dependent changes in the oligomeric state.

Table 2.5 DLS data of Geph-P2 in the absence and presence of DYNLL1/2

Protein	Theoretical monomer mass (kDa)	Theoretical oligomeric state	Experimental molecular mass (kDa)[a]	Temperature	Polydispersity (%)[a]
Geph-P2	83	Trimer (249 kDa)	285±39	4˚C	~15.2
Geph-P2+DYNLL1	83 + 10	Trimer+Dimer (269 kDa)	336±54	4˚C	~14.7
Geph-P2+DYNLL2	83 + 10	Trimer+Dimer (269 kDa)	236±41	4˚C	~29.9
Geph-P2	83	Trimer (249 kDa)	274±41	10˚C	~4.6
Geph-P2+DYNLL1	83 + 10	Trimer+Dimer (269 kDa)	315±50	10˚C	~17.6
Geph-P2+DYNLL2	83 + 10	Trimer+Dimer (269 kDa)	330±10	10˚C	~18.4
Geph-P2	83	Trimer (249 kDa)	226±93	20˚C	~21.7
Geph-P2+DYNLL1	83 + 10	Trimer+Dimer (269 kDa)	263±118	20˚C	~17.4
Geph-P2+DYNLL2	83 + 10	Trimer+Dimer (269 kDa)	266±20	20˚C	~13.0

[a]Each experimental value (molecular weight and polydispersity) represents the average of two or three independent measurements at 4°C, 10°C and 20°C, each consisting of 30 individual measurements of 10 second data acquisitions.

Gephyrin therefore represents an example where DYNLL does not induce dimerization in its binding partner, which seems surprising since there is an unoccupied DYNLL binding site in one of the gephyrin monomers in each trimer. Possibly topological constraints prevent the DYNLL-induced dimerization of gephyrin, however, it remains unclear why an additional DYNLL could not bind to the vacant binding site in an asymmetric manner, leaving the second binding site unoccupied. Although a weak cooperativity has been described (63) for the binding of DYNLL to its ligands, it appears too small to prevent binding in this situation.

C. Structures of DYNLL1/2 in their apo-state

To characterize the molecular details of the DYNLL-gephyrin interaction, structural studies of DYNLL in its apo-state and in complex with the gephyrin peptide were conducted. Apo-crystals of DYNLL1 belong to the monoclinic space group C2 with unit cell dimensions of a=164.3 Å, b=38.7 Å and c=44.8 Å and data were collected to 2.4 Å resolution (Table 2.6). The crystals contain three molecules in the asymmetric unit organized into a non-crystallographic dimer and an additional monomer, which dimerizes via a crystallographic twofold axis of symmetry. Despite the high sequence identity of 93% and similarity of 98%, apo-DYNLL2 crystals belong to a different space group ($P6_122$) with unit cell dimensions of a=b=44.5 Å, c=202.8 Å. These crystals diffract to 1.6 Å resolution and contain one molecule in the asymmetric unit. The DYNLL1 and DYNLL2 apo-structures have been refined to an R-factor of 0.19 (R_{free}=0.28) and 0.18 (R_{free}=0.21), respectively (Table 2.6). The three DYNLL1 monomers present in the asymmetric unit display an average pairwise root mean square (rms) deviation of 0.10 Å for the Cα atoms of residues 5 to 89, however, due to the limited resolution NCS restraints were employed during refinement. Each DYNLL1 monomer can be superimposed with the

Table 2.6 Data collection and refinement statistics of DYNLL1/2 structures

	Apo-DYNLL1	Apo-DYNLL2	DYNLL1-gephyrin	DYNLL2-gephyrin	DYNLL1-IC1
Data collection					
Space group	C2	$P6_122$	$P6_122$	$P6_122$	C2
Cell dimensions (a,b,c(Å)/ α,β,γ(°))	164.3,38.7,44.8 /90.0,100.1,90.0	44.5,44.5,202.8 /90.0,90.0,120.0	44.1,44.1,205.5 /90.0,90.0,120.0	44.3,44.3,204.6 /90.0,90.0,120.0	122.4,71.9,70.3 /90.0,122.7,90.0
Resolution limits (Å)	50-2.4	50-1.6	50-2.8	50-1.75	50-1.88
R_{sym} (highest shell)	0.071 (0.420)	0.050 (0.228)	0.105 (0.228)	0.052 (0.277)	0.059 (0.179)
Completeness (highest shell) (%)	99.0 (93.8)	97.2 (90.2)	97.4 (80.1)	98.9 (93.1)	99.4 (94.4)
<I/sig I>	28.6 (2.9)	41.9 (5.0)	31.9 (4.6)	67.4 (4.0)	34.2 (6.8)
Redundancy	6.8	9.0	14.0	17.3	3.6
Unique reflections	11,004	16,345	3,337	12,846	41,572
Refinement					
Resolution limits (Å)	20.0-2.4	30.0-1.6	20.0-2.8	30-1.75	20-1.88
Number of reflections used in refinement	10,454	15,503	3,124	12,125	39,354
R_{cryst} / R_{free}	0.192 / 0.275	0.181 / 0.207	0.197 / 0.287	0.194 / 0.219	0.149 / 0.191
Completeness(%)	98.79	97.52	97.03	98.98	99.14
Number of protein / ligand / solvent atoms	2135 / - / 43	722 / - / 104	709 / 68 / 7	742 / 89 / 61	2833 / 360 / 356
Deviations from ideal values in					
Bond distances (Å)	0.019	0.020	0.017	0.021	0.017
Bond angles (°)	1.849	1.619	1.522	1.834	1.557
Chiral volumes ($Å^3$)	0.096	0.099	0.083	0.131	0.098
Planar groups (Å)	0.006	0.008	0.004	0.011	0.007
Average B-factors for protein / peptide / solvent atoms ($Å^2$)	88.4 / - / 77.9	27.7 / - / 46.7	47.7 / 57.0 / 44.3	40.1 / 48.0 / 52.3	26.8 / 27.6 / 45.2
Estimated overall coordinate error (DPI) based on R_{free} (Å)	0.328	0.099	0.412	0.116	0.134
Ramachandran statistics Favored / Allowed (%)	92.1 / 97.2	95.3 / 98.8	92.3 / 98.9	97.9 / 98.9	97.6 / 98.9

$R_{sym} = \Sigma_{hkl}\Sigma_i |I_i - \langle I \rangle| / \Sigma_i \langle I \rangle$ where I_i is the i^{th} measurement and $\langle I \rangle$ is the weighted mean of all measurements of I. $\langle I/sigI \rangle$ indicates the average of the intensity divided by its standard deviation. $R_{cryst} = \Sigma| |F_o| - |F_c| | / \Sigma |F_o|$, where F_o and F_c are the observed and calculated structure factor amplitudes. R_{free} same as R_{cryst} for 5% of the data randomly omitted from refinement. Numbers in parentheses refer to the highest resolution data shell. Ramachandran statistics indicate the fraction of residues in the favored/allowed regions as calculated with MOLPROBITY (92).

DYNLL2 apo-structure with an average rms deviation of 0.3 Å. Based on the high amino acid sequence identity this low value was expected and taking the experimental error limits into account the two structures are virtually identical. Interestingly, DYNLL1 shows a significantly reduced thermostability with a T_m of 60°C compared to DYNLL2 with a T_m of 71.5°C (Figure 2.6).

Both apo-structures feature the expected α/β architecture with a central four-stranded antiparallel β-sheet (Figure 2.7) formed by β1, β4, β5 and β2 packed against two α-helices and the remaining strand β3 (68,71,93). Two monomers form a rectangular homodimer such that β3 of one monomer interacts in an antiparallel fashion with β2 of the other monomer, thus forming a five-stranded antiparallel β-sheet (Figure 2.7). Dimerization leads to the burial of ~950 $Å^2$ (17.5%) of the monomer surface. The dimer interface is predominantly hydrophobic in nature but also includes 14 H-bonds and 8 salt bridges (Table 2.7).

The oligomeric state of apo-DYNLL 1/2 was analyzed by analytical size exclusion chromatography and SV analytical ultracentrifugation yielding molecular masses of 20 kDa and 24 kDa for DYNLL1 and DYNLL2 by size exclusion chromatography (Table 2.4) and 21 kDa and 19 kDa for DYNLL1 and DYNLL2 by SV analytical ultracentrifugation (Figure 2.8). Both techniques therefore indicate that in the concentration range studied (15 to 200 µM) both DYNLLs exist only in a dimeric form.

Recently, the first crystallographic analysis of a *Drosophila* DYNLL1 homologue LC8 apo-structure has been reported which shows 94% identity and 98% similarity to DYNLL1 (71) and its dimerization potential was analyzed. As expected, this structure is highly similar to the structure reported here. In addition, an upper value for the dissociation constant of 500 nM has been estimated, significantly lower than previously

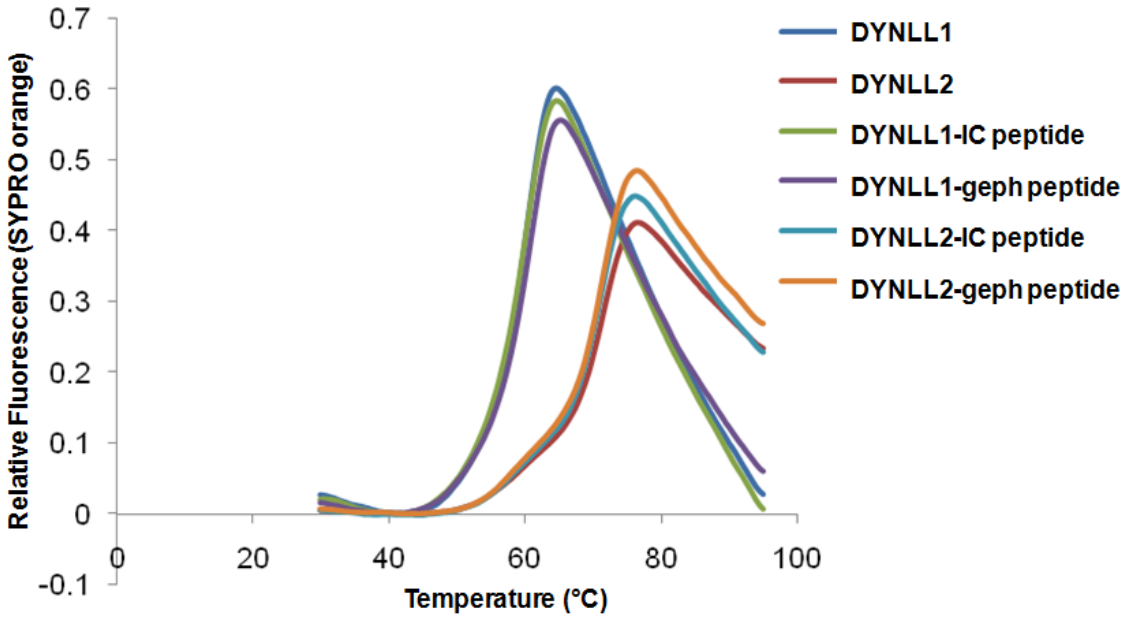

Figure 2.6 Thermal stability of DYNLL1/2. Melting curves of DYNLL1/2 with or without either the gephyrin or dynein intermediate chain (IC1) derived peptides. The fluorescence change was monitored in the temperature range from 30°C to 95°C using an Opticon real time PCR cycler (Bio-Rad). DYNLL2 is more thermostable than DYNLL1 and neither the gephyrin derived peptide nor the intermediate chain derived peptide affect the thermostability of DYNLL1/2.

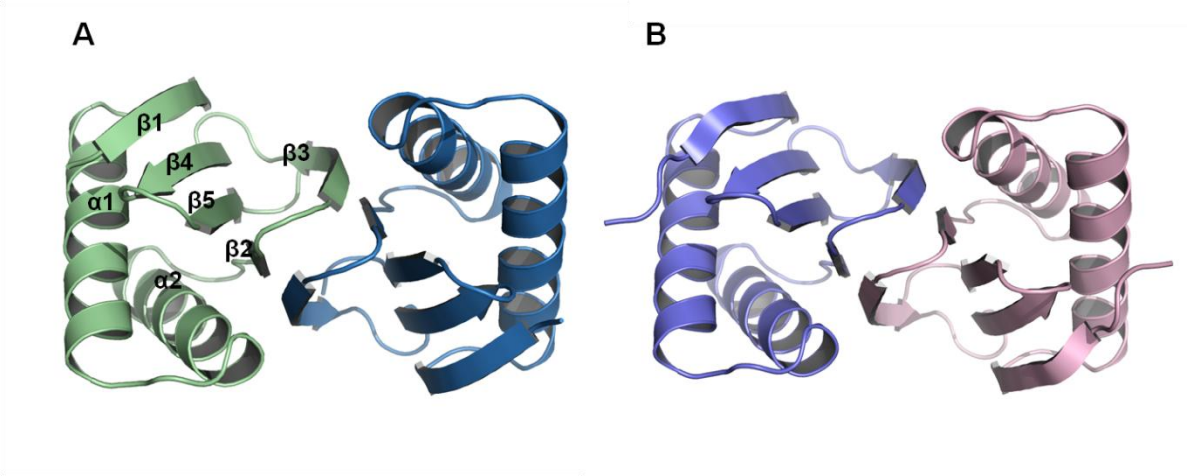

Figure 2.7 Ribbon diagram of the DYNLL1/2 homodimer. (A) One monomer of DYNLL1 is colored in pale green and the other in sky blue. Secondary structure elements are labeled for one monomer. (B) The two monomers of DYNLL2 are colored in slate and pink, respectively.

Table 2.7 Interactions between two monomers on the dimer interface of DYNLL2

Monomer1	Dist.(Å)	Monomer2
GLY 63 [N]	3.50	GLU 35 [OE1]
ASN 61 [ND2]	2.50	GLU 35 [OE2]
TYR 65 [N]	2.91	CYS 56 [O]
GLY 63 [N]	2.76	VAL 58 [O]
ARG 60 [N]	3.12	ASN 61 [O]
ASN 61 [N]	2.98	ASN 61 [O]
VAL 58 [N]	2.89	GLY 63 [O]
LYS 44 [NZ]	3.13	TYR 65 [OH]
CYS 56 [N]	3.05	TYR 65 [O]
LYS 43 [NZ]	2.77	THR 67 [OG1]
HIS 55 [NE2]	3.10	THR 67 [O]
GLU 35[OE1]	3.50	GLY 63 [N]
GLU 35[OE2]	2.50	ASN 61 [ND2]
CYS 56[O]	2.91	TYR 65 [N]
VAL 58[O]	2.76	GLY 63 [N]
ASN 61[O]	3.12	ARG 60 [N]
ASN 61[O]	2.98	ASN 61 [N]
GLY 63[O]	2.89	VAL 58 [N]
TYR 65[OH]	3.13	LYS 44 [NZ]
TYR 65[O]	3.05	CYS 56 [N]
THR 67[OG1]	2.77	LYS 43 [NZ]
THR 67[O]	3.10	HIS 55 [NE2]

http://www.ebi.ac.uk/msd-srv/prot_int/pistart.html

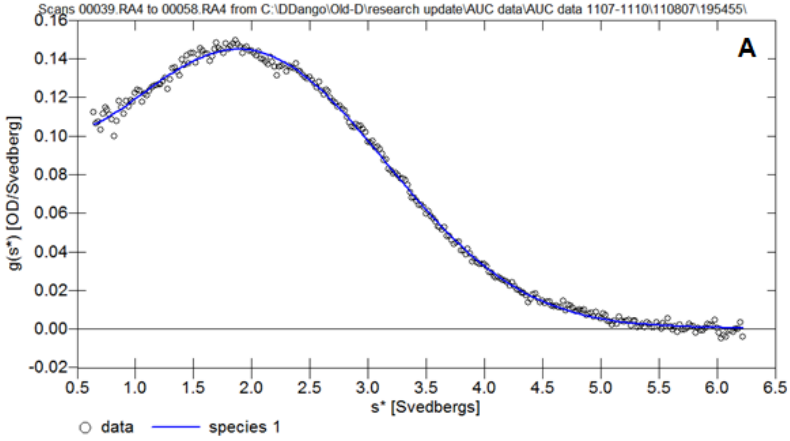

Parameter	Value
Co[OD]	0.38
S[S]	2.25±0.01
M[kDa]	21.25±0.19

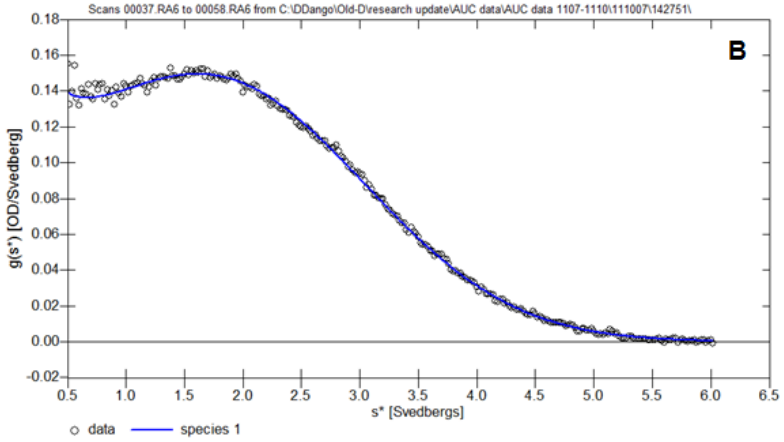

Parameter	Value
Co[OD]	0. 41
S[S]	2.13±0.01
M[kDa]	19.98±0.11

Figure 2.8 Sedimentation velocity analytical ultracentrifugation data for DYNLL1(A) and DYNLL2(B).

anticipated (94). However, it agrees well with the observed lack of monomeric protein in our studies.

D. Crystal structures of DYNLL1/2-gephyrin peptide complexes

The complex structures of DYNLL1 and DYNLL2 with the gephyrin-derived peptide KQTEDKGVQCEE crystallized in space group $P6_122$ (DYNLL1: a=b=44.1 Å and c=205.5 Å; DYNLL2: a=b=44.3 Å and c=204.6 Å) and are nearly isomorphous to the apo-DYNLL2 crystals. The binary complexes have been refined at 2.8 and 1.75 Å resolution, respectively, to R-factors of 0.20 and 0.19 (R_{free} of 0.29 and 0.22) (Table 2.6). Despite the differences in resolution between the two complex structures, omit difference electron density maps indicate that nine residues of the gephyrin-derived dodecapeptide bind tightly to DYNLL1/2 and are consequently well defined in the electron density maps (Figure 2.9). In agreement with the ITC studies in which DYNLL was titrated with the gephyrin peptide each DYNLL dimer binds two peptides consistent with an n-value of 1. The peptides are positioned in the ~22 Å long and ~13 Å wide groove at the monomer-monomer interface. In both structures the peptide binds in an antiparallel arrangement to β3, thus resulting in the formation of a 6-stranded antiparallel β-sheet, which is composed of four strands from one monomer, one strand from the other monomer and the bound peptide (Figure 2.10) The bound peptide is surrounded by α-helix 2 of one monomer and β-strands 3, 4 and 5 of the other monomer. The peptide-binding site of DYNLL1/2 is enriched in hydrophobic residues (Figure 2.9), which nicely complement apolar atoms in the peptide, including atoms in residues that are polar or even charged such as Asp207 and Lys208. In the following discussion residue numbers >200 identify residues in gephyrin and numbers <100 refer to residues in DYNLL1/2.

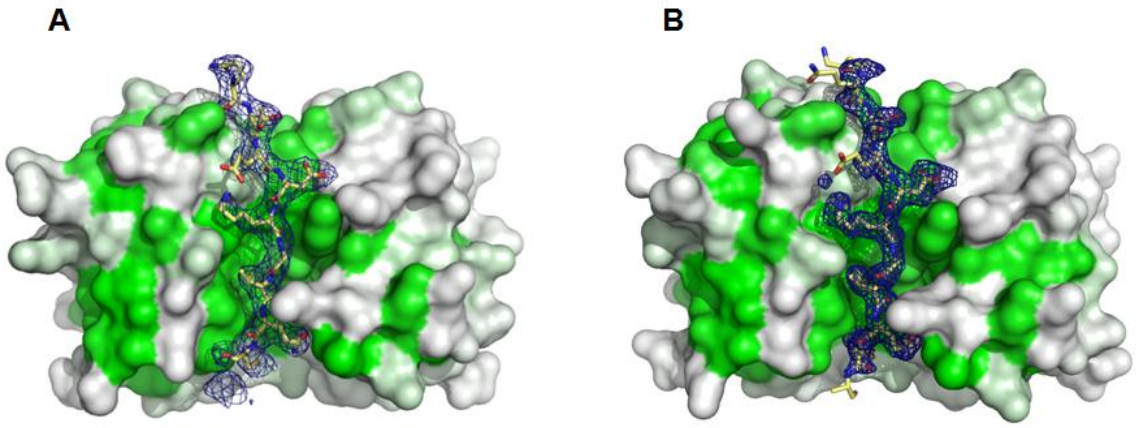

Figure 2.9 Surface representation of DYNLL1 (A) and DYNLL2 (B) with hydrophobic residues highlighted in green based on a hydrophobicity analysis (95). The bound peptide is displayed in stick representation with C-atoms in yellow, N-atoms in blue, O-atoms in red and the S-atom in orange. An omit SIGMAA weighted $2F_o$-F_c electron density map contoured at three times the rms deviation is shown as a blue wire mesh.

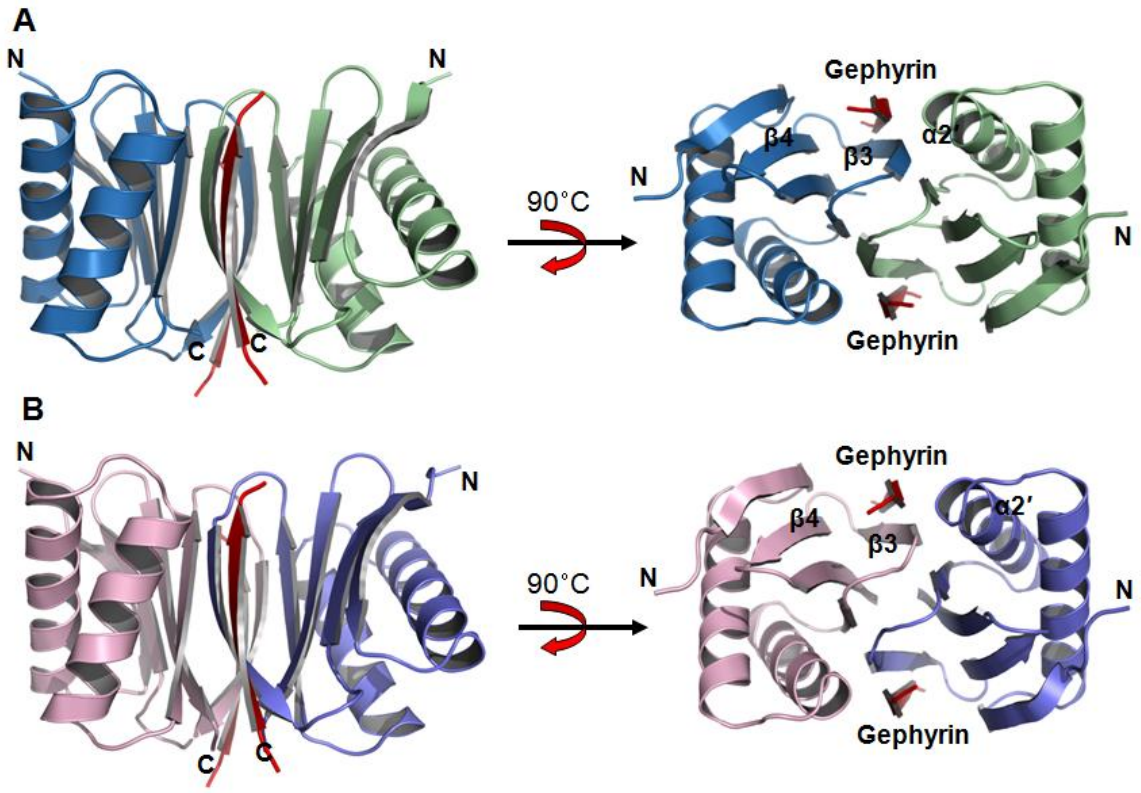

Figure 2.10 Ribbon diagram of DYNLL1/2 in complex with the gephyrin-derived peptide. DYNLL1 (A) and DYNLL2 (B) are colored as described for apo-DYNLL1/2 while the peptide is colored in red. The two views are related by a 90° rotation around the horizontal axis. Secondary structure elements in the vicinity of one of the peptides are labeled.

The most extensive hydrophobic contacts involve Gly209 and Val210; the former residue is tugged below the side chain of Tyr65 and the latter is inserted into a hydrophobic pocket formed by Phe62, Tyr75 and Leu84. On the basis of structural considerations alone, this interaction appears to be crucial for complex formation.

E. Comparison of gephyrin-bound and apo-DYNLL2

To detect whether gephyrin peptide-binding leads to conformational changes, and to analyze the structural differences in detail, the structure of apo-DYNLL2 has been compared with the structure of DYNLL2-peptide complex due to the higher resolution of the DYNLL2 models with 1.6 Å and 1.75 Å, respectively. As described earlier a comparison of the DYNLL1 and DYNLL2 apo structures revealed a high degree of structural similarity. The interaction pattern with gephyrin is highly conserved between DYNLL1/2 which will be described in detail the next paragraph. In addition, upon binding to gephyrin both DYNLL1/2 do not show any change in their thermostability although DYNLL2 is still more thermostable than DYNLL1 (Figure 2.6).

A superposition of the DYNLL2 crystal structures results in an rms deviation of 0.28 Å for all Cα atoms and 0.72 Å for all atoms of residues 3 to 87. By comparison the average coordinate error as calculated by Refmac is 0.099 Å for the apo-structure and 0.116 Å for the complex. Overall the structures of both DYNLLs are very similar (Figure 2.11A), however, small but significant movements are observed for the main chain atoms of β3, which move in a concerted fashion towards the twofold axis of the dimer, thus slightly increasing the width of the binding cleft from 13.0 Å in apo-DYNLL2 to 13.4 Å in the DYNLL2-gephyrin peptide complex (Table 2.8). At the same time, the side chains of residues Lys36, Phe62 and His68 undergo conformational changes with a

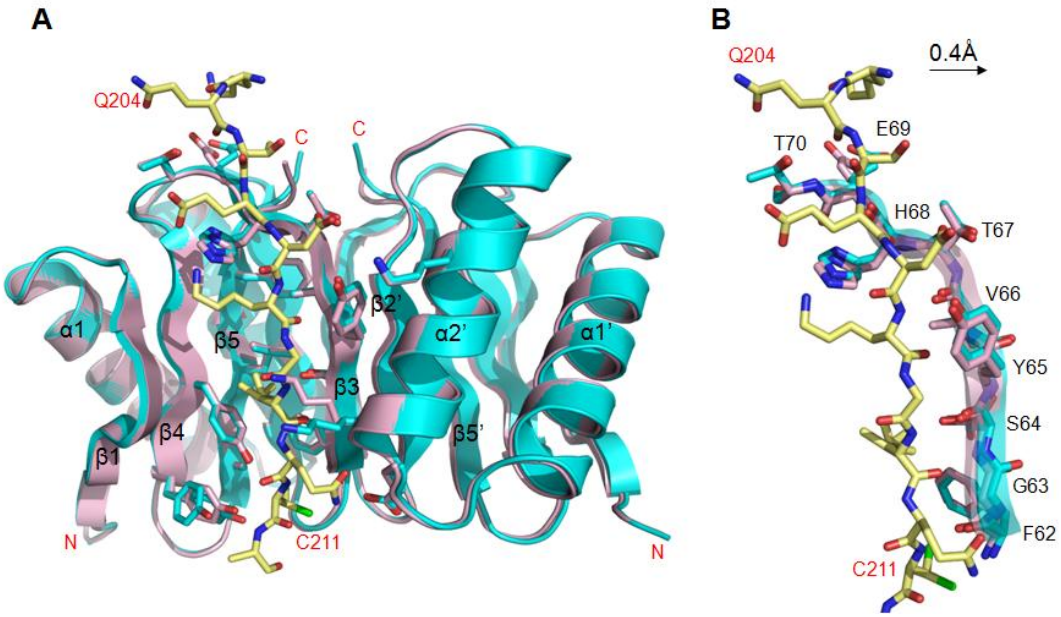

Figure 2.11 Structural changes between apo-DYNLL2 and the DYNLL2-gephyrin peptide complex. (A) Superposition of both structures represented as ribbon diagrams (apo-DYNLL2 in pink, peptide-bound DYNLL2 in cyan with the peptide in stick representation colored according to atom type) with selected side chains undergoing conformational changes in pink and cyan, respectively. Val210 and Cys212 of gephyrin, and Tyr77 of DYNLL2 each exhibit two, and Ser64 three alternate conformations. (B) Enlarged view of the peptide colored as in (A) and β3 with C-atoms in pink (apo) and cyan (complex) in the same orientation as in (A). As a consequence of binding the main chain atoms of β3 are pushed away from the bound peptide by 0.4 Å.

Table 2.8 Width of peptide binding pocket in DYNLL/LC8

	[b]63Cα to 9Cα(Å)	64Cα to 10Cα(Å)	65Cα to 11Cα(Å)	66Cα to 12Cα(Å)	Average cleft width (Å)
[a]*Apo-DYNLL1(3GHO)	12.5	11.9	13.8	12.8	12.8
*Apo-DYNLL2(3GHK)	12.8	12.2	14.1	13.0	13.0
Apo-LC8(3BRI)	12.3	12.0	13.9	12.9	12.8
*DYNLL1-geph(3GHL)	13.2	12.5	14.5	13.2	13.4
*DYNLL2-geph(3GHI)	13.4	12.7	14.4	13.1	13.4
DYNLL1-nNOS(1CMI)	14.1	13.4	15.1	13.8	14.1
*DYNLL1-IC1(3GM4)	13.4	12.8	14.4	13.1	13.4
LC8-IC2(2PG1)	13.5	12.6	14.2	13.2	13.4
LC8-swallow(2P1K)	13.4	12.7	14.2	13.1	13.3
LC8K36P-Pak1(3DVP)	12.7	12.5	13.7	12.8	12.9
Apo-LC8K36P(3DVH)	12.2	12.1	14.1	12.9	12.8

*[a]This study

[b]Measured distance between two Cα atoms of β3 and β1 of DYNLL as illustrated in Figure 2.12B to calculate the width of groove surrounding Asp207 to Gln211 of the gephyrin peptide and the corresponding residues in the other peptides

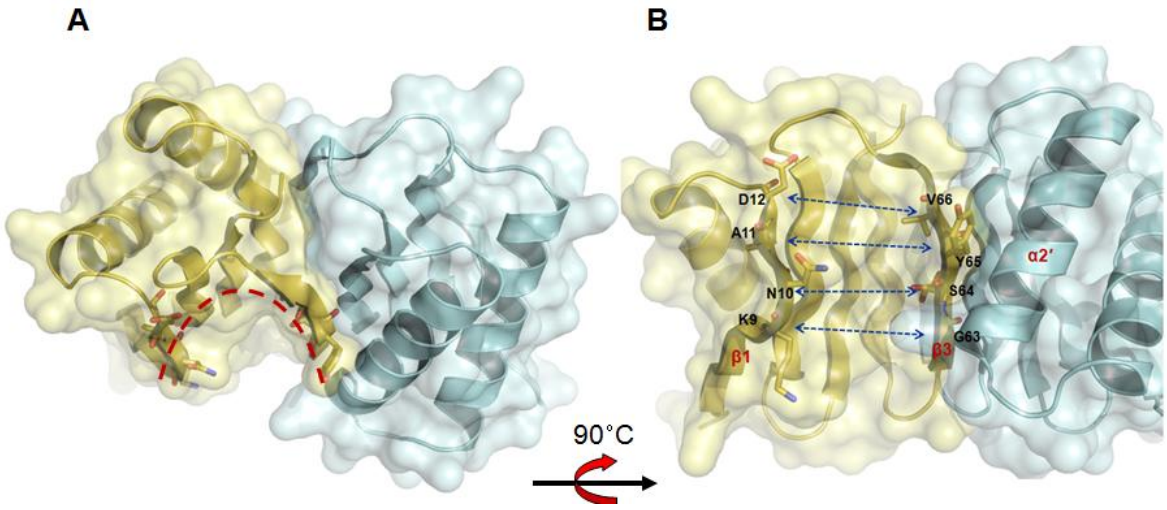

Figure 2.12 Gephyrin protein binding cleft on DYNLL2. One monomer is colored in yellow and the other in cyan. (A) Top view of the dimer interface. (B) Distances between two Cα atoms of β1 and β3 are represented by double-headed arrows. The corresponding amino acid residues in β1 and β3 are shown in stick representation.

maximum displacement of 0.9 Å for the Nδ1 atom of residue His68 (Figure 2.11B). These observations indicate that binding of the gephyrin peptide to DYNLL2 can be described to a first approximation as a lock-and-key interaction coupled with a shear movement at the domain interface (93).

F. Molecular basis of gephyrin recognition

As described above, the gephyrin-derived peptide is bound in a predominantly hydrophobic groove, which is formed by both DYNLL monomers and runs approximately parallel to the twofold axis of the dimer. Residues 204-212 of gephyrin are located towards the N-terminal end of the central linker connecting the N- and C-terminal domains, and, based on secondary structure predictions (Figure 2.13), these residues do not appear to form stable secondary structure elements in the absence of a binding partner as in other DYNLL binding proteins. CD experiments with gephyrin derived peptides confirmed that the DYNLL-binding motif by itself does not form a defined structure (Figure 2.14A). Nevertheless, the crystal structure reveals that in the proper environment these residues adopt the conformation of a β-strand.

Peptide binding results in the burial of ~670 $Å^2$ of surface area and the formation of 12 H-bonds as well as numerous van der Waals contacts (Table 2.9). Out of all the H-bonds six result from the extension of the antiparallel β-sheet and hence involve two main chain atoms. An additional H-bond involving two main chain atoms is present between the main chain nitrogen of Thr70 and the main chain oxygen of Gln203. Among the remaining H-bonds, the side chain of Gln211 appears critical: In the DYNLL1-peptide complex it engages in a bifurcated interaction, involving its side chain oxygen and the main chain nitrogen of Lys36, and its side chain nitrogen and the side chain oxygen of

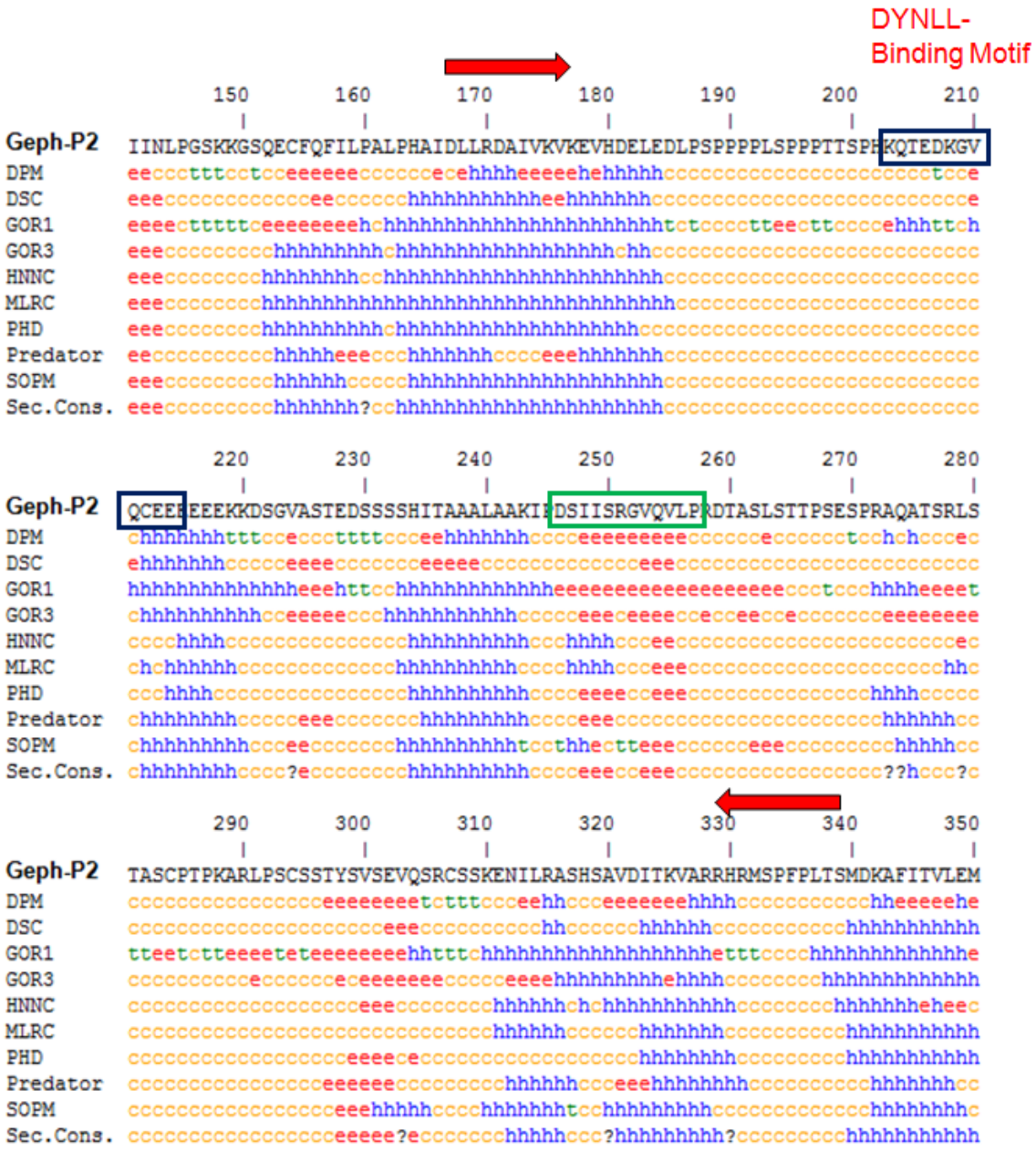

http://npsa-pbil.ibcp.fr/cgi-bin/npsa_automat.pl?page=/NPSA/npsa_seccons.html

Figure 2.13 Secondary structure predictions of gephyrin's linker region. The linker region is indicated with red arrows and is comprised of residues 168 to 340. The DYNLL-binding region in the linker is shown as a blue box and the sequence in the green box indicates the possible DYNLL binding region with also harbors the GVQV core residues. h: α-helix, e: extended conformation (β-strand), c: Random coli, t: β-turn.

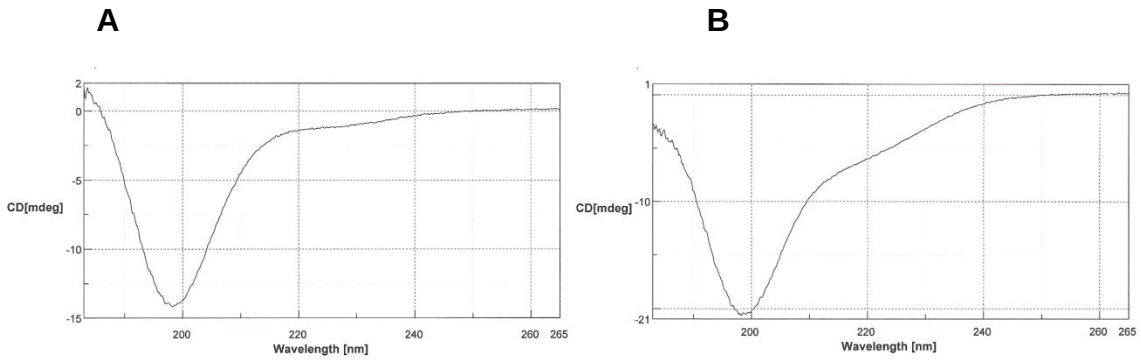

Figure 2.14 Circular dichroism spectra of gephyrin-derived peptides. The gephyrin peptide 1 (KQTEDKGVQCEE, 12-mer) (A) and the gephyrin peptide 2 (DSIISRGVQVLP, 12-mer) (B).

Table 2.9 Interactions between DYNLL1/2 and gephyrin

Gephyrin	Dist. [Å]	DYNLL1
GLU 206[N]	2.83	HIS 68[O]
LYS 208[N]	2.95	VAL 66[O]
VAL 210[N]	3.09	SER 64[O]
GLN 204[O]	2.64	THR 70[N]
GLN 204[O]	2.67	THR 70[OG1]
GLU 206[O]	2.90	HIS 68[N]
ASP 207[OD1]	3.29	THR 67[OG1]
ASP 207[OD2]	3.67	TYR 65[OH]
LYS 208[O]	3.06	VAL 66[N]
VAL 210[O]	3.00	SER 64[N]

Gephyrin	Dist. [Å]	DYNLL2
GLU 206[N]	2.94	HIS 68[O]
LYS 208[N]	2.94	VAL 66[O]
VAL 210[N]	3.08	SER 64[O]
CYS 212[N]	3.00	PHE 62[O]
CYS 212[SG]	3.35	TYR 75[OH]
ALA 213[N]	3.37	TYR 77[OH]
GLN 204[O]	3.09	THR 70[N]
GLU 206[O]	2.85	HIS 68[N]
ASP 207[OD1]	2.79	THR 67[OG1]
ASP 207[OD2]	3.76	TYR 65[OH]
LYS 208[O]	3.09	VAL 66[N]
VAL 210[O]	2.96	SER 64[N]
LYS 203[NZ]	3.99	GLU 69[OE1]
GLU 206[OE1]	3.88	HIS 68[NE2]

http://www.ebi.ac.uk/msd-srv/prot_int/pistart.html

Glu35 (Figure 2.15A). In the DYNLL2-peptide complex the side chain oxygen of Gln211 interacts only with the main chain nitrogen of Lys36 and an additional hydrogen bond exists between the main chain nitrogen of Cys212 and the main chain oxygen of Phe62 (Figure 2.15B). The remaining 3 H-bonds involve only side chain atoms. Strong van der Waals interactions, defined by the burial of more than 50 $Å^2$ per residue, involve Glu206, Asp207, Lys208, Val210 and Cys212 of gephyrin and Tyr65, His68, Glu69, Thr70 and Tyr75 of DYNLL. Based on structural considerations the central Gly-Val-Gln tripeptide of gephyrin appears to be crucial for the interaction with the DYNLLs: The glycine is required since larger residues presumably lead to steric interference. The valine resides in a hydrophobic pocket which is too small for larger aliphatic (Leu and Ile) and aromatic residues, yet Ala would be too small for this pocket. Finally, the Gln fits with the aliphatic moiety of its side chain nicely into a sub-pocket of the hydrophobic groove; its side chain oxygen engages in at least one hydrogen bond with the main chain atoms at the N-terminus of α2, while its side chain nitrogen forms an additional H-bond with the side chain of Glu35. At the position of Val210 a Thr could also be envisioned since this residue is almost isosteric with Val and its side chain OH-group could also form a hydrogen bond with Ser64. In contrast to that a Q211E variant would be expected to disrupt the binding interactions due to the loss of the H-bond acceptor required to interact with the side chain of Glu35 and the resulting electrostatic repulsion between both glutamate residues.

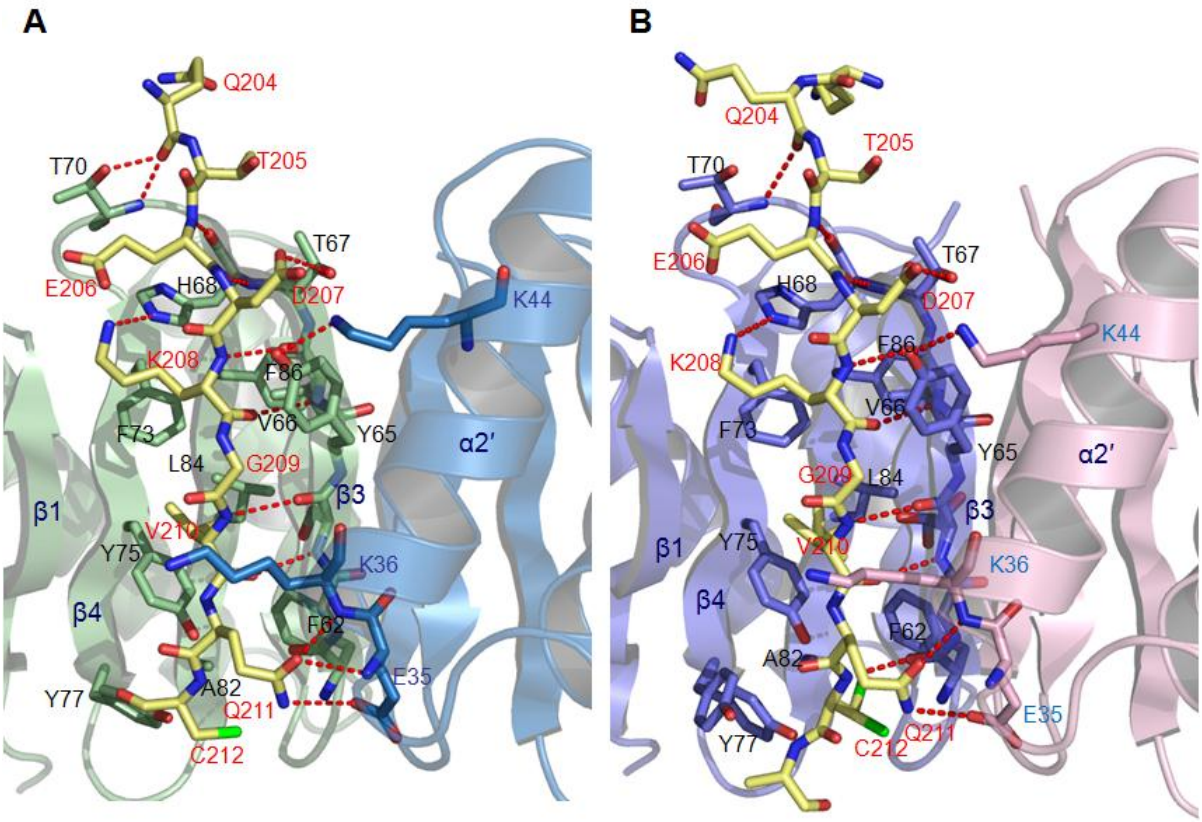

Figure 2.15 Interactions between gephyrin and DYNLL1/2. Detailed views of the interactions between DYNLL1 and the gephyrin peptide (A), and DYNLL2 and the gephyrin peptide (B). DYNLL is shown in ribbon representation (one monomer in green and the other in sky blue for DYNLL1, and slate and pink for DYNLL2) with residues involved in hydrogen-bonded interactions shown in all bond representation with O-atoms in red, N-atoms in blue and C-atoms either in slate or pink. The gephyrin peptide is shown in stick representation with C-atoms in yellow and a single S-atom in green. Hydrogen bonds are shown as red dashed lines. Selected residues of the binding interface are numbered in red for the gephyrin peptide, in black for one DYNLL monomer and blue for the other monomer.

G. Probing the gephyrin-DYNLL interface

To analyze the contribution of residues in the gephyrin and DYNLL interface as detected in the crystal structure, gephyrin and DYNLL variants were introduced into the full-length proteins and subjected to ITC studies.

A detailed structure-function analysis revealed that the contribution of individual residues to complex formation cannot always be predicted from the structure. On the one hand substitutions of Gln211 within the Gly209-Val210-Gln211 tripeptide, which based on the structure appears crucial for DYNLL binding, with either Ala or Glu prevent binding as measured by ITC (Table 2.10). On the other hand, the situation is more complex for the two other residues, Gly209 and Val210. As expected, larger residues such as a Glu at position 209 cannot be tolerated, however, an Ala can be introduced with hardly any decrease in affinity. For Val210 the situation is equally complex since truncation to Ala only leads to an 8-fold increase in K_d, while substitution with the larger and hydrophilic Asn does not disrupt binding but only decreases the affinity 20-fold. In addition, the almost isosteric Thr leads to barely any changes in affinity. Outside this tripeptide, the binding affinity of the T205A, D207A and K208A variants was reduced between fourfold and tenfold compared to wild type indicating that these residues contribute to complex stability via their polar side chains. Cys212 adopts two alternate conformations which are both involved in limited van der Waals interaction with DYNLL. In agreement with this the C212A variant resulted in a threefold lowered binding affinity.

From the perspective of DYNLL the interactions involving Tyr65, His68 and Phe73 appear crucial since substituting any of these residues with Ala completely abolishes binding in the ITC experiments (Table 2.11). In the case of Tyr65 it is clear that hydrophobic interactions mediated by the phenyl ring are crucial since the Y65F

Table 2.10 Binding parameters of Geph-P2 mutants and DYNLL1 wild-type

Cell(Geph-P2)	Injector(DYNLL1)	N	K_d (μM)	ΔH (kcal mol^{-1})	ΔS (cal mol^{-1} K^{-1})
WT	DYNLL1	0.77±0.02	3.3±0.3	-8.1±0.2	-1.3
Q204A	DYNLL1	0.99±0.03	4.3±0.5	-7.5±0.3	0.4
T205A	DYNLL1	0.98±0.06	11.5±1.2	-6.2±0.5	2.7
E206A	DYNLL1	0.96±0.02	2.3±0.3	-10.1±0.3	-6.6
E206K	DYNLL1	1.07±0.04	3.8±0.5	-9.2±0.4	-4.9
D207A	DYNLL1	0.77±0.25	31.0±6.3	-10.8±0.4	-14.4
K208A	DYNLL1	1.01±0.17	20.0±3.9	-8.3±1.7	-5.2
G209A	DYNLL1	0.7 [*a]	5.5±1.2	-6.3±0.5	3.7
G209E	DYNLL1	n.d.[b]	n.d.	n.d.	n.d.
V210A	DYNLL1	0.7 [*]	24.6±1.8	-7.3±0.2	-2.3
V210N	DYNLL1	0.61±1.2	56.8±3.8	-23.9±1.0	-57.9
V210T	DYNLL1	0.7 [*]	4.3±0.9	-10.6±0.7	-9.5
Q211A	DYNLL1	n.d.	n.d.	n.d.	n.d.
Q211E	DYNLL1	n.d.	n.d.	n.d.	n.d.
C212A	DYNLL1	0.83±0.06	10.0±1.5	-5.8±0.5	4.3

[*a]For mutants where refinement is not stable n-values were fixed at wild-type levels (n=0.7) and then the other parameters were refined

[b]Experiments where binding could not be detected have been labeled n.d. (non-detectable)

Raw data for the wild type and variants of gephyrin is represented in Figure 2.16

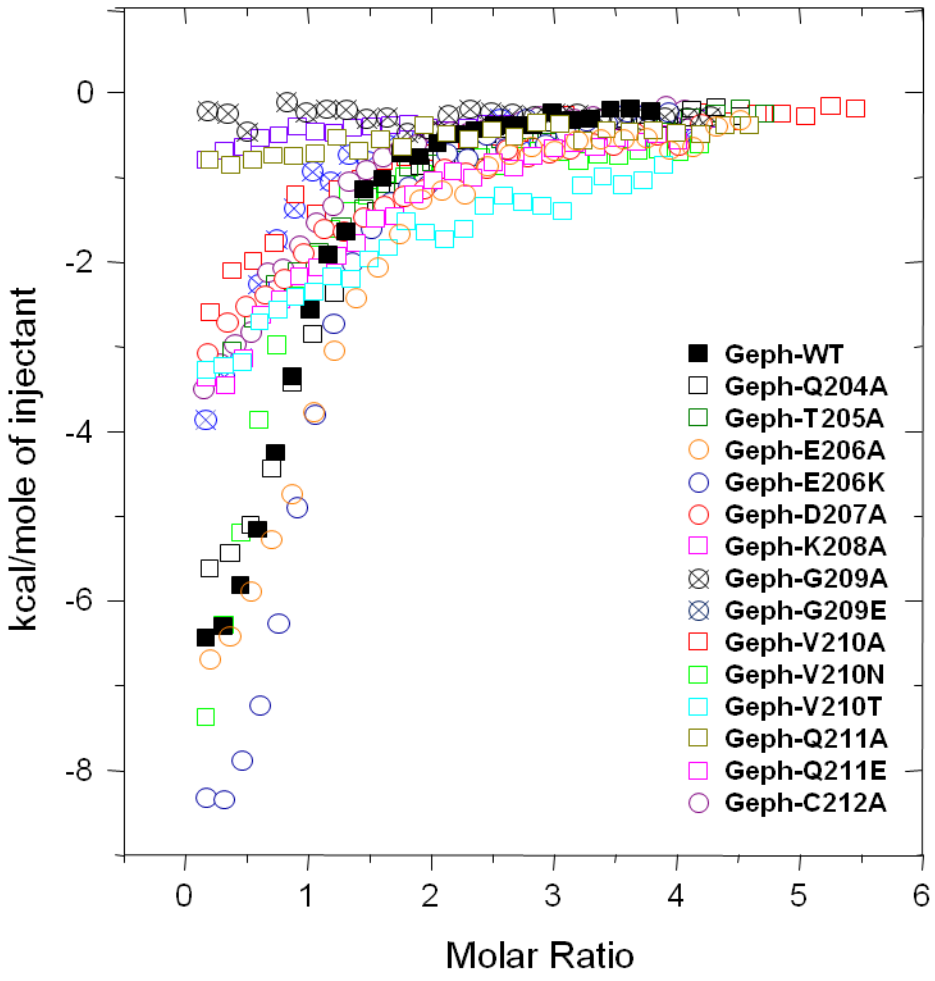

Figure 2.16 ITC data of gephyrin variants. Raw ITC data resulting from titrations of gephyrin wild-type and mutants with the DYNLL1 wild-type protein.

Table 2.11 Binding parameters of Geph-P2 wild-type and DYNLL1 mutants

Cell(Geph-P2)	Injector(DYNLL1)	N	K_d (μM)	ΔH (kcal mol^{-1})	ΔS (cal mol^{-1} K^{-1})
WT	WT	0.77±0.02	3.3±0.3	-8.1±0.2	-1.3
WT	E35K	0.71±0.02	0.5±0.1	-1.9±0.1	22.7
WT	K36A	0.7*	27.9±2.5	-3.5±0.2	9.5
WT	K36P	n.d.	n.d.	n.d.	n.d.
WT	K44A	0.75±0.07	11.3±1.6	-4.6±0.6	7.7
WT	N61A	0.7*	3.8±0.8	-3.4±0.2	13.9
WT	Y65A	n.d.	n.d.	n.d.	n.d.
WT	Y65F	0.7*	4.2±0.9	-7.7±0.5	-0.3
WT	Y65D	n.d.	n.d.	n.d.	n.d.
WT	H68A	n.d.	n.d.	n.d.	n.d.
WT	T70A	0.98±0.06	8.5±1.0	-8.5±0.6	-4.3
WT	F73A	n.d.	n.d.	n.d.	n.d.
WT	Y77A	0.7*	11.8±0.9	-12.1±0.4	-16.5

*[a]For mutants where refinement is not stable n-values were fixed at wild-type levels (n=0.7) and then the other parameters were refined

[b]Experiments where binding could not be detected have been labeled n.d. (non-detectable)

Raw ITC data are shown in Figure 2.17

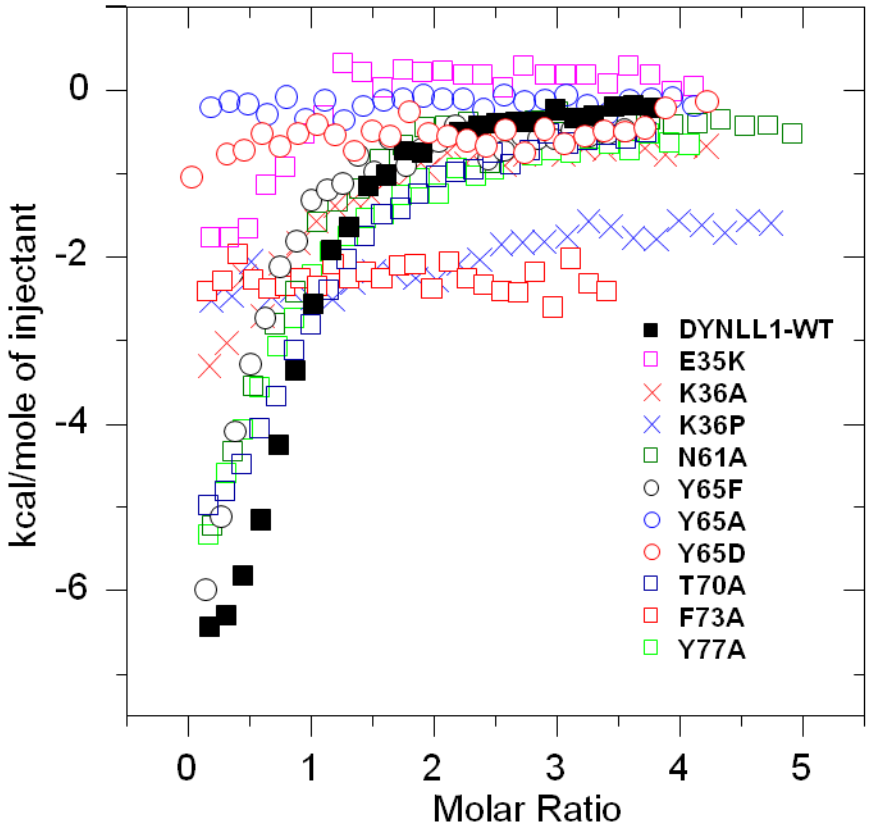

Figure 2.17 ITC data of DYNLL variants. In these ITC experiments gephyrin wild-type was titrated with DYNLL1 wild-type or mutants.

variant still retains almost full affinity whereas the Y65D substitution abolishes binding. Interestingly this mutation also shifts the monomer-dimer equilibrium of DYNLL1 almost completely towards the monomer (Figure 2.18). This observation seems surprising since one would expect the Asp side chain to engage in electrostatic interactions with the side chains of Lys43 and Lys44 across the dimer interface, thus stabilizing the dimer. Interestingly, Tyr65 is a predicted phosphorylation site in both DYNLL1/2 according to the NetPhos server (www.cbs.dtu.dk/services/NetPhos/). However, the Y65D mutant of DYNLL2 continues to form a stable dimer. DYNLL2 harbors an additional predicted phosphotyrosine site at Tyr32. Since the Y65D substitution represents a phosphomimetic substitution the question arises whether phosphorylation at this position might lead to dissociation of the dimer of DYNLL1 but not DYNLL2.

Like Tyr65, the side chain of His68 appears to make important van der Waals contacts, but also engages in an H-bond with Lys208 of gephyrin. Since the K208A variant displays a 7-fold reduced affinity one could assign this defect to the H-bond but more likely it is due to the missing interaction between the aliphatic moiety of Lys208 and the phenyl ring of Phe73 since the F73A variant displays no binding. However, an explanation for why the F73A variant is so severely impaired must also take into account the van der Waals contact at a distance of 3.9 Å between the Cβ of Lys208 and the side chain of Phe73 which is present in the K208A variant but no longer in the F73A mutant. Besides the three residues where substitution with Ala completely eliminates binding, I have identified three additional residues that contribute to a lesser extent to binding. The K36A mutant displays a ninefold lower affinity, indicating that in the absence of a polar contact of this side chain the aliphatic moiety of this residue contributes to binding.

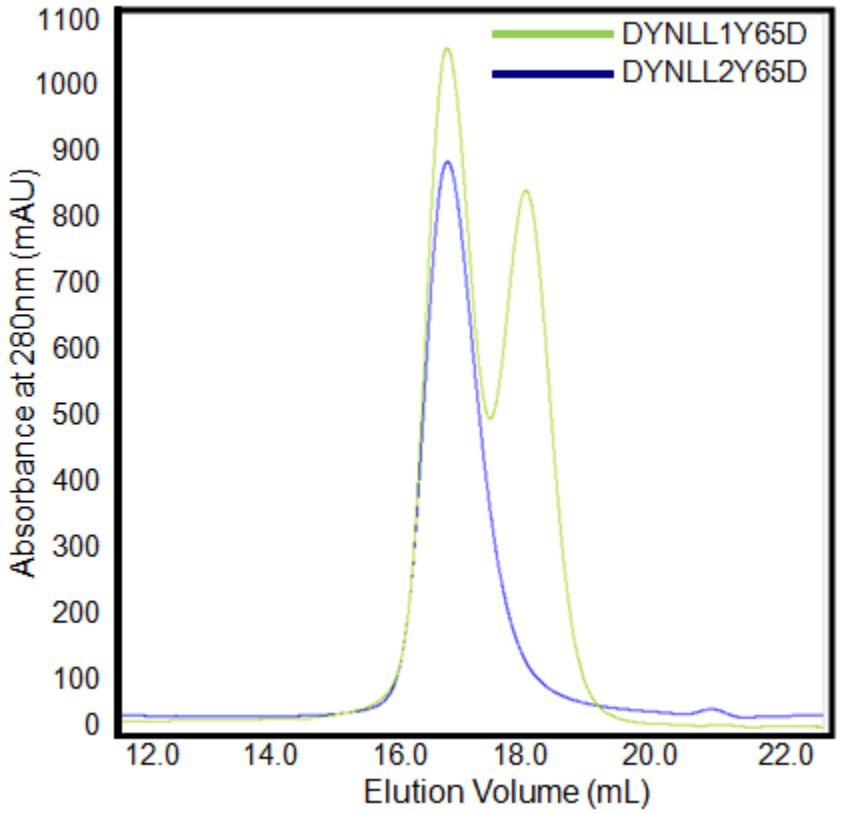

Figure 2.18 Size exclusion chromatography experiments of DYNLLY65D mutants. The elution profiles of DYNLL1Y65D and DYNLL2Y65D at pH 8.0.

As expected due to its location at the periphery of the interface, Tyr77 is not as important for complex formation as Tyr65 and His68, nevertheless, this mutant has a 4-fold reduced affinity. Unfortunately, I was not able to probe the contribution of the hydrophobic residues Phe62 and Tyr75 which together form a consecutive hydrophobic patch on the apo-DYNLL surface since the corresponding Ala-variants could not be stably expressed and purified.

The H-bonded interactions involving the side chain of Thr70 do not appear to be crucial since the T70A binding only shows a less than threefold reduction in affinity, but I cannot rule out the possibility that the H-bond involving the main chain of Thr70 is important for binding. Finally, the E35K variant surprisingly displays a roughly 6-fold tighter binding than the wild-type DYNLL1 protein with a dissociation constant of 0.5 μM coupled with a 4-fold decrease in enthalpy and a significant increase in entropy. Attempts to investigate the E35A variant were unsuccessful since this mutant expressed in an insoluble form.

While I analyzed the DYNLL1/2-peptide complex structures I noted that an additional putative DYNLL binding site with the sequence DSIISRGVQVLP appears to exist between residues 246 and 257 of gephyrin (Figure 2.13). Although the overall degree of sequence conservation is rather low, the important Gly-Val-Gln tripeptide is also present and hence binding to this site appeared possible. Based on the secondary structure prediction this region would form two short β-stands. However, CD experiments revealed that the isolated gephyrin-derived peptide2 (DSIISRGVQVLP) did not display a defined secondary structure in CD experiments either (Fig 2.14B) although it appears somewhat more structured than the gephyrin-derived peptide1 (residues 203-214, KQTEDKGVQCEE).

C-terminal to the tripeptide this alternative sequence features a valine that one would predict to be a good substitute for the cysteine observed in the structure, while the two remaining residues (Leu and Pro) should not be relevant since they would be beyond the binding groove in DYNLL1/2. On the N-terminal side of the tripeptide the possible DYNLL binding site features an arginine instead of a lysine, a type-conserved and hence presumably tolerable solution, preceded by a serine and two isoleucine residues, which would correspond to Asp207, Glu206 and Thr205. Using a chemically synthesized peptide (DSIISRGVQVLP, 12-mer, Anaspec) I could, however, not detect any binding in ITC experiments, indicating that additional residues beyond the tripeptide are required for binding, in agreement with our structure-function analysis. If I only focus on Thr205 and Asp207 the site directed mutagenesis study revealed that their combined replacement with Ala would result in a ~40-fold reduction in affinity, clearly indicating that the accumulation of a few subtle changes in the peptide will be sufficient to abolish binding since residues across almost the entire length of the peptide (from 205 to 212) contribute to the interaction of the two proteins.

H. Crystal structure of DYNLL1-intermediate chain peptide complex

The complex structure of DYNLL1 with the human intermediate chain isoform 1 (IC1)-derived peptide VVSYSKETQTPL (residues 164-172, PDB entry 3GM4) was crystallized in space group C2 (a=122.4 Å, b=71.9 Å, c=70.38 Å and β=122.7°) and refined at a resolution of 1.88 Å to an R-factor of 0.15 and an R_{free} of 0.19 (Table 2.6).

The crystals contain four binary complexes in the asymmetric unit organized into two non-crystallographic dimers. Each dimer interacts with two IC peptides that are surrounded by β-strands 3, 4 and 5 of the one monomer and α-helix 2 of the other

monomer bind in an antiparallel arrangement to β3 (Figure 12.19A) in complete analogy to the DYNLL1/2-gephyrin complexes. Twelve residues of the IC-derived dodecapeptide are well defined in the electron density maps (Figure 12.19B).

I. Comparison with known DYNLL1/LC8 crystal structures

The crystal structures of dynein light chains in complex with peptides from nNOS (68), the dynein intermediate chain (63), swallow (93) and Pak1 (71) have been determined so far. A superposition of these complexes onto the DYNLL1/2-gephyrin peptide complexes reveals a striking overall similarity between the different complexes (Table 2.12). Although all other DYNLL-peptide complexes involve DYNLL1 in the following I will use the complex with DYNLL2 as reference structure for comparison since the rms deviations with DYNLL2 are slightly smaller than those with DYNLL1, presumably reflecting the higher resolution and corresponding higher accuracy of the DYNLL2 structure. For comparison the rms deviation of DYNLL1 and DYNLL2 with the gephyrin peptide is 0.3 Å for the Cα atoms and 0.8 Å for all atoms. Consistent with the small rms deviation of the Cα atoms there is a conserved pattern of interactions involving backbone and side chain atoms in both complexes. Again, in the following discussion residue numbers <100 refer to DYNLL and those >100 to their different binding partners.

The superposition of the complexes between DYNLL2 and the gephyrin peptide with the sequence QTEDKGVQC (residues 204-212) and DYNLL1 in complex with the nNOS derived peptide (EMKDTGIQV, residues 227-235, PDB entry 1CMI) (68) that contain a similar G(I/V)QV(D/E) motif results in a rms deviation of 0.4 and 0.9 Å for the Cα positions and all atoms, respectively. This results not only in virtually identical atom

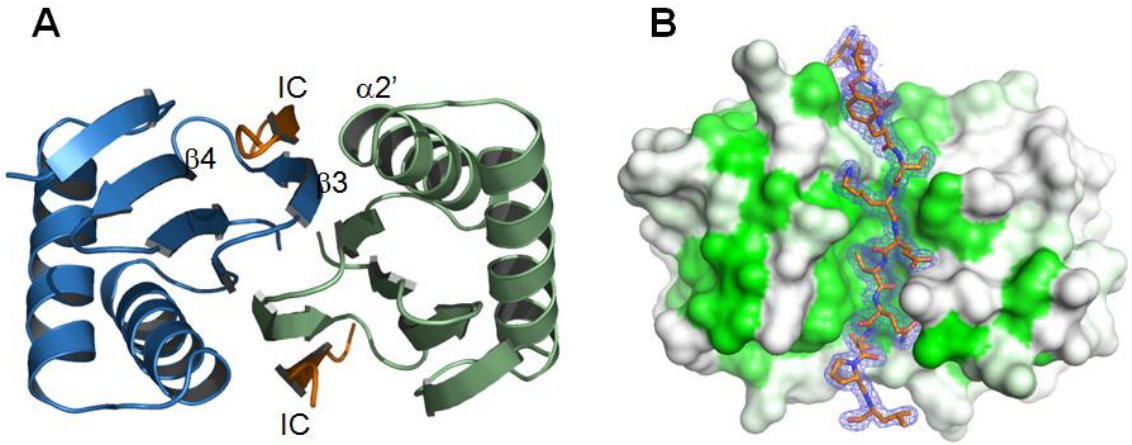

Figure 2.19 Structure of DYNLL1 in complex with the dynein intermediate chain-derived peptide. (A) Ribbon diagram of DYNLL1 and the IC peptide. DYNLL1 is colored as described for apo-DYNLL1 and the IC peptide is colored in orange. Secondary structure elements in the vicinity of one of the peptides are labeled. (B) Surface representation of DYNLL1 with hydrophobic residues highlighted in green based on a hydrophobicity analysis (95). The bound peptide is displayed in stick representation with C-atoms in orange, N-atoms in blue and O-atoms in red. An omit SIGMAA weighted $2F_o$-F_c electron density map contoured at three times the rms deviation is shown as a blue wire mesh.

Table 2.12 Amino acid sequences of peptides from DYNLL/LC8 complexes and rms deviations between DYNLL/LC8-peptide complexes

Protein (PDB entry): resolution	Peptide residues	Sequence	[a]Rms deviations to DYNLL1-Geph complex (Å)	[a]Rms deviations to DYNLL2-Geph complex (Å)
nNos(1CMI): 2.5 Å	227-235	EMKDTGIQV	0.5/1.0	0.4/0.9
*[b]IC1 (3GM4):1.88 Å	164-172	VSYSKETQT	0.5/1.1	0.4/0.9
IC2 (2PG1): 2.8 Å	128-136	VTYTKETQT	0.4/1.1	0.4/1.0
Swallow(2P1K): 2.0 Å	287-295	ATSAKATQT	0.3/0.9	0.3/0.7
Pak1(3DVP): 2.5 Å	213-221	PTRDVATSP	0.4/1.0	0.4/0.9
*Gephyrin from DYNLL1 complex (3GHL): 2.8 Å	204-212	QTEDKGVQC	-	0.3/0.8
*Gephyrin from DYNLL2 complex (3GHI): 1.75 Å	204-212	QTEDKGVQC	0.3/0.8	-

[a]Rms deviations for Cα and all atoms when residues 6-87 of DYNLL/LC8 were superimposed

*[b]From this study

positions but also in a conservation of most interactions (Figure 2.20A). As demonstrated by my ITC results with the gephyrin E206K variant, the substitution of Glu206 with Lys (corresponding to Lys229 of nNOS) does not influence the binding affinity because the van der Waals interactions with His68 are maintained (Table 2.10). Thr231 of nNOS interacts with His68 via its side chain oxygen, a similar interaction of the corresponding residue Lys208 of gephyrin, however, here this contact involves the side chain nitrogen. The most significant difference involves Ile233 in nNOS (corresponding to Val209 of gephyrin) since the Ile side chain induces a 20° rotation around the Cα-Cβ bond of Tyr75, thus generating additional space to accommodate its larger aliphatic side chain in the hydrophobic pocket. The rotation of Tyr75 in turn leads to a 90° rotation around the Cβ-Cγ bond of Tyr77 compared with Tyr77 from DYNLL1-gephyrin complex. Since the complex of DYNLL2-gephyrin harbors two alternate conformations at this position, 15° and 85° rotations around the Cβ-Cγ bond of Tyr77 are observed dependent on the compared conformation. These changes are clustered around the C-terminal end of the peptide and represent the only area where significant changes are observed.

The (K/R)XTQT peptide represents the other canonical sequence motif present in DYNLL binding partners and structurally characterized examples include the mouse intermediate chain isoform 2 (PDB entry 2PG1) (63) and the swallow peptide (PDB entry 2P1K) (93). As described in the previous paragraph I have also determined the crystal structure of DYNLL1 in complex with a peptide derived from the human intermediate chain isoform 1 (VSYSKETQT, residues 164-172, PDB entry 3GM4) at a resolution of 1.88 Å (Table 2.6) and used it also for comparison. The two intermediate chain (IC) sequences differ in two residues, Ser165 and Ser167 in our DYNLL1-IC1 structure,

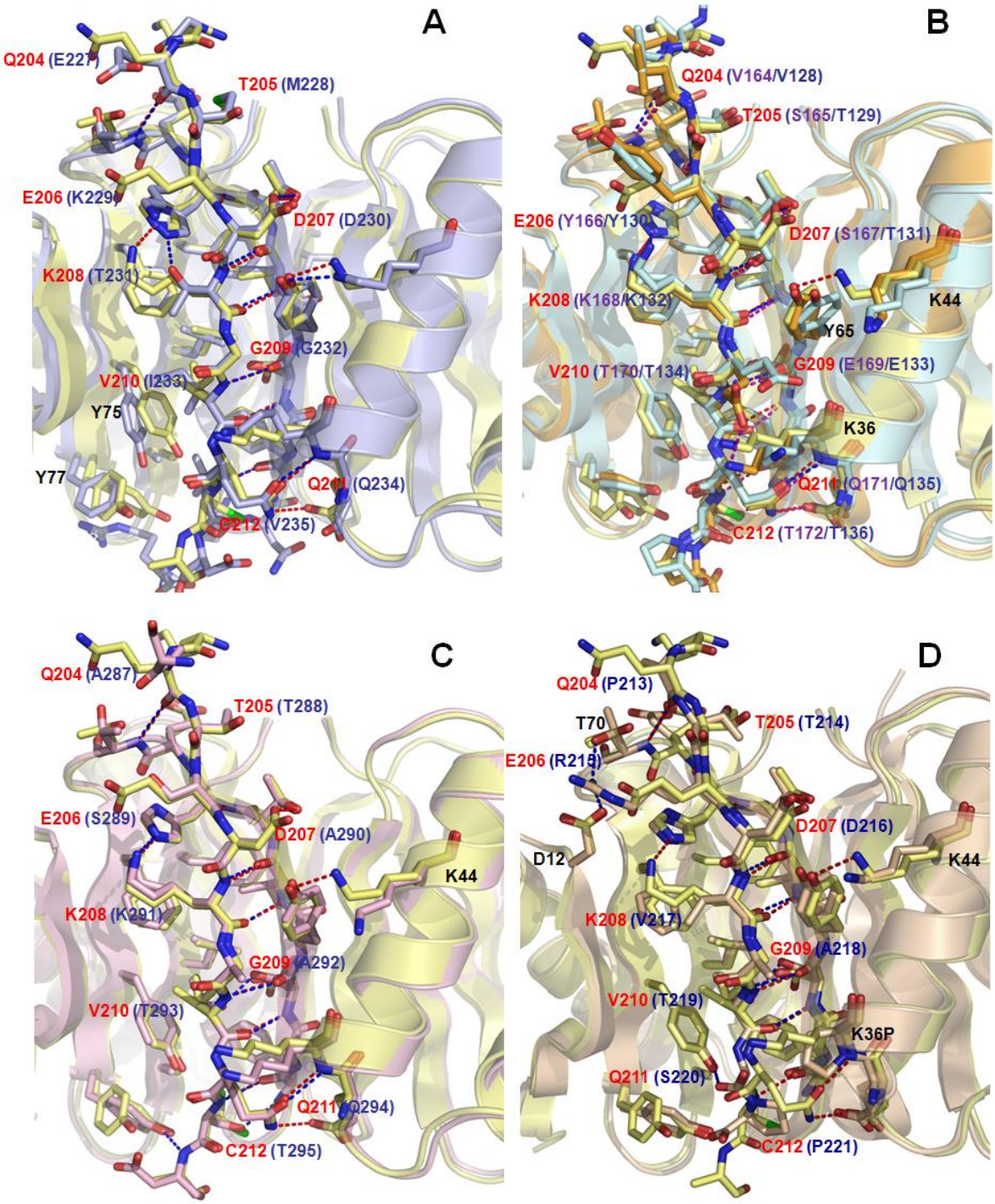

Figure 2.20 Comparison of dynein light chain-ligands complexes. Ribbon diagram of the superimposed structure of DYNLL2-gephyrin (yellow) with (A) the DYNLL1-nNOS complex: light blue (G(I/V)QV(D/E)), (B) DYNLL1-IC1: orange/ LC8-IC2 complex: pale cyan ((K/R)XTQT motif), (C) LC8-swallow complex: pink (D) LC8K36P-Pak1 complex: wheat (RDVATS motif). Peptide residues are numbered in red for the gephyrin peptide and blue for the other peptides. Hydrogen bonds between the gephyrin peptide and the DYNLL1 are shown as red dashed lines, IC1 and DYNLL1 as purple dashed lines, and the other peptides and DYNLL/LC8 as blue dashed lines, respectively.

which are replaced by Thr129 and Thr131 in the published structure (2PG1) (63), and obviously also in their residue numbering.

As expected from the conservative substitution the H-bond between the side chain oxygens of Thr131/Ser167 and Thr67 of DYNLL is present in both structures. The rms deviation between the two DYNLL-IC structures is 0.3 Å and 0.9 Å for the Cα and all atoms. Surprisingly, the gephyrin and intermediate chain (IC) peptides can be superimposed with similarly low rms deviations of 0.4/0.9 Å in Cα positions and all atoms, respectively (Table 2.12) although the (K/R)XTQT motif clearly differs from the G(I/V)QV(D/E) motif with the exception of the common Gln residue. All together only 4 of 9 superimposed residues are identical; Thr205, Lys208, Val210, and Gln211 of gephyrin match Ser165/Thr129, Lys168/Lys132, Thr170/Thr134, and Gln171/Gln135 of the intermediate chain.

The side chain of Thr205 is not involved in any interaction, and I have demonstrated that the V210T variant of gephyrin corresponding to Thr170/Thr134 of the intermediate chain does not change the affinity towards DYNLL. In the structure with the IC1 peptide, the side chain oxygen and nitrogen of Gln171 interact with the main chain nitrogen of Lys36 and side chain oxygen of Glu35 as in the DYNLL2-gephyrin complex. The major difference between the gephyrin and IC peptides is the replacement of gephyrin's Gly209 residue with Glu169/Glu133 (Figure 2.20B). Gly209 of gephyrin could not be mutated to Glu which I attributed to severe steric clashes with Tyr65. The complexes with the IC peptides demonstrate that this explanation cannot be correct and that a Glu at this position can be tolerated in the appropriate sequence context. To accommodate the side chain of Glu169/Glu133, the main chain of the peptide is slightly twisted to move the Glu side chain away from Tyr65 coupled to the formation of an H-bond between the side chain oxygens of Thr170/Thr134 and Ser64 of DYNLL. At the

same time the side chain of Tyr65 of DYNLL is rotated around the Cβ-Cγ bond by 140° which in turn leads to a different position of the side chain of Lys44. Alternatively, a glutamate at this position can also be accommodated by a 180° rotation around the Cα-Cβ bond leading to the formation of an H-bond and strong salt bridge with Lys36, as illustrated by Glu169 of our DYNLL1-IC1 complex. In this arrangement, only a slight rotation of the side chain of Tyr65 is observed. The introduction of Ala instead of Gly at position 209 (gephyrin peptide numbering) leads to almost no change in affinity in our ITC experiments and the accommodation of the additional methyl group can be seen in the complex with the swallow peptide (Figure 2.20C).

I have measured the affinity of the DYNLL-IC1 complex in ITC experiments by titrating DYNLL1/2 with the IC1-derived peptide (VVSYSKETQTPL) at 37°C (Table 2.13). The dissociation constant for the intermediate chain with values around 6 µM is basically identical to the K_d for the gephyrin peptide, however, the reaction is significantly more exothermic as reflected in a twofold decrease in ΔH from approximately -6 kcal/mol for the gephyrin peptide to roughly -12 kcal/mol for the IC1 peptide. The decrease in ΔH is offset by a decrease in the reaction entropy from about +5 cal mol^{-1} K^{-1} for the gephyrin peptide to approximately -15 cal mol^{-1} K^{-1} in the IC1 peptide. I attribute the increase in the exothermic character of the interaction to the additional ionic interaction between the Glu at position 169 and the Lys residue at position 36 which is absent when a Gly is present at the corresponding position (Gly209 in gephyrin).

Finally, a comparison between the DYNLL complexes with the gephyrin peptide and Pak1 peptide (PTRDVATSP, residues 213-221, PDB entry 3DVP) (71) results in an rms deviation of 0.4 Å and 0.9 Å for the Cα positions and all atoms, respectively, which is not higher than for the other bound peptides (Table 2.12). The Pak1 peptide is unusual as it does not contain a conserved Gln residue (Gln211 of gephyrin) which is

Table 2.13 ITC data of wild-type DYNLL1/2 titrated with the dynein intermediate chain1 peptide

Cell(DYNLL)	Injector(Peptide)	N	K_d(μM)	ΔH (kcal mol^{-1})	ΔS (cal mol^{-1} K^{-1})
DYNLL1	IC1-peptide	0.81±0.02	7.6±0.4	-11.9±0.4	-14.9
DYNLL2	IC1-peptide	0.89±0.01	5.0±0.2	-12.7±0.2	-16.6

The raw ITC data are shown in Figure 2.21

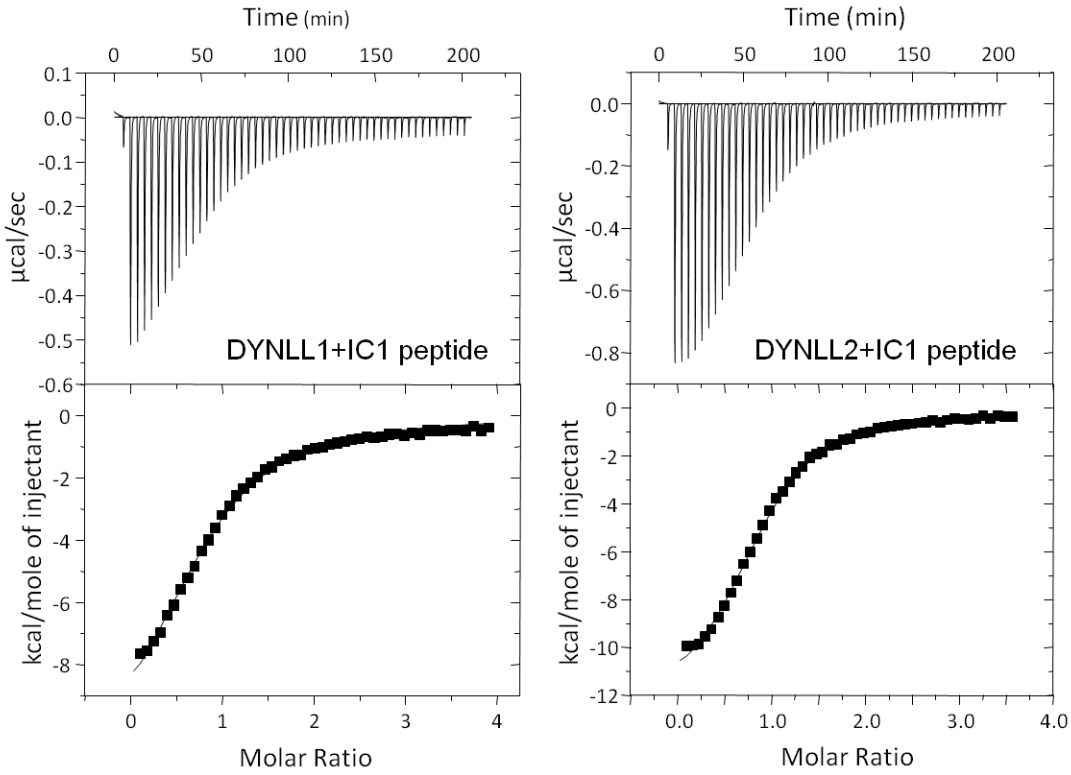

Figure 2.21 Raw ITC data with intermediate chain peptide. The titration results of DYNLL1 (left) and DYNLL2 (right) with the dynein intermediate chain derived peptide.

essential for the DYNLL gephyrin interaction due to its H-bond with the main chain of Lys36. In Pak1 a serine (Ser220) replaces the glutamine at this position, however, a DYNLL1 mutant (K36P) was utilized in the Pak1 complex which would be too short to interact with the main chain nitrogen of Lys36. ITC experiment with the K36P variant of DYNLL1 demonstrate that a canonical peptide with a conserved Gln cannot bind to the DYNLL mutant (Table 2.10), however, I have not investigated whether a peptide containing Ser instead of Glu would bind the DYNLL K36P variant. Additional differences between the gephyrin and Pak1 peptides are Arg215 and Val217 of Pak1 which correspond to Glu206 and Lys208 of gephyrin (Figure 2.20D). The Arg215 substitution contributes to form two additional H-bonds with the side chains of Thr70 and Asp12. At the same time two H-bonds, one between the side chain of Lys208 and His68 and the aforementioned H-bond involving the main chain nitrogen of Lys36 and Gln211 are lost due to the combined replacement of Lys208 with Val217 and Gln211 with Ser220.

The comparison of all available DYNLL-peptide complexes reveals a surprising degree of sequence variation in the peptides, however, the rms deviations between the DYNLL-gephyrin and other known DYNLL-peptide complexes are almost identical irrespective of whether the peptides belong to either of the two recognized consensus motifs. The observed sequence variability is compensated by changes in the peptide-binding groove of DYNLL resulting in a significant level of structural plasticity (Figure 2.22) which is afforded by conformational changes of Lys36, Lys44, Ser64, Tyr 65, His68, Thr70, Phe73, and Tyr75 in DYNLL. While there are many small variations a couple of major changes are obvious: (1) The presence of an Ile in the nNOS at the position corresponding to Val210 of gephyrin leads to a widening of the binding groove (Table 2.8) due to the conformational changes in Tyr75 described above (2). The presence of a longer residue (Glu in the intermediate chain, Ala in the swallow and Pak1

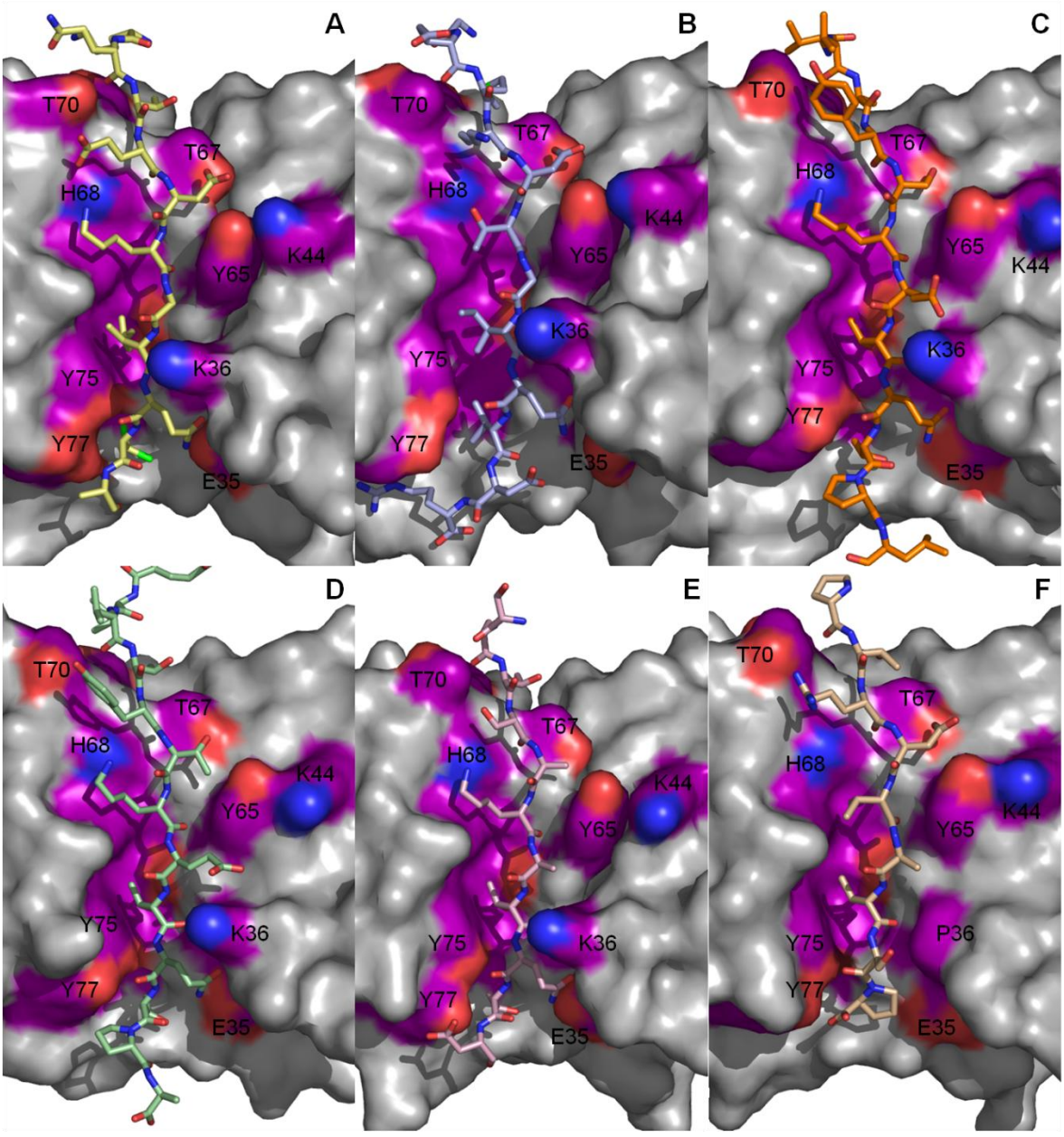

Figure 2.22 Structural changes in DYNLL induced by peptide binding. Surface representation of DYNLL with the bound peptide in stick representation. Residues which differ significantly from the gephyrin complex are highlighted in purple and O-atoms and N-atoms of the side chains are colored in red and blue, respectively. Dimeric forms of (A), (B), and (D) are generated by a crystallographic twofold axis of symmetry. (A) DYNLL2-gephyrin complex, (B) DYNLL1-nNOS complex, (C) DYNLL1-IC1 complex, (D) LC8-IC2 complex, (E) LC8-swallow complex and (F) LC8K36P-Pak1 complex.

peptides) instead of Gly209 in gephyrin (Gly232 in nNOS) pushes the side chain of Tyr65 towards the N-terminal end of the peptide which is obvious when the position of its OH-group is compared to the Nε-atom of Lys44 (3). The Glu in the intermediate chain peptides engages in a tight interaction with Lys36 (H-bond and ionic interaction). At the same time the H-bond between the side chains of Tyr65 and Lys44 is broken (4). In addition, the main chain conformations of the peptides display flexibility, in particular to allow for the incorporation of the larger Glu in the IC peptides at the position corresponding to Gly209 of gephyrin. In general, almost all residues in the peptide from a given target protein contribute to interaction with DYNLLs, thus compensating for substitutions in residues which based on a structure alone would be considered critical.

CHAPTER3:
BIOCHEMICAL CHARACTERIZATION OF GEPHYRIN'S LINKER REGION

I. Introduction

X-ray crystallographic analysis and cross linking experiments revealed that in solution the isolated gephyrin N-terminal G-domain forms trimers (38,43) and that the C-terminal E-domain dimerizes (37,42). Although neither the structure of holo-gephyrin nor the linker region has been defined yet, it is believed that the linker region between the G- and E-domains is highly flexible to allow the G- and E-domains to generate the highly condensed and ordered gephyrin scaffold below the inhibitory postsynaptic membranes.

Recent studies characterized the linker region (also referred to as central domain, C-domain, in the literature) as a binding domain for gephyrin interacting proteins. The linker region contains binding sites for Pin1, DYNLL1/2 and collybistin (Figure 3.1). Furthermore, our collaborator expressed the full-linker domain of gephyrin with the aid of an intein-fusion expression system and showed that the isolated gephyrin linker region forms a tetramer by analytical size exclusion chromatography (unpublished data).

To investigate in more detail the structural features of the linker of gephyrin, constructs encoding only this region, the G-domain with linker (GL) and the linker with the E domain (LE) were cloned and expressed as His_6-tag fusion proteins. Since the full-linker region could not successfully be expressed, the oligomeric states and thermostability of truncated gephyrin proteins including the linker region (GL and LE) were biochemically characterized and the effects on gephyrin upon binding the established gephyrin linker region interaction partner DYNLL were investigated.

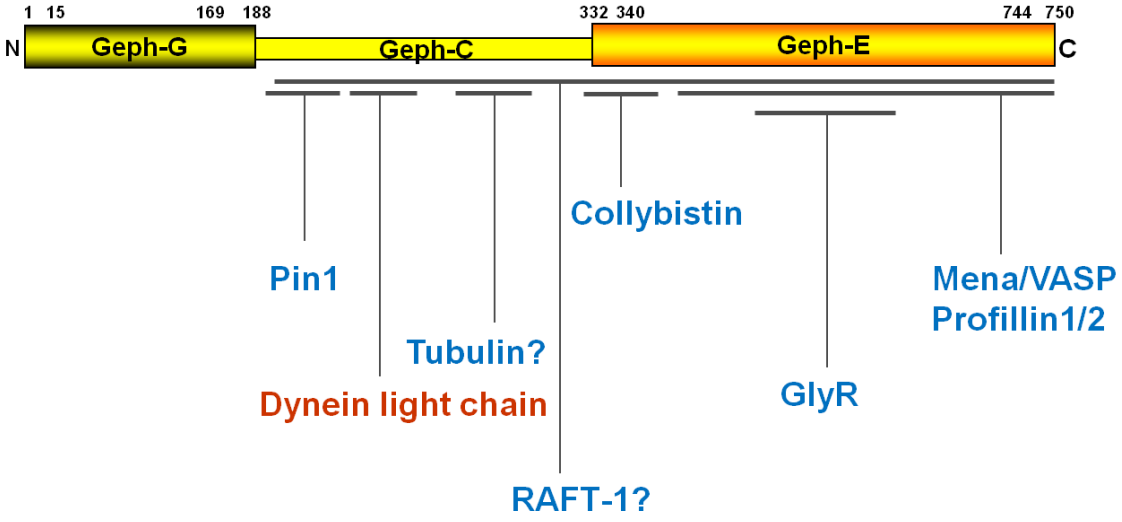

Figure 3.1 Interacting regions on gephyrin for its binding partners. Geph-E has been known to harbor the binding sites for its interaction partners GlyR, Mena/VASP and profillin1/2. The binding motifs of Pin 1, DYNLL1/2 and collybistin are located in gephyrin's linker region (C-domain), while no binding partners have so far been identified which target the G-domain.

II. Materials and methods

A. Molecular cloning

By using site directed mutagenesis, a stop codon was introduced into the Geph-P2 construct after the identified DYNLL binding motif to generate Geph-GL230 which contains one third of the linker region and an N-terminal His_6-tag (G-domain with partial linker). The Geph-G and Geph-GL303 (G-domain with the full-linker) constructs with a C-terminal His_6-tag in the pET28a vector had already been generated by Florian Sauer, a former diploma student in the lab. For the Geph-LE189 protein in which the G-domain is deleted from full-length gephyrin, the gene sequence corresponding to residues 189-750 was sub-cloned into the SapI/XmaI restriction enzyme sites of the pTYB11 vector (IMPACT TM-CN, New England Biolabs) by a former graduate student Dr. Eunyoung Kim.

To generate the linker-E domain constructs, and the linker constructs with an N-terminal His_6-tag, the corresponding regions of the Geph-P2 gene were amplified by PCR. The gene sequence corresponding to the linker-only was inserted into the NdeI/HindIII restriction sites, and linker-E domain constructs was introduced into the NheI/HindIII restriction sites of the pET28a vector.

B. Protein overexpression and purification

For overexpression, Geph-LE189 (pTYB11), Geph-GL303 (pET28a), or Geph-LEs (pET28a) were transformed into *E. coli* BL21 (DE3) cells and Geph-GL230 (pQE30) was cotransformed with pREP4 into *E. coli* BL21 (DE3) cells. Fresh overnight cultures were inoculated in LB medium containing 100 μg/mL of ampicillin or 50 μg/mL of

Table 3.1 Primers' sequence for E domain + linker constructs

Primers	Sequence
LE309-750/pET28a	LE309NheIF / ELHindIIIR
Forward	5' TCCAGGTGCAGCGCTAGCAGCAAGGAGAACA 3'
Reverse	3' CAGGTCGACCCGGAAGCTTTCATAGCCGTCCG 5'
LE208-750/pET28a	LE208NheIF / ELHindIIIR
Forward	5' AGACAGAAGACGCTAGCAAAGGAGTTC 3'
Reverse	5' CAGGTCGACCCGGAAGCTTTCATAGCCGTCCG 5'
LE260-750/pET28a	LE260NheIF / ELHindIIIR
Forward	5' CTCCCACGAGACGCTAGCACAGCCTCCCTTAGCAC 3'
Reverse	3' CAGGTCGACCCGGAAGCTTTCATAGCCGTCCG 5'
LE188-750/pET28a	EL188NheIF / ELHindIIIR
Forward	5' GATTTACCTTCCGCTAGCCCACCACCTCC 3'
Reverse	3' CAGGTCGACCCGGAAGCTTTCATAGCCGTCCG 5'
LE167-750/pET28a	LinkNheIF / ELHindIIIR
Forward	5' GCTCTACCTGCTAGC GACCTTTTACGTGAT 3'
Reverse	3' CAGGTCGACCCGGAAGCTTTCATAGCCGTCCG 5'

Table 3.2 Primers' sequence for linker constructs

Primers	Sequence
Linker208-331/pET28a	LE208NdeIF / Link331stopHind3R
Forward	5’ AGACAGAAGACCATATGAAAGGAGTTC 3’
Reverse	3’ TCAGAGGAAAAGGAGACATAAGCTTCTAGCGATGTCTTC 5’
Linker208-260/pET28a	LE208NdeIF / Link260stopHind3R
Forward	5’ AGACAGAAGACCATATGAAAGGAGTTC 3’
Reverse	3’ GTGCTAAGGGAGGCTGTAAGCTTCTAGTCTCGTGGGAG 5’
Linker260-331/pET28a	LE260NdeIF / Link331stopHind3R
Forward	5’ CTCCCACGAGACCATATGACAGCCTCCCTTAGCAC 3’
Reverse	3’ TCAGAGGAAAAGGAGACATAAGCTTCTAGCGATGTCTTC 5’
Linker167-340/pET28a	LinkerNdeIF / Link340stopHindIIIR
Forward	5’ GCTCTACCTCATATGGACCTTTTACGTGAT 3’
Reverse	3’ CGTAATGAAGGCAAGCTTCTACATAGACGTCAGAGG 5’

kanamycin. The cells were grown at 37°C until the optical density (OD_{600}) reached 1.0 and then IPTG was added to a final concentration of 0.5 mM. After IPTG induction, cells were grown for 16-20 h at 16°C and harvested by centrifugation at 4,000 x g for 30 min. Cell pellets were resuspended in lysis buffer containing 40 mM Tris-HCl (pH 8.0), 300 mM NaCl, 10% glycerol and a protease inhibitor cocktail (Roche), and lysed by passing them twice through a French pressure cell operating at 1,000-1,500 psi. The cleared lysate with the intein-fused Geph-LE189 was incubated with chitin agarose beads (New England Biolabs) for 1 h at 4°C with constant rocking. Beads were washed with 20 column volumes of wash buffer containing 40 mM Tris-HCl (pH 8.0), 1 M NaCl and 1 mM EDTA. The Geph-LE189 protein was eluted with 20 mM Tris-HCl (pH 8.0), 250 mM NaCl and 50 mM DTT, following cleavage of the intein with 50 mM DTT for 2 days at 4°C and then for 2 days at room temperature. Pooled untagged Geph-LE189 was loaded onto a Q sepharose anion exchange chromatography and eluted by using a linear NaCl gradient (Buffer A: 50 mM NaCl, 5 mM DTT, 20 mM Tris-HCl (pH 8.0); Buffer B: same as Buffer A with 1 M instead of 20 mM NaCl). The peak fractions from the Q sepharose were loaded on a Superdex 200 (26/60) column (GE Healthcare), which was pre-equilibrated with 20 mM Tris-HCl (pH 8.0), 250 mM NaCl and 5 mM DTT.

Soluble fractions of Geph-GL230 (pQE30), Geph-GL303 (pET28a), Geph-LE (pET28a) proteins and linker proteins containing a His_6-tag were directly transferred onto a column with Ni-nitrilotriacetic acid (NTA) superflow beads (Qiagen) at 4°C and beads were washed with 20 mM Tris-HCl (pH 8.0), 250 mM NaCl and 10 mM imidazole. After elution with 10 column volumes of buffer containing 20 mM Tris-HCl (pH 8.0), 250 mM NaCl and 250 mM imidazole the resulting protein pool was further purified as described above.

The purity of the final protein batches was analyzed by SDS-PAGE and the protein concentration was calculated by UV spectroscopy at 280 nm on the basis of calculated extinction coefficients of 6970 $M^{-1}cm^{-1}$, 8250 $M^{-1}cm^{-1}$, 21584 $M^{-1}cm^{-1}$ for Geph-GL230, Geph-GL303, Geph-LE189, respectively. All purified proteins were flash frozen in liquid nitrogen after concentrating them to 5~10 mg/ml with Centricon-20 (Millipore).

C. Fluorescence-based thermal shift assay

Gephyrin proteins were diluted with buffer containing 20 mM Tris-HCl (pH 8.0), 250 mM NaCl and 5 mM DTT to 1 mg/mL. The fluorescence change was monitored in the temperature range from 20°C to 90°C using a MaxPro real time PCR cycler (STRATAGENE). SYPRO Orange was diluted 2500-fold and added to the protein (25 µg total).

D. Analytical size exclusion chromatography

Geph-GL, or Geph-LE in complex with DYNLL1/2, and Geph-GL, Geph-LE, Geph-E or Geph-G in the absence of DYNLLs were diluted to a final concentration of 0.15-1 mg/mL. 500 µL of each protein sample was injected onto a Superdex 200 10/300 analytical size exclusion chromatography column (GE Healthcare) equilibrated with buffer containing 20 mM Tris-HCl (pH 8.0), 250 mM NaCl and 5 mM DTT.

The column was calibrated with a molecular weight standard (GE Healthcare) containing blue dextran (2000 kDa, V_o), ferritin (440 kDa), catalase (232 kDa), aldolase (158 kDa), ovalbumin (43 kDa), chymotrypsinogen (25 kDa), ribonuclease A (13.7 kDa) in order to estimate the molecular mass of the analyzed proteins.

E. Analytical Ultracentrifugation (AUC)

Sedimentation velocity (SV) experiments were performed by using a Beckman XL-I Optima analytical ultracentrifuge (Beckman Coulter, Fullerton, CA) with an eight-hole An-50 Ti rotor at 40,000 rpm and 20°C. Before each experiment, the samples were dialyzed overnight at 4°C against a buffer containing 10 mM Tris-HCl (pH 8.0), 250 mM NaCl and 1 mM β-mercaptoethanol. Data were collected using absorbance optical detection at a wavelength of 280 nm and were analyzed using the c(s) continuous distribution of Lamm equation solutions with the program SEDFIT (www.analyticalultracentrifugation.com). The c(s) analysis was performed with regularization at a confidence level of 0.68-0.95 and a floating frictional ratio (f/f_o), time-independent noise, baseline, and meniscus position. The c(s) distribution was transformed to the c(M) distribution. The partial specific volume of the proteins as well as the density and the viscosity of the buffer solution were calculated with the program SEDNTERP (www.jphilo.mailway.com).

III. Results and discussion

A. Secondary structure and folding prediction of the gephyrin linker region, and design of truncated gephyrin constructs

The secondary structure prediction (Figure 3.2) suggests that the linker region of gephyrin is largely unstructured, however, a consensus prediction gives small regions of defined secondary structure elements including two α-helices for residues 212-219 (CEEEEEEK) and 234-243 (HITAAALAAK), and two short β-strands between residues 248-250 (IIS) and 253-255 (VQV). Additionally, two α-helices are predicted at the end of the linker region which include residues 311-316 with the sequence ENILRA and 321-329 (VDITKVARR) prior to the E-domain. The Fold Index program (Figure 3.3) shows that the region around residues 240-260 could be folded.

Based on these predictions, truncated gephyrin constructs have been engineered (Figure 3.4) to investigate whether this region of the linker either forms secondary structure in solution or contributes to oligomerization. GL230 contains the G-domain with a third of linker region and GL303 has the G-domain with almost the complete linker except for the two predicted helices before the start of the E-domain. The linker-E domain constructs, LE (309-750) features the E domain with two predicted helices, LE (260-750) harbors the E domain with one half of the linker, and LE (208-750) contains the E-domain with all possible structured regions of the linker region. LE (167-750) is the longest LE construct, and it contains the C-terminal end of Geph-G which shows structural differences from that of MogA.

Linker only constructs were also made. The first short linker construct (208-260) includes the first two predicted α helices and two β strands. The long linker construct (208-331) in addition includes the region devoid of predicted secondary structure and the

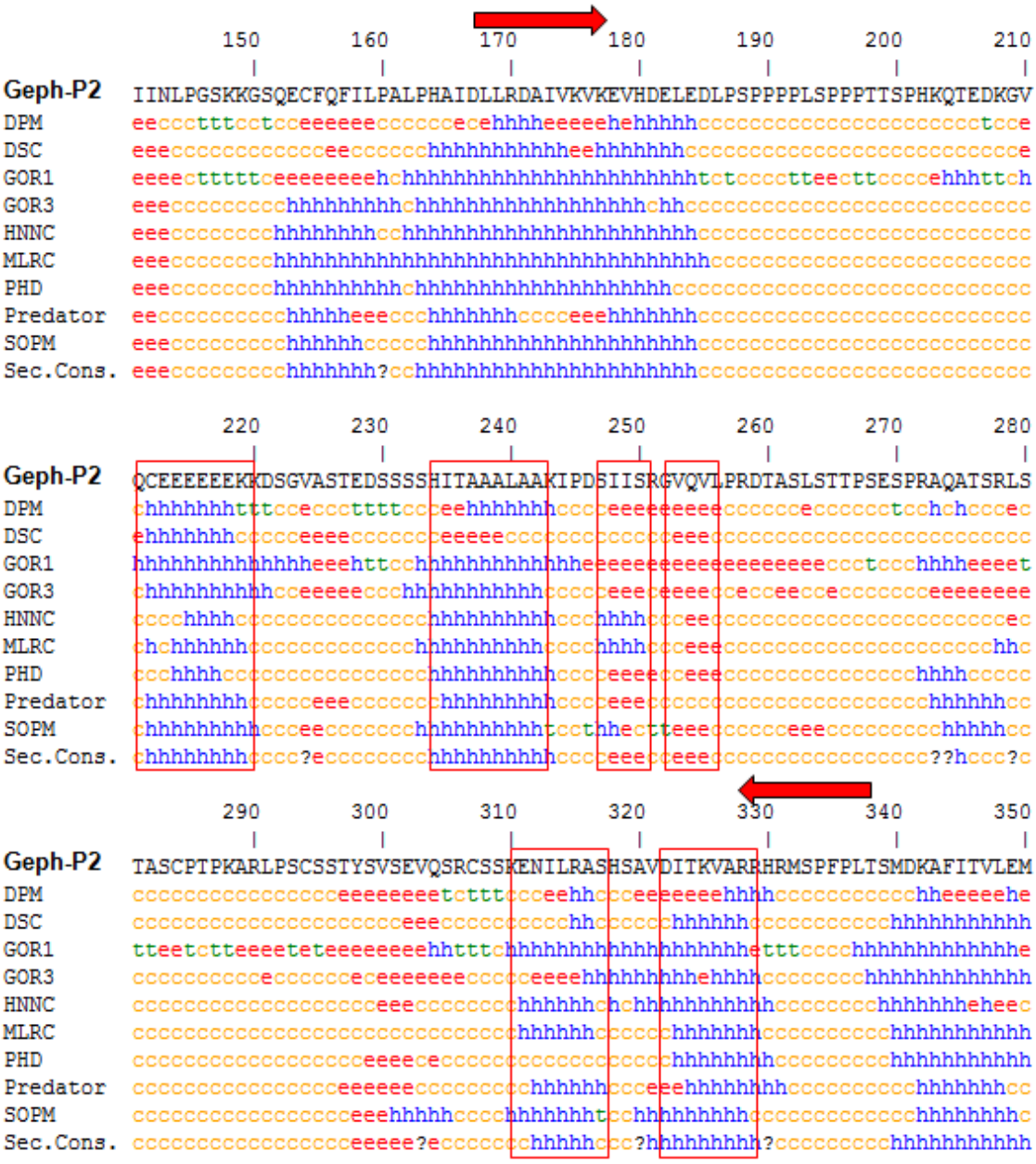

http://npsa-pbil.ibcp.fr/cgi-bin/npsa_automat.pl?page=/NPSA/npsa_seccons.html

Figure 3.2 Secondary structure predictions of gephyrin's linker region. The linker region is indicated with red arrows and is comprised of residues 168 to 340. The consensus predicted secondary structures are shown in red colored boxes. h: α-helix, e: extended conformation (β-strand), c: Random coli, t: β-turn.

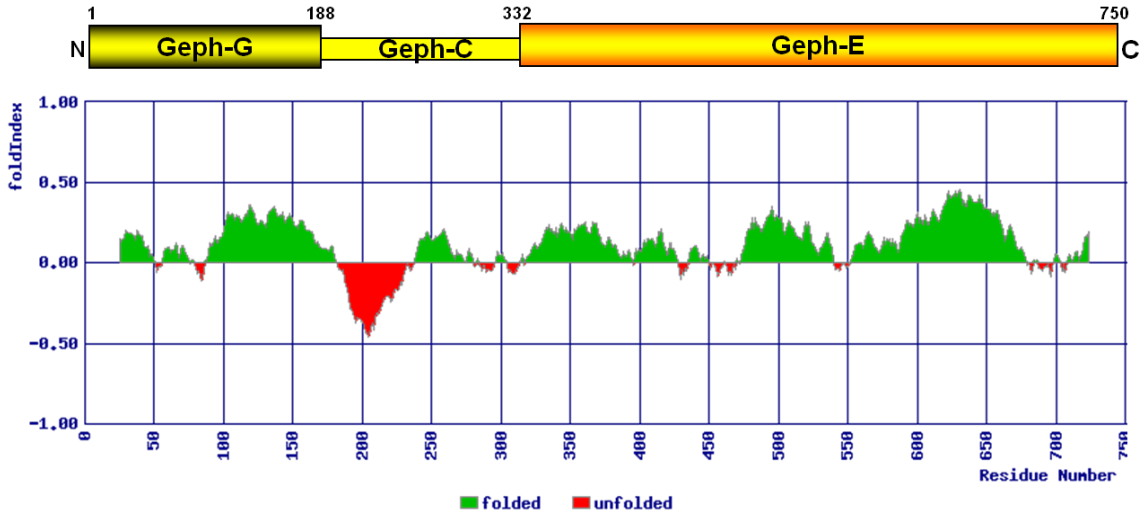

http://bioportal.weizmann.ac.il/fldbin/findex

Figure 3.3 Fold index prediction for full-length gephyrin. The N-terminal half of the linker has a high probability of being unfolded, however, the C-terminal region has a significant probability of being folded.

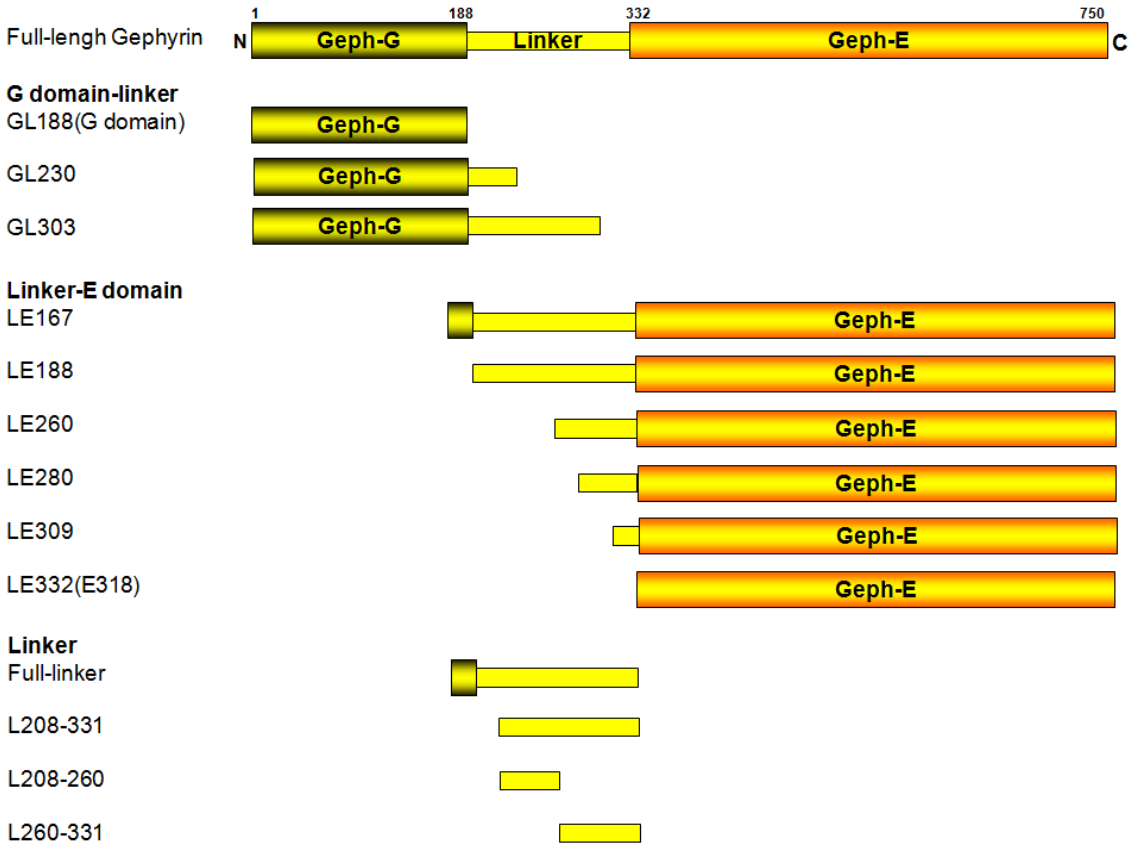

Figure 3.4 Domain architectures of truncated gephyrin proteins.

two C-terminal α helices. The second short linker construct (260-331) contains the C-terminal half of the longer linker. However, neither the full- linker region nor the (260-331) shorter linker construct could be stably expressed as His_6-tagged fusion proteins presumably due to their high sensitivity to proteolytic degradation.

B. Fluorescence-based thermal shift assay

First, the thermal stability of the various gephyrin proteins was analyzed by fluorescence changes. The melting temperature (T_m) of Geph-G is 79°C while that of Geph-E is 59°C. Full-length gephyrin has two major unfolding transitions with T_m-values of 61°C and 79°C which apparently correspond to the E- and G-domains, In addition, a minor transition is observed around 45°C (Figure 3.5) which might be due to the linker region. The G-linker construct shows the same thermostability as the G-domain with a T_m of 79°C, however, the stability of the linker-E domain proteins is slightly higher than that of the isolated E-domain which suggests that the linker region influences the stability of the E-domain. A more thorough analysis using the various LE-constructs reveals that residues 309-317 are mostly responsible for the stabilization of the E-domain. According to the secondary structure prediction this region features one of the predicted α-helices at the C-terminal end of the linker. Although proteins containing the linker region showed a small unfolding transition around 45 to 50°C which is highlighted by the red arrows in Figure 3.5, all truncated linker proteins did not show any SYPRO fluorescence signal upon an increase in temperature indicating that they cannot independently fold. A further characterization of the truncated linker proteins has therefore not been conducted.

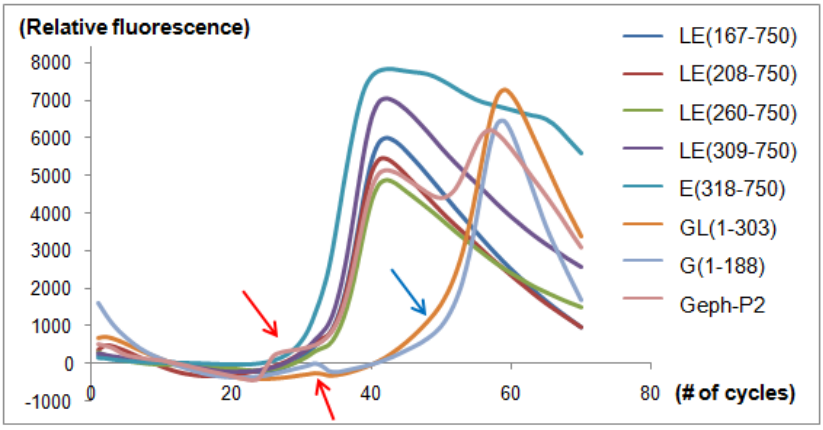

Proteins	T_m(°C)
LE(167-750)	62.0
LE (208-750)	62.0
LE (260-750)	62.0
LE (309-750)	61.0
E (318-750)	59.0
GL(1-303)	79.0
G(1-188)	79.0
Geph-P2	61.0/79.0

Figure 3.5 Thermostability of gephyrin wild-type and truncated proteins. The presumed unfolding transition of the linker region is highlighted with red arrows and the difference between Geph-G and G with the full linker with a blue arrow.

C. Oligomeric states of truncated gephyrin

To determine whether the fused linker region affects the oligomerization of Geph-G and Geph-E, size exclusion chromatography studies were performed (Figure 3.6). These studies were motivated by the observation that the isolated linker has the ability to oilgomerize since it apparently runs as a tetramer in size exclusion chromatography experiments (Günter Schwarz, personal communication). As reference points the isolated G- and E-domains as well as full-length gephyrin were analyzed. The masses deduced for the G- and E-domains of 79 kDa and 104 kDa, respectively, correspond to a trimer in the case of the G-domain and a dimer for the E-domain in agreement with published data. In contrast, full-length gephyrin displayed a mass of 540 kDa which is larger than the previously estimated mass of 420 kDa. With the larger mass of 540 kDa it appears as if gephyrin forms a hexamer, however, as discussed earlier, the elongated shape of the molecule is responsible for a larger than expected mass which is already reflected in the published value of 420 kDa. The additional increase from 420 kDa to 540 kDa cannot be explained at present.

Interestingly the G-domain with a full-linker region displayed a mass of 435 kDa which is significantly larger than the value expected if the trimer interface of the G-domain was the only site for oligomerization. If one considers the putative tetramerization of the linker region observed by our collaborators the mass of 435 kDa could possibly be explained through the combination of two sequential oligomerizations involving the trimerization of G-domain and the tetramerization of linker. At the same time the E-domain with a full-linker eluted from the column at a position corresponding to a mass of 484 kDa which approximately corresponds to an octamer. This oligomeric form could again be explained through the known dimerization of Geph-E and the tetramerization of the linker region. A progressive truncation of the linker region, in

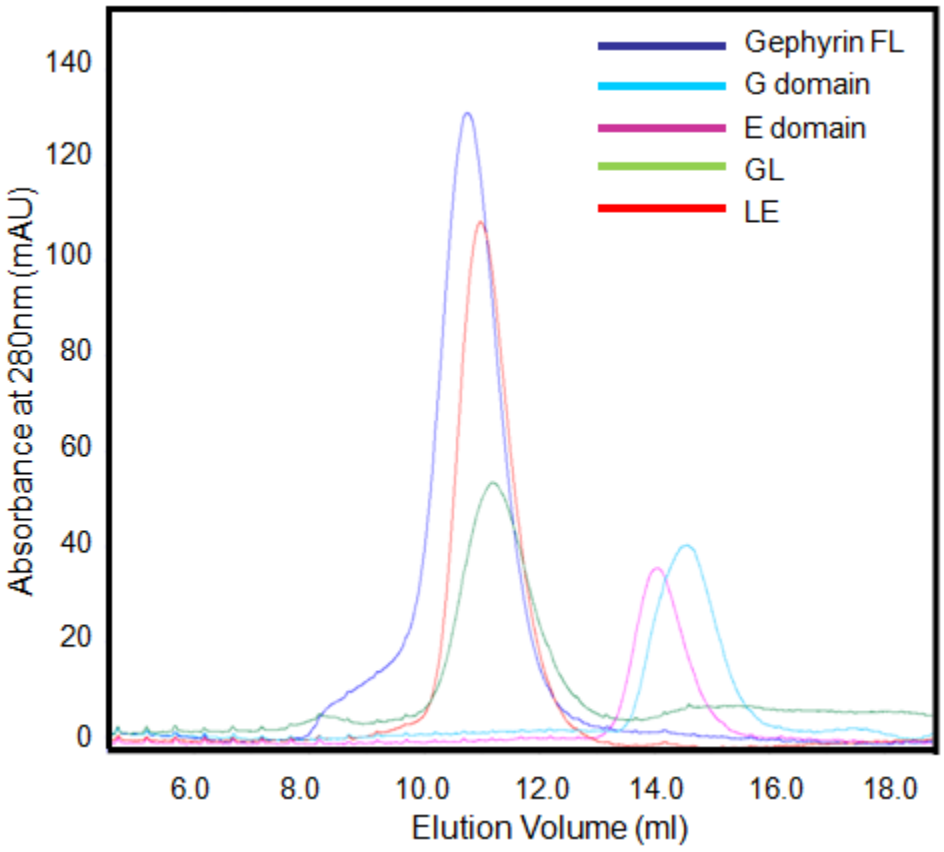

Figure 3.6 Size exclusion chromatography results of gephyrin wild-type and truncated mutants. Full-length gephyrin (blue), Geph-G (cyan), Geph-E (purple), Geph-GL (green), and Geph-LE (red).

particular this can be seen for the various LE constructs, results in a reduction of the calculated oligomeric state, eventually approaching the known G-domain trimer and E-domain dimer values (Table 3.3). Although it remains unclear at the molecular level which regions of the linker are responsible for the observed oligomerization residues167-260 seem to play an important role as do residues between 260 and 330. Within residues 167-260 the C-terminal end of the G-domain encompassing residues 167-188 appears to play a more significant role than residues 208-260. The latter region harbors most of the predicted secondary structure elements of gephyrin.

In addition to analytical size exclusion chromatography the molecular masses of the different proteins were estimated by native gel electrophoresis. On 5-20% native gradient PAGE gels the major protein bands of Geph-E and Geph-G show masses of ~70 kDa and ~100 kDa, respectively, corresponding to the expected dimer and trimer. Furthermore, full-length gephyrin behaves like a trimer under these conditions (Figure 3.7B) in agreement with earlier assumptions and in contrast to the size exclusion chromatography results reported here. The positions of the bands corresponding to the linker-E proteins (LE167, LE188, LE208 and LE260) all approximately match that of full-length gephyrin with the exception of LE (309-750) which shows two bands, of which the prominent band has a faster mobility and the minor band runs approximately like the other E-domain constructs (Figure 3.7A). A similar behavior with two bands is also observed for Geph-E where the major band runs at a mass corresponding to the E-domain dimer whereas the larger and in this case very minor band runs approximately at a mass of ~200 kDa. The G domain with a partial linker region (GL230) migrated at ~90 kDa which would correspond to a trimer (Figure 3.7C), whereas the GL303 construct shows a diffuse and low intensity band with a mass of ~240 kDa. Although the masses for LE and GL constructs deduced from native gels are generally smaller than those

Table 3.3 Size exclusion chromatography data of full-length and truncated gephyrin proteins

Protein	Theoretical Monomer Mw (kDa)	Experimental Mw (kDa)	Oligomer
Linker-E-domain proteins			
LE167	66	484	7.5(2x4)
LE188	63	374	5.9
LE208	61	320	5.3
LE260	55	189	3.4
LE309	51	128	2.5
E318	46	104	2.3(2x1)
G-domain-linker proteins			
GL303	36	435	12.2(3x4)
GL230	27	199	7.4
G	24	79	3.3(3x1)
Full-length gephyrin			
Geph-P2	83	524	6.3(3x2)

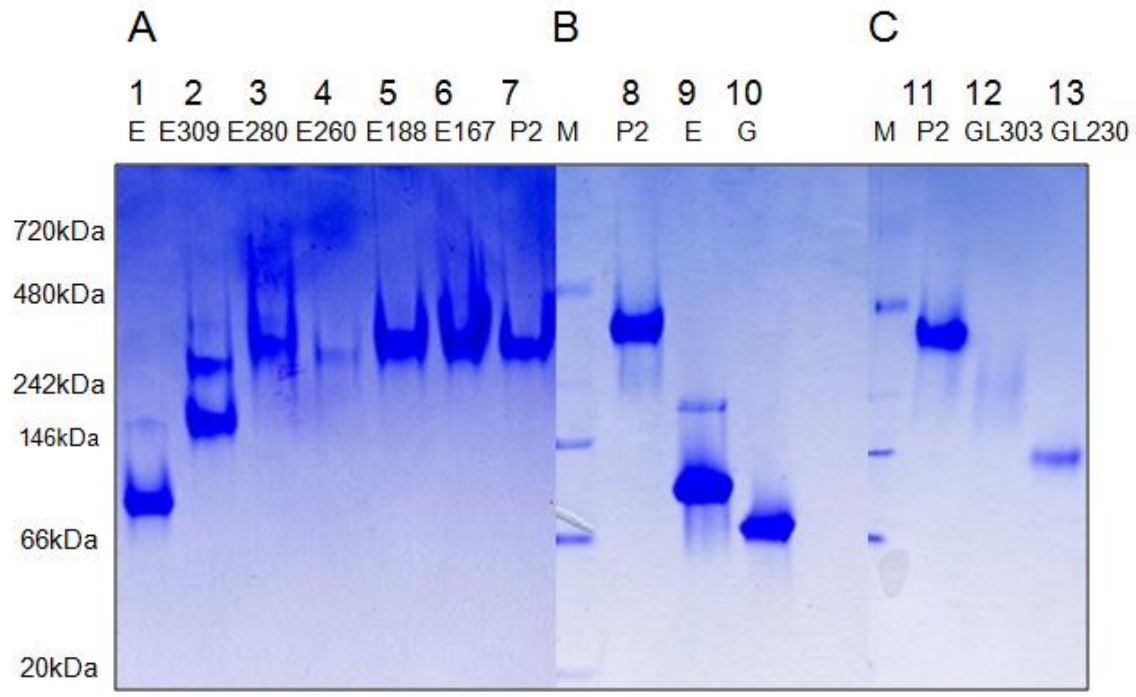

Figure 3.7 Migration of full-length and truncated gephyrin proteins on native gels. All samples (10 μg) were loaded on native PAGE gradient gels (5-20%) and visualized with Coomassie Brilliant Blue staining. The molecular weights were estimated with a native standard protein marker (Invitrogen).

observed by size exclusion chromatography experiments, they are larger than what would be expected on the basis of the monomer mass and the E-domain dimerization or G-domain trimerization with the exception of GL230. These observations again indicate that the linker, in additiol to the G- and E-domains has the ability to oligomerize, however, the precise oligomeric state cannot be deduced at present. One possible mechanism to be considered could involve the formation of an intermolecular disulfide bond involving Cys284 and Cys294 located in the linker region. In fact size exclusion chromatography experiments with the LE-construct show an even higher estimated molecular mass in buffers without DTT (data not shown), nevertheless, the masses reported in Table 3.3 were deduced in the presence of 5 mM DTT where disulfide bond formation should not occur.

Additionally, the oligomeric state of the truncated proteins was analyzed by SV analytical ultracentrifugation (Table 3.4). The resulting molecular masses of Geph-G and Geph-E are 83 kDa and 91 kDa which correspond to the dimer and trimer, respectively. Truncated versions of gephyrin with the full-linker did not behave well as they tend to aggregate. In the case of the E-domain with a full linker, this sample shows two minor absorbance peaks corresponding to a dimer and tetramer.

D. Does DYNLL binding influence the oligomeric state of GL and LE?

As mentioned earlier no change in the oligomeric state of full-length gephyrin occurs upon binding to DYNLLs as judged by size exclusion chromatography and dynamic light scattering. In contrast, the elution volume of the full-linker with E domain construct is retarded when DYNLLs interact with its linker region on the basis of size exclusion chromatography experiments. In complex with DYNLL the LE construct elutes

Table 3.4 Sedimentation velocity analytical ultracentrifugation data of truncated gephyrin proteins in the absence and presence of DYNLLs

Protein	Theoretical Monomer mass (kDa)	Theoretical Oligomeric state	Experimental Mw (kDa)
G domain	24	Trimer (72 kDa)	82.4
E domain	46	Dimer (92kDa)	90.8
G-full linker	36	Trimer (108 kDa)	-*
Full linker-E domain	63	Dimer (126 kDa)	109/219
G-partial linker	27	Trimer (81 kDa)	92.6
Full linker-E + DYNLL1	63+10	Dimer+Dimer 126+20	36.8 /190
G-full linker + DYNLL1	36+10	Trimer+Dimer 108+20	-
G-partial linker + DYNLL1	27+10	Trimer+Dimer 81+20	93.2
G-partial linker + DYNLL2	27+10	Trimer+Dimer 81+20	112

* indicates experiments which could not be analyzed due to aggregation.

G-partial linker contains residues 1-230.

at a volume corresponding to a mass of 440 kDa in contrast to a mass of 484 kDa in the absence of DYNLL (Table 3.5). The GL construct in the presence of DYNLL elutes at the same volume as the same construct in the absence of DYNLL corresponding to a mass of 420 kDa. Given that there are now two components, gephyrin and DYNLL which can independently oligomerize both molecular masses can be explained by more than one oligomeric assembly. Despite the difficulties in assigning an oligomeric state to these masses these results indicate that there is either a substantial conformational change which gives rise to the delayed elution from the column (this is clearly the case for the LE-DYNLL complex but also for the GL-DYNLL complex which due to the added DYNLL should elute earlier), or due to a change in the oligomeric state upon binding DYNLLs.

To distinguish whether there is a change in the oligomeric state or a conformational change of truncated gephyrin upon binding to DYNLL as observed in the size exclusion chromatography experiments, SV analytical ultracentrifugation experiments were conducted. Unfortunately, AUC could not provide any information about the GL and LE constructs, neither in the absence nor in the presence of DYNLLs which is presumably due to protein instability at 20°C (Table 3.4). Only data for the complex of GL230 and DYNLL could be collected which show that a G-domain trimer with a partial linker interacts with a dimer of DYNLL without any change in the oligomeric state.

Since it was not possible to obtain information about the oligomeric state of truncated gephyrin containing a full-linker (GL and LE), which is presumably due to proteolytic instability of the linker, full-length gephyrin on its own and in complex with DYNLL have been subjected to SV analytical ultracentrifugation experiments.

Table 3.5 Size exclusion chromatography data of truncated gephyrin proteins in complex with DYNLL1/2

Protein	Theoretical Monomer Mw (kDa)	Experimental Mw (kDa)
G-full linker (GL)	36	424
GL+DYNLL1	36+10	426
GL+DYNLL2	36+10	420
Full linker-E (LE)	65	484
LE+DYNLL1	65+10	430
LE+DYNLL2	65+10	454

Preliminary analysis with the SEDFIT program showed a somewhat surprising result since full-length gephyrin was observed predominantly in a dimeric form, plus additional peaks corresponding to monomeric, and possibly tetrameric and hexameric forms (Figure 3.8). Upon binding to DYNLLs, gephyrin tends to be more homogeneous since the monomeric, tetrameric and hexameric forms decreased in intensity.

G. Crystallization of the G domain with partial linker

Various truncated forms of gephyrin in the absence or presence of DYNLLs have been subjected to crystallization experiments utilizing the sitting drop vapor diffusion method with the aid of a crystallization robot and the hanging drop vapor diffusion method in manual setups. Most of these attempts were unsuccessful except for the GL230 fragment in complex with DYNLL1. The complex was prepared by purification through size exclusion chromatography after incubation of the GL230 and DYNLL1 proteins at a molar ratio of 1 to 2 at 4°C for 1 h. The resulting complex at a concentration of 5 mg/mL could be crystallized as very thin needles against a mother liquor containing 0.1 M sodium cacodylate (pH 6.5), 0.4 M sodium acetate and 18% w/v PEG 4000 at 18°C by the hanging drop vapor diffusion method (Figure 3.9). The crystals were reproducible, however, the quality of crystals could not be improved and these small crystals easily dissolved during freezing. Therefore diffraction experiments could not be carried out.

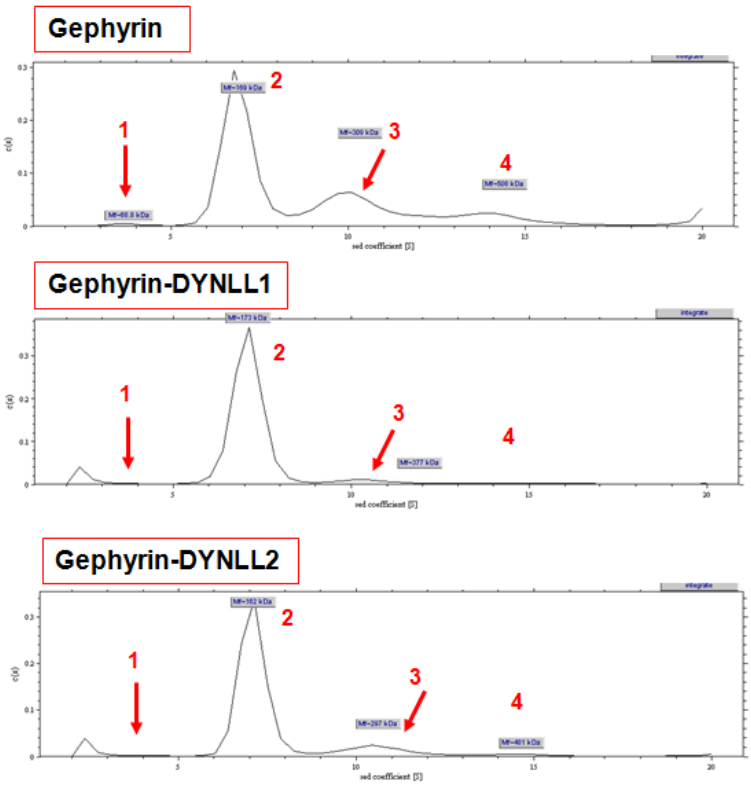

Peak #	Experimental Mw (KDa)	# of monomer
1	68.8	0.8
2	163	2.0
3	309	3.7
4	508	6.0

Peak #	Experimental Mw (KDa)	# of monomer
1	-	-
2	173	1.8
3	377	4.0
4	-	-

Peak #	Experimental Mw (KDa)	# of monomer
1	-	-
2	162	1.7
3	297	3.2
4	481	5.1

Figure 3.8 Sedimentation velocity analytical ultracentrifugation results of full-length gephyrin in the absence and presence of DYNLL1/2.

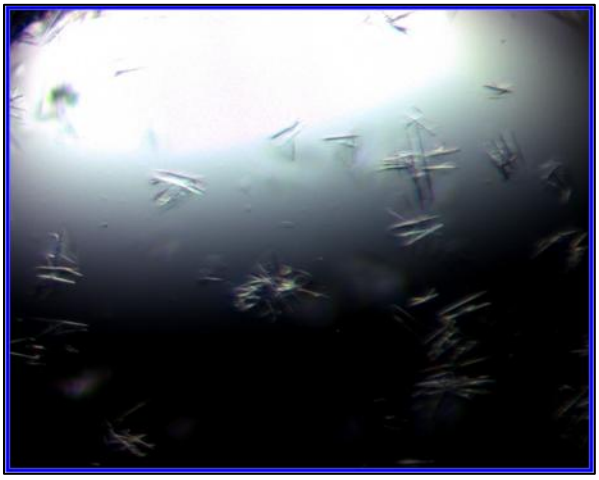

Figure 3.9 Crystals of GL (1-230) in complex with DYNLL1.

CHAPTER4:

CONCLUDING DISCUSSION

I. The implications of the DYNLL-gephyrin interaction

The structural and biophysical studies presented here demonstrate that gephyrin interacts with both DYNLL1/2 in a similar manner although the two proteins differ in six amino acid residues. Currently the functional differences between the two isoforms *in vivo* are not clear, however, DYNLL2 is more thermostable than DYNLL1, and DYNLL1/2 have different predicted phosphorylation sites due to their different primary structures. For example, Tyr65 is a predicted phospho-tyrosine site in DYNLL1. This residue is located near the dimer interface and its substitution with Asp induces a dimer to monomer transition in DYNLL1, whereas the Y65D mutant of DYNLL2 continues to form a stable dimer. DYNLL2 harbors an additional predicted phospho-tyrosine site at Tyr32, due to the presence of Met 29 which replaces Leu29 in DYNLL1. The Drosophila DYNLL1 homologue LC8 shows the same predicted Tyr-phosphorylation as DYNLL1, however, the phosphomimetic Y65E mutant of LC8 forms a dimer and behaves like the wild-type in pull-down experiments with the IC fragment (96). Interestingly, the thermostability of LC8 (T_m=76°C) is similar to DYNLL2's (T_m=71.5°C) (71) and actually LC8 shows a higher sequence identity to DYNLL2 than DYNLL1. A previous study demonstrated that the amino acid at position 41 which is a histidine in DYNLL1 and a tyrosine in DYNLL2 is important for DYNLL1/2's selective localization to either the dynein or myosin motor (67). If the gephyrin-GlyR complex is transported through both microtubule and actin-based motor systems *in vivo,* the selective binding to either DYNLL1 or DYNLL2 would be determined by DYNLL and could be influenced by phosphorylation.

In vitro a DYNLL dimer does not bind to two different gephyrin trimers. Rather a DYNLL dimer binds to a gephyrin trimer while leaving the third binding site unoccupied

according to our ITC, DLS and size exclusion chromatography experiments. Therefore, at least *in vitro* DYNLLs do not directly induce any change in the oligomeric state of gephyrin. However, known DYNLL target proteins tend to be dimeric when bound to DYNLLs (76). Along this line one could speculate that DYNLL-induced changes might influence gephyrin in a way that would lead to tighter binding with the GlyR, or that an oligomerization of gephyrin requires the simultaneous presence of the receptor. CD experiments with the entire linker region of gephyrin in the presence and absence of DYNLL1/2 by our collaborator show that DYNLL1/2 do not induce a defined structure in the linker region (Günter Schwarz, unpublished data).

As described above, the gephyrin-derived peptide which contains the sequence GVQCE and hence belongs to the first canonical DYNLL binding motif (G(I/V)QV(D/E)) has near identical affinity for DYNLL1/2 compared to the peptide from the dynein intermediate chain, which with its KETQT sequence belongs to the second canonical DYNLL binding motif (K/R)XTQT despite the prominent Gly→Glu substitution. Therefore, the question remains as to how DYNLLs bind at the same time to two different target proteins, the cargo (gephyrin) and dynein intermediate chain. It has recently been speculated that DYNLLs act as dimerization hubs where the dimeric DYNLLs induce dimerization in the partner proteins which involves a cooperative process where an initial lower affinity binding to the ligand by the first DYNLL monomer is followed by a higher affinity binding in the second binding site (63). How gephyrin with its trimeric architecture fits into this scheme is not clear. However, for gephyrin a scenario is possible where the binding site in this monomer could interact asymmetrically with a DYNLL dimer and the remaining binding site of this monomer could then interact with an intermediate chain of the dynein motor, thus linking the cargo (gephyrin) to the motor (Figure 4.1). Alternatively, one could speculate that *in vivo* higher oligomeric forms of gephyrin are

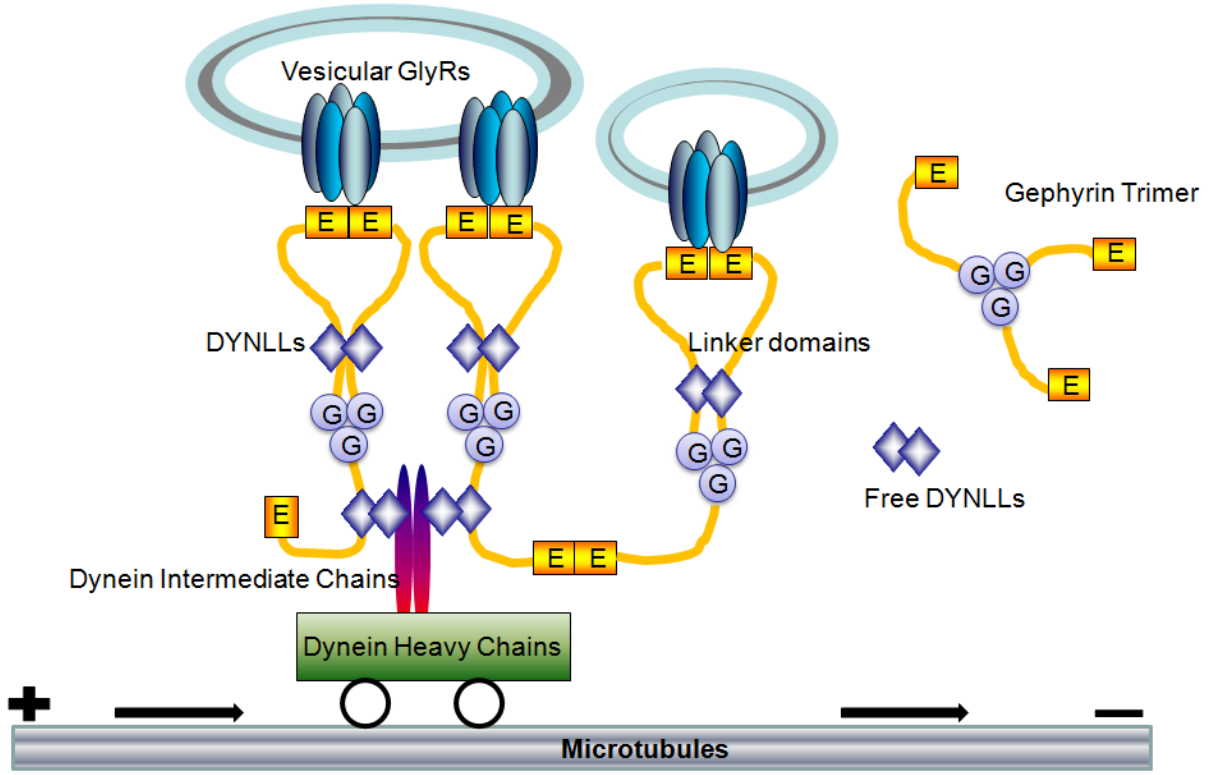

Figure 4.1 Model of the GlyR-gephyrin-dynein motor complex. DYNLL is postulated to act both as a dimerization hub for gephyrin and as an adaptor to the dynein motor via simultaneous binding to gephyrin and the intermediate chains.

induced by DYNLL binding despite the results presented here which only reveal trimeric gephyrin in the presence of DYNLL. Further experiments are necessary to clarify this issue.

II. Functional significance of the linker region and gephyrin oligomerization

Although bacterially expressed full-length gephyrin has been shown to form predominately a trimer (42,44), ammonium acetate treated gephyrin can be reversibly assembled into dimers, tetramers and hexamers as demonstrated by electrospray ionization mass spectroscopy (42) and also a hexameric gephyrin has been identified in blue native PAGE after recombinant expression in Xenopus oocytes (97). Even *in vitro* without its interacting partners, depending on the experimental conditions, there are various oligomeric states of gephyrin. In contrast, several independent experimental methods including crystallographic analysis and biochemical experiments have consistently revealed that the isolated Geph-G and Geph-E domains form trimers and dimers, respectively. Based on this observation gephyrin has been proposed to assemble into a hexagonal lattice which would be located below the postsynaptic membrane.

Experiments have been conducted that analyze the oligomerization behaviour of the G and E-domains in the presence of either the full-length linker or fragments thereof. These experiments are complicated by the fact that the linker is sensitive to proteolytic degradation and hence expression and purification of the proteins is difficult. In addition, purified proteins are still susceptible to proteolytic degradation. Despite these experimental difficulties a picture has emerged which is consistent with an additional oligomerization site in the linker region since the GL and LE constructs differ in their

oligomeric state from the isolated G- and E-domains. It seems that when the influence of at least either trimerization by G-domains or dimerization by E-domains was removed the oligomerization potential of linker region has been increased.

A previous study showed that the LE construct containing the complete linker tends to be predominately in a monomeric form, indicating that the linker region inhibits dimerization of the E-domain (98). However, truncated gephyrins including the linker region show that the E-domain is thermostabilized by the C-terminal end of the linker region. Dissociation of an E-domain dimer with a fused-linker region has not been observed. In contrast, the possible tetramerization of the linker induced a higher oligomeric state of LE which could be octameric.

On the basis of size exclusion chromatography and the migration pattern in native gels, the linker region might harbor an additional oligomerization domain which would be located between residues 167 to 188, toward the N-terminal end of the linker region and the C-terminal end of the G-domain. Without the remaining linker region (residues 190-310), however, the oligomerization potential of residues 167-188 might be too weak to form independent oligomers on the basis of the results of G-domain with a partial linker which like the G-domain trimerizes. Residues 190 to 310 include the predicted secondary structured regions as well as the unstructured regions, located in between them. According to one possible scenario the predicted two α helices and two β strands between 210-260 of the linker form a small structured domain which might be involved in oligomerization of the linker region, together with residues 167-188. At the same time it cannot be ruled out that the predicted unstructured region of the linker could also be important for oligomerization. Clearly a further characterization of the truncated linker proteins is necessary. For example various truncated linker proteins rather than the full-length linker protein could be expressed and subjected to biochemical and

biophysical experiments since expression and purification of the full-length linker described here was not successful.

Currently it is not clear how binding of DYNLL in the linker of gephyrin might regulate dimerization of E-domain or oligomerization of the linker region. Recent studies support the notion that proteins binding to the linker can modulate the binding affinity of Geph-E to GlyRs. In a phosphorylation dependent manner, Pin1 induces a conformational change of gephyrin and enhances the binding affinity of gephyrin to GlyRs (45). The binding motifs for Pin1 and DYNLL in gephyrin are located near the N-terminus of the linker region in a presumably unstructured region prior to the predicted secondary structured elements following the C-terminal end of G-domain (residues 167-188). Residues 167-188 contain one of 4 hydrophobic amino acid residues which are located at the Geph-G trimer interface and are important for trimerization. A possible mechanism is that binding by gephyin-interacting proteins in the linker region would influence the G-domain trimerization through the C-terminal residues of the G-domain. Therefore, binding proteins on the linker region might regulate indirectly the function of Geph-E through directly controlling Geph-G. In cases when the oligomerization potential of either G- or E-domains is modulated by its binding partners, the remaining linker region would regulate the dynamics of gephyrin at inhibitory synapses.

REFERENCES

1. Kneussel, M., and Loebrich, S. (2007) **Trafficking and synaptic anchoring of ionotropic inhibitory neurotransmitter receptors.** *Biol Cell* **99**, 297-309
2. Moss, S. J., and Smart, T. G. (2001) **Constructing inhibitory synapses.** *Nat Rev Neurosci* **2**, 240-250
3. Maas, C., Tagnaouti, N., Loebrich, S., Behrend, B., Lappe-Siefke, C., and Kneussel, M. (2006) **Neuronal cotransport of glycine receptor and the scaffold protein gephyrin.** *J Cell Biol* **172**, 441-451
4. Setou, M., Seog, D. H., Tanaka, Y., Kanai, Y., Takei, Y., Kawagishi, M., and Hirokawa, N. (2002) **Glutamate-receptor-interacting protein GRIP1 directly steers kinesin to dendrites.** *Nature* **417**, 83-87
5. Setou, M., Nakagawa, T., Seog, D. H., and Hirokawa, N. (2000) **Kinesin superfamily motor protein KIF17 and mLin-10 in NMDA receptor-containing vesicle transport.** *Science* **288**, 1796-1802
6. Miki, H., Okada, Y., and Hirokawa, N. (2005) **Analysis of the kinesin superfamily: insights into structure and function.** *Trends Cell Biol* **15**, 467-476
7. Vallee, R. B., Williams, J. C., Varma, D., and Barnhart, L. E. (2004) **Dynein: An ancient motor protein involved in multiple modes of transport.** *J Neurobiol* **58**, 189-200
8. Bridgman, P. C. (2004) **Myosin-dependent transport in neurons.** *J Neurobiol* **58**, 164-174
9. Rudolph, U., and Mohler, H. (2006) **GABA-based therapeutic approaches: GABAA receptor subtype functions.** *Curr Opin Pharmacol* **6**, 18-23
10. Smith, M. J., Pozo, K., Brickley, K., and Stephenson, F. A. (2006) **Mapping the GRIF-1 binding domain of the kinesin, KIF5C, substantiates a role for GRIF-1 as an adaptor protein in the anterograde trafficking of cargoes.** *J Biol Chem* **281**, 27216-27228
11. McGuire, J. R., Rong, J., Li, S. H., and Li, X. J. (2006) **Interaction of Huntingtin-associated protein-1 with kinesin light chain: implications in intracellular trafficking in neurons.** *J Biol Chem* **281**, 3552-3559
12. Harjes, P., and Wanker, E. E. (2003) **The hunt for huntingtin function: interaction partners tell many different stories.** *Trends Biochem Sci* **28**, 425-433
13. Wang, H., Bedford, F. K., Brandon, N. J., Moss, S. J., and Olsen, R. W. (1999) **GABA(A)-receptor-associated protein links GABA(A) receptors and the cytoskeleton.** *Nature* **397**, 69-72
14. Keller, C. A., Yuan, X., Panzanelli, P., Martin, M. L., Alldred, M., Sassoe-Pognetto, M., and Luscher, B. (2004) **The gamma2 subunit of GABA(A) receptors is a substrate for palmitoylation by GODZ.** *J Neurosci* **24**, 5881-5891
15. Chen, L., Wang, H., Vicini, S., and Olsen, R. W. (2000) **The gamma-aminobutyric acid type A (GABAA) receptor-associated protein (GABARAP) promotes GABAA receptor clustering and modulates the channel kinetics.** *Proc Natl Acad Sci U S A* **97**, 11557-11562
16. Kneussel, M., Haverkamp, S., Fuhrmann, J. C., Wang, H., Wassle, H., Olsen, R. W., and Betz, H. (2000) **The gamma-aminobutyric acid type A receptor (GABAAR)-associated protein GABARAP interacts with gephyrin but is not**

involved in receptor anchoring at the synapse. *Proc Natl Acad Sci U S A* **97**, 8594-8599
17. O'Sullivan, G. A., Kneussel, M., Elazar, Z., and Betz, H. (2005) **GABARAP is not essential for GABA receptor targeting to the synapse.** *Eur J Neurosci* **22**, 2644-2648
18. Bavro, V. N., Sola, M., Bracher, A., Kneussel, M., Betz, H., and Weissenhorn, W. (2002) **Crystal structure of the GABA(A)-receptor-associated protein, GABARAP.** *EMBO Rep* **3**, 183-189
19. Bedford, F. K., Kittler, J. T., Muller, E., Thomas, P., Uren, J. M., Merlo, D., Wisden, W., Triller, A., Smart, T. G., and Moss, S. J. (2001) **GABA(A) receptor cell surface number and subunit stability are regulated by the ubiquitin-like protein Plic-1.** *Nat Neurosci* **4**, 908-916
20. Kittler, J. T., and Moss, S. J. (2003) **Modulation of GABAA receptor activity by phosphorylation and receptor trafficking: implications for the efficacy of synaptic inhibition.** *Curr Opin Neurobiol* **13**, 341-347
21. Essrich, C., Lorez, M., Benson, J. A., Fritschy, J. M., and Luscher, B. (1998) **Postsynaptic clustering of major GABAA receptor subtypes requires the gamma 2 subunit and gephyrin.** *Nat Neurosci* **1**, 563-571
22. Kneussel, M., Brandstatter, J. H., Gasnier, B., Feng, G., Sanes, J. R., and Betz, H. (2001) **Gephyrin-independent clustering of postsynaptic GABA(A) receptor subtypes.** *Mol Cell Neurosci* **17**, 973-982
23. Kneussel, M., and Betz, H. (2000) **Receptors, gephyrin and gephyrin-associated proteins: novel insights into the assembly of inhibitory postsynaptic membrane specializations.** *J Physiol* **525 Pt 1**, 1-9
24. Tretter, V., Jacob, T. C., Mukherjee, J., Fritschy, J. M., Pangalos, M. N., and Moss, S. J. (2008) **The clustering of GABA(A) receptor subtypes at inhibitory synapses is facilitated via the direct binding of receptor alpha 2 subunits to gephyrin.** *J Neurosci* **28**, 1356-1365
25. Becker, C. M., Hoch, W., and Betz, H. (1988) **Glycine receptor heterogeneity in rat spinal cord during postnatal development.** *EMBO J* **7**, 3717-3726
26. Grudzinska, J., Schemm, R., Haeger, S., Nicke, A., Schmalzing, G., Betz, H., and Laube, B. (2005) **The beta subunit determines the ligand binding properties of synaptic glycine receptors.** *Neuron* **45**, 727-739
27. Pfeiffer, F., Graham, D., and Betz, H. (1982) **Purification by affinity chromatography of the glycine receptor of rat spinal cord.** *J Biol Chem* **257**, 9389-9393
28. Meyer, G., Kirsch, J., Betz, H., and Langosch, D. (1995) **Identification of a gephyrin binding motif on the glycine receptor beta subunit.** *Neuron* **15**, 563-572
29. Kirsch, J., Wolters, I., Triller, A., and Betz, H. (1993) **Gephyrin antisense oligonucleotides prevent glycine receptor clustering in spinal neurons.** *Nature* **366**, 745-748
30. Feng, G., Tintrup, H., Kirsch, J., Nichol, M. C., Kuhse, J., Betz, H., and Sanes, J. R. (1998) **Dual requirement for gephyrin in glycine receptor clustering and molybdoenzyme activity.** *Science* **282**, 1321-1324
31. Kins, S., Kuhse, J., Laube, B., Betz, H., and Kirsch, J. (1999) **Incorporation of a gephyrin-binding motif targets NMDA receptors to gephyrin-rich domains in HEK 293 cells.** *Eur J Neurosci* **11**, 740-744
32. Kirsch, J., Kuhse, J., and Betz, H. (1995) **Targeting of glycine receptor subunits to gephyrin-rich domains in transfected human embryonic kidney cells.** *Mol Cell Neurosci* **6**, 450-461

33. Prior, P., Schmitt, B., Grenningloh, G., Pribilla, I., Multhaup, G., Beyreuther, K., Maulet, Y., Werner, P., Langosch, D., Kirsch, J., and et al. (1992) **Primary structure and alternative splice variants of gephyrin, a putative glycine receptor-tubulin linker protein.** *Neuron* **8**, 1161-1170
34. Fritschy, J. M., Harvey, R. J., and Schwarz, G. (2008) **Gephyrin: where do we stand, where do we go?** *Trends Neurosci* **31**, 257-264
35. Ramming, M., Kins, S., Werner, N., Hermann, A., Betz, H., and Kirsch, J. (2000) **Diversity and phylogeny of gephyrin: tissue-specific splice variants, gene structure, and sequence similarities to molybdenum cofactor-synthesizing and cytoskeleton-associated proteins.** *Proc Natl Acad Sci U S A* **97**, 10266-10271
36. Stallmeyer, B., Schwarz, G., Schulze, J., Nerlich, A., Reiss, J., Kirsch, J., and Mendel, R. R. (1999) **The neurotransmitter receptor-anchoring protein gephyrin reconstitutes molybdenum cofactor biosynthesis in bacteria, plants, and mammalian cells.** *Proc Natl Acad Sci U S A* **96**, 1333-1338
37. Kim, E. Y., Schrader, N., Smolinsky, B., Bedet, C., Vannier, C., Schwarz, G., and Schindelin, H. (2006) **Deciphering the structural framework of glycine receptor anchoring by gephyrin.** *EMBO J* **25**, 1385-1395
38. Schwarz, G., Schrader, N., Mendel, R. R., Hecht, H. J., and Schindelin, H. (2001) **Crystal structures of human gephyrin and plant Cnx1 G domains: comparative analysis and functional implications.** *J Mol Biol* **312**, 405-418
39. Liu, M. T., Wuebbens, M. M., Rajagopalan, K. V., and Schindelin, H. (2000) **Crystal structure of the gephyrin-related molybdenum cofactor biosynthesis protein MogA from Escherichia coli.** *J Biol Chem* **275**, 1814-1822
40. Xiang, S., Nichols, J., Rajagopalan, K. V., and Schindelin, H. (2001) **The crystal structure of Escherichia coli MoeA and its relationship to the multifunctional protein gephyrin.** *Structure* **9**, 299-310
41. Schwarz, G., and Mendel, R. R. (2006) **Molybdenum cofactor biosynthesis and molybdenum enzymes.** *Annu Rev Plant Biol* **57**, 623-647
42. Sola, M., Bavro, V. N., Timmins, J., Franz, T., Ricard-Blum, S., Schoehn, G., Ruigrok, R. W., Paarmann, I., Saiyed, T., O'Sullivan, G. A., Schmitt, B., Betz, H., and Weissenhorn, W. (2004) **Structural basis of dynamic glycine receptor clustering by gephyrin.** *EMBO J* **23**, 2510-2519
43. Sola, M., Kneussel, M., Heck, I. S., Betz, H., and Weissenhorn, W. (2001) **X-ray crystal structure of the trimeric N-terminal domain of gephyrin.** *J Biol Chem* **276**, 25294-25301
44. Schrader, N., Kim, E. Y., Winking, J., Paulukat, J., Schindelin, H., and Schwarz, G. (2004) **Biochemical characterization of the high affinity binding between the glycine receptor and gephyrin.** *J Biol Chem* **279**, 18733-18741
45. Zita, M. M., Marchionni, I., Bottos, E., Righi, M., Del Sal, G., Cherubini, E., and Zacchi, P. (2007) **Post-phosphorylation prolyl isomerisation of gephyrin represents a mechanism to modulate glycine receptors function.** *EMBO J* **26**, 1761-1771
46. Kins, S., Betz, H., and Kirsch, J. (2000) **Collybistin, a newly identified brain-specific GEF, induces submembrane clustering of gephyrin.** *Nat Neurosci* **3**, 22-29
47. Kneussel, M., and Betz, H. (2000) **Clustering of inhibitory neurotransmitter receptors at developing postsynaptic sites: the membrane activation model.** *Trends Neurosci* **23**, 429-435

48. Sabatini, D. M., Barrow, R. K., Blackshaw, S., Burnett, P. E., Lai, M. M., Field, M. E., Bahr, B. A., Kirsch, J., Betz, H., and Snyder, S. H. (1999) **Interaction of RAFT1 with gephyrin required for rapamycin-sensitive signaling.** *Science* **284**, 1161-1164
49. Mammoto, A., Sasaki, T., Asakura, T., Hotta, I., Imamura, H., Takahashi, K., Matsuura, Y., Shirao, T., and Takai, Y. (1998) **Interactions of drebrin and gephyrin with profilin.** *Biochem Biophys Res Commun* **243**, 86-89
50. Giesemann, T., Schwarz, G., Nawrotzki, R., Berhorster, K., Rothkegel, M., Schluter, K., Schrader, N., Schindelin, H., Mendel, R. R., Kirsch, J., and Jockusch, B. M. (2003) **Complex formation between the postsynaptic scaffolding protein gephyrin, profilin, and Mena: a possible link to the microfilament system.** *J Neurosci* **23**, 8330-8339
51. Kirsch, J., Langosch, D., Prior, P., Littauer, U. Z., Schmitt, B., and Betz, H. (1991) **The 93-kDa glycine receptor-associated protein binds to tubulin.** *J Biol Chem* **266**, 22242-22245
52. King, S. M., and Patel-King, R. S. (1995) **The M(r) = 8,000 and 11,000 outer arm dynein light chains from Chlamydomonas flagella have cytoplasmic homologues.** *J Biol Chem* **270**, 11445-11452
53. Delanoue, R., and Davis, I. (2005) **Dynein anchors its mRNA cargo after apical transport in the Drosophila blastoderm embryo.** *Cell* **122**, 97-106
54. Stokin, G. B., and Goldstein, L. S. (2006) **Axonal transport and Alzheimer's disease.** *Annu Rev Biochem* **75**, 607-627
55. Vale, R. D. (2003) **The molecular motor toolbox for intracellular transport.** *Cell* **112**, 467-480
56. Hirokawa, N., Noda, Y., and Okada, Y. (1998) **Kinesin and dynein superfamily proteins in organelle transport and cell division.** *Curr Opin Cell Biol* **10**, 60-73
57. King, S. M. (2000) **The dynein microtubule motor.** *Biochim Biophys Acta* **1496**, 60-75
58. Vaughan, K. T., and Vallee, R. B. (1995) **Cytoplasmic dynein binds dynactin through a direct interaction between the intermediate chains and p150Glued.** *J Cell Biol* **131**, 1507-1516
59. Ligon, L. A., Karki, S., Tokito, M., and Holzbaur, E. L. (2001) **Dynein binds to beta-catenin and may tether microtubules at adherens junctions.** *Nat Cell Biol* **3**, 913-917
60. Purohit, A., Tynan, S. H., Vallee, R., and Doxsey, S. J. (1999) **Direct interaction of pericentrin with cytoplasmic dynein light intermediate chain contributes to mitotic spindle organization.** *J Cell Biol* **147**, 481-492
61. King, S. M., Barbarese, E., Dillman, J. F., III, Patel-King, R. S., Carson, J. H., and Pfister, K. K. (1996) **Brain cytoplasmic and flagellar outer arm dyneins share a highly conserved Mr 8,000 light chain.** *J Biol Chem* **271**, 19358-19366
62. Schnorrer, F., Bohmann, K., and Nusslein-Volhard, C. (2000) **The molecular motor dynein is involved in targeting swallow and bicoid RNA to the anterior pole of Drosophila oocytes.** *Nat Cell Biol* **2**, 185-190
63. Williams, J. C., Roulhac, P. L., Roy, A. G., Vallee, R. B., Fitzgerald, M. C., and Hendrickson, W. A. (2007) **Structural and thermodynamic characterization of a cytoplasmic dynein light chain-intermediate chain complex.** *Proc Natl Acad Sci U S A* **104**, 10028-10033
64. Benison, G., Karplus, P. A., and Barbar, E. (2007) **Structure and dynamics of LC8 complexes with KXTQT-motif peptides: swallow and dynein intermediate chain compete for a common site.** *J Mol Biol* **371**, 457-468

65. Espindola, F. S., Suter, D. M., Partata, L. B., Cao, T., Wolenski, J. S., Cheney, R. E., King, S. M., and Mooseker, M. S. (2000) **The light chain composition of chicken brain myosin-Va: calmodulin, myosin-II essential light chains, and 8-kDa dynein light chain/PIN.** *Cell Motil Cytoskeleton* **47**, 269-281
66. Naisbitt, S., Valtschanoff, J., Allison, D. W., Sala, C., Kim, E., Craig, A. M., Weinberg, R. J., and Sheng, M. (2000) **Interaction of the postsynaptic density-95/guanylate kinase domain-associated protein complex with a light chain of myosin-V and dynein.** *J Neurosci* **20**, 4524-4534
67. Day, C. L., Puthalakath, H., Skea, G., Strasser, A., Barsukov, I., Lian, L. Y., Huang, D. C., and Hinds, M. G. (2004) **Localization of dynein light chains 1 and 2 and their pro-apoptotic ligands.** *Biochem J* **377**, 597-605
68. Liang, J., Jaffrey, S. R., Guo, W., Snyder, S. H., and Clardy, J. (1999) **Structure of the PIN/LC8 dimer with a bound peptide.** *Nat Struct Biol* **6**, 735-740
69. Crepieux, P., Kwon, H., Leclerc, N., Spencer, W., Richard, S., Lin, R., and Hiscott, J. (1997) **I kappaB alpha physically interacts with a cytoskeleton-associated protein through its signal response domain.** *Mol Cell Biol* **17**, 7375-7385
70. Lo, K. W., Kan, H. M., Chan, L. N., Xu, W. G., Wang, K. P., Wu, Z., Sheng, M., and Zhang, M. (2005) **The 8-kDa dynein light chain binds to p53-binding protein 1 and mediates DNA damage-induced p53 nuclear accumulation.** *J Biol Chem* **280**, 8172-8179
71. Lightcap, C. M., Sun, S., Lear, J. D., Rodeck, U., Polenova, T., and Williams, J. C. (2008) **Biochemical and structural characterization of the Pak1- LC8 interaction.** *J Biol Chem*
72. Tan, G. S., Preuss, M. A., Williams, J. C., and Schnell, M. J. (2007) **The dynein light chain 8 binding motif of rabies virus phosphoprotein promotes efficient viral transcription.** *Proc Natl Acad Sci U S A* **104**, 7229-7234
73. Rayala, S. K., den Hollander, P., Manavathi, B., Talukder, A. H., Song, C., Peng, S., Barnekow, A., Kremerskothen, J., and Kumar, R. (2006) **Essential role of KIBRA in co-activator function of dynein light chain 1 in mammalian cells.** *J Biol Chem* **281**, 19092-19099
74. Fuhrmann, J. C., Kins, S., Rostaing, P., El Far, O., Kirsch, J., Sheng, M., Triller, A., Betz, H., and Kneussel, M. (2002) **Gephyrin interacts with Dynein light chains 1 and 2, components of motor protein complexes.** *J Neurosci* **22**, 5393-5402
75. Navarro-Lerida, I., Martinez Moreno, M., Roncal, F., Gavilanes, F., Albar, J. P., and Rodriguez-Crespo, I. (2004) **Proteomic identification of brain proteins that interact with dynein light chain LC8.** *Proteomics* **4**, 339-346
76. Barbar, E. (2008) **Dynein light chain LC8 is a dimerization hub essential in diverse protein networks.** *Biochemistry* **47**, 503-508
77. Jaffrey, S. R., and Snyder, S. H. (1996) **PIN: an associated protein inhibitor of neuronal nitric oxide synthase.** *Science* **274**, 774-777
78. Nyarko, A., Hare, M., Hays, T. S., and Barbar, E. (2004) **The intermediate chain of cytoplasmic dynein is partially disordered and gains structure upon binding to light-chain LC8.** *Biochemistry* **43**, 15595-15603
79. Wagner, W., Fodor, E., Ginsburg, A., and Hammer, J. A., 3rd. (2006) **The binding of DYNLL2 to myosin Va requires alternatively spliced exon B and stabilizes a portion of the myosin's coiled-coil domain.** *Biochemistry* **45**, 11564-11577

80. Jung, Y., Kim, H., Min, S. H., Rhee, S. G., and Jeong, W. (2008) **Dynein light chain LC8 negatively regulates NF-kappaB through the redox-dependent interaction with IkappaBalpha.** *J Biol Chem* **283**, 23863-23871
81. den Hollander, P., and Kumar, R. (2006) **Dynein light chain 1 contributes to cell cycle progression by increasing cyclin-dependent kinase 2 activity in estrogen-stimulated cells.** *Cancer Res* **66**, 5941-5949
82. Rodriguez-Crespo, I., Yelamos, B., Roncal, F., Albar, J. P., Ortiz de Montellano, P. R., and Gavilanes, F. (2001) **Identification of novel cellular proteins that bind to the LC8 dynein light chain using a pepscan technique.** *FEBS Lett* **503**, 135-141
83. Otwinowski, Z., and Minor, W. (1997) **Processing of X-ray Diffraction Data Collected in Oscillation Mode.** *Macromolecular crystallography-Methods in Enzymology, New York: Academic Press* **276a**, 307-326
84. Navaza, J. (1994) **AMoRe: an automated package for molecular replacement.** *Acta Crystallographica* **A50**, 157-163
85. Lebedev, A. A., Vagin, A. A., and Murshudov, G. N. (2008) **Model preparation in MOLREP and examples of model improvement using X-ray data.** *Acta Crystallogr D Biol Crystallogr* **64**, 33-39
86. CCP4. (1994) **The CCP4 suite: programs for protein crystallography.** *Acta Crystallogr D Biol Crystallogr* **50**, 760-763
87. Murshudov, G. N., Vagin, A. A., and Dodson, E. J. (1997) **Refinement of macromolecular structures by the maximum-likelihood method.** *Acta Crystallogr D Biol Crystallogr* **53**, 240-255
88. Winn, M. D., Murshudov, G. N., and Papiz, M. Z. (2003) **Macromolecular TLS refinement in REFMAC at moderate resolutions.** *Methods Enzymol* **374**, 300-321
89. Perrakis, A., Morris, R., and Lamzin, V. S. (1999) **Automated protein model building combined with iterative structure refinement.** *Nat Struct Biol* **6**, 458-463
90. Jones, T. A., Zou, J. Y., Cowan, S. W., and Kjeldgaard, M. (1991) **Improved methods for building protein models in electron density maps and the location of errors in these models.** *Acta Crystallogr A* **47 (Pt 2)**, 110-119
91. Emsley, P., and Cowtan, K. (2004) **Coot: model-building tools for molecular graphics.** *Acta Crystallogr D Biol Crystallogr* **60**, 2126-2132
92. Lovell, S. C., Davis, I. W., Arendall, W. B., 3rd, de Bakker, P. I., Word, J. M., Prisant, M. G., Richardson, J. S., and Richardson, D. C. (2003) **Structure validation by Calpha geometry: phi,psi and Cbeta deviation.** *Proteins* **50**, 437-450
93. Benison, G., Karplus, P. A., and Barbar, E. (2008) **The interplay of ligand binding and quaternary structure in the diverse interactions of dynein light chain LC8.** *J Mol Biol* **384**, 954-966
94. Barbar, E., Kleinman, B., Imhoff, D., Li, M., Hays, T. S., and Hare, M. (2001) **Dimerization and folding of LC8, a highly conserved light chain of cytoplasmic dynein.** *Biochemistry* **40**, 1596-1605
95. Zhao, G., and London, E. (2006) **An amino acid "transmembrane tendency" scale that approaches the theoretical limit to accuracy for prediction of transmembrane helices: relationship to biological hydrophobicity.** *Protein Sci* **15**, 1987-2001
96. Song, Y., Benison, G., Nyarko, A., Hays, T. S., and Barbar, E. (2007) **Potential role for phosphorylation in differential regulation of the assembly of dynein light chains.** *J Biol Chem* **282**, 17272-17279

97. Saiyed, T., Paarmann, I., Schmitt, B., Haeger, S., Sola, M., Schmalzing, G., Weissenhorn, W., and Betz, H. (2007) **Molecular basis of gephyrin clustering at inhibitory synapses: role of G- and E-domain interactions.** *J Biol Chem* **282**, 5625-5632
98. Bedet, C., Bruusgaard, J. C., Vergo, S., Groth-Pedersen, L., Eimer, S., Triller, A., and Vannier, C. (2006) **Regulation of gephyrin assembly and glycine receptor synaptic stability.** *J Biol Chem* **281**, 30046-30056